Naval Research Laboratory
Washington, DC 20375-5000

NRL Memorandum Report 6204

Design, Test and Evaluation of a Pair of Bootlace Lenses

P. D. STILWELL, JR, M. G. PARENT, H. P. COLEMAN AND B. D. WRIGHT

Electromagnetics Branch
Radar Division

July 6, 1988

SECURITY CLASSIFICATION OF THIS PAGE

REPORT DOCUMENTATION PAGE

Form Approved OMB No. 0704-0188

1a REPORT SECURITY CLASSIFICATION UNCLASSIFIED	1b RESTRICTIVE MARKINGS
2a SECURITY CLASSIFICATION AUTHORITY	3 DISTRIBUTION / AVAILABILITY OF REPORT Approved for public release; distribution unlimited.
2b DECLASSIFICATION / DOWNGRADING SCHEDULE	
4 PERFORMING ORGANIZATION REPORT NUMBER(S) NRL Memorandum Report 6204	5 MONITORING ORGANIZATION REPORT NUMBER(S)
6a NAME OF PERFORMING ORGANIZATION Naval Research Laboratory 6b OFFICE SYMBOL (If applicable) Code 5374	7a NAME OF MONITORING ORGANIZATION
6c ADDRESS (City, State, and ZIP Code) Washington, DC 20375-5000	7b ADDRESS (City, State, and ZIP Code)
8a NAME OF FUNDING / SPONSORING ORGANIZATION Space and Naval Warfare Systems Command 8b OFFICE SYMBOL (If applicable)	9 PROCUREMENT INSTRUMENT IDENTIFICATION NUMBER
8c ADDRESS (City, State, and ZIP Code) Washington, DC 20362-5101	10 SOURCE OF FUNDING NUMBERS PROGRAM ELEMENT NO: 62712N PROJECT NO: XF12-141-100 TASK NO WORK UNIT ACCESSION NO
11 TITLE (Include Security Classification) Design, Test and Evaluation of a Pair of Bootlace Lenses	
12 PERSONAL AUTHOR(S) Stilwell, P.D. Jr., Parent, M.G., Coleman, H.P. and Wright, B.D.	
13a TYPE OF REPORT Final 13b TIME COVERED FROM _____ TO _____ 14 DATE OF REPORT (Year, Month, Day) 1988 July 6 15 PAGE COUNT 76	
16 SUPPLEMENTARY NOTATION	

17 COSATI CODES			18 SUBJECT TERMS (Continue on reverse if necessary and identify by block number)
FIELD	GROUP	SUB-GROUP	Beamforming, Array matching, Bootlace lens, Rotman lens,

19 ABSTRACT (Continue on reverse if necessary and identify by block number)

This report details the design, test, and evaluation of two 3.2 GHz bootlace lenses. They were designed to be used to provide time delay beamforming for a 33 element linear array. The lenses were fabricated using a parallel plane medium with coaxial probes lining the entire perimeter. In this manner a true time delay lens performance was achieved displaying good impedance matching over 200 MHz and excellent beam match over ±45°. Extensive performance results are given as measured with an HP-8510 Network Analyzer for both the individual lenses and for their back-to-back configuration.

20 DISTRIBUTION / AVAILABILITY OF ABSTRACT ☒ UNCLASSIFIED/UNLIMITED ☐ SAME AS RPT ☐ DTIC USERS	21 ABSTRACT SECURITY CLASSIFICATION UNCLASSIFIED
22a NAME OF RESPONSIBLE INDIVIDUAL P.D. Stilwell, Jr.	22b TELEPHONE (Include Area Code) (202) 767-3355 22c OFFICE SYMBOL Code 5374

DD Form 1473, JUN 86 Previous editions are obsolete SECURITY CLASSIFICATION OF THIS PAGE

S/N 0102-LF-014-6603

CONTENTS

DESIGN, TEST AND EVALUATION OF A PAIR OF BOOTLACE LENSES

I. INTRODUCTION

This report concerns the development of a microwave lens of the bootlace type for use as a beamformer for linear, phased array antennas. Such devices prove to be a practical implementation of the type of time delay beamformer required in ECCM systems identified by Gabriel and others [1,2,3]. They constitute hardware which maps from a sampled (elemental antenna) space to beamspace, where beamspace denotes one of the many discrete sets of directional antenna patterns possible, e.g., a Fourier transform of the antenna samples.

Successful implementation of a wide angle, wideband lens places strong conditions on impedance match over frequency and scan direction. Further, operation in beamspace implies the existence of a significant number of beam ports and a commensurate number of antenna elements. Of the numerous types of beamforming circuitry (Blass [4], Butler [5], Gent [6], Ruze [7], Rotman-Turner [8], etc., [9, 10]) none display the exact features desired. It was decided that a generic bootlace lens using a parallel plane medium designed with an emphasis on channel matching offered the greatest potential for a high quality beamformer with a moderate number of beams. A key ingredient in obtaining the requisite match is a uniform spacing of the probes feeding the parallel plate region. This uniform spacing although compromising the independence of adjacent beams, allows a common probe element pattern to be used and maintains good match to large scanning angles. In spite of the intrinsic advantages of a stripline design, it was felt that a beamformer with approximately 30 beams using an air filled parallel plane medium connected to coaxial probes would offer experimental convenience and be more amenable to modification and fine tuning. The use of two such lenses would allow a laboratory evaluation of performance in a back-to-back arrangement while avoiding the necessity of operating with an array on an antenna range during the development of the lenses.

II. BACKGROUND

A bootlace beamformer is an M input port device with N output ports, see Fig. II-1. The N output ports can be attached to an N element array with a linear spacing, a circularily disposed set of elemental antennas or some other type of array. The attachment of a source to any of the M input ports will create an antenna beam in the m^{th} direction. The RF "lacing" between the input and output ports constitutes the body of the lens and therefore dominates the RF performance of the device. The lens medium can either be stripline or space between parallel planes, in either case, probes provide the coupling to and from the lens. There is strong

Manuscript approved March 26, 1988.

coupling between adjacent probes since each is embedded in an array consisting of all nearby probes. This may cause severe problems in cases where non-uniform probe spacing is used to make each of the M beams intersect adjacent beams at the 4 dB points. A non-uniform feed probe spacing greatly complicates the matching of each probe to its transmission line impedance and simultaneously to the 2D modes in the parallel plane medium.

Total matching of the input ports of a multiport lens involves two distinct matching conditions. The first is the impedance transformation from the transmission line to that of the parallel plane medium. The second is the match or coupling to different propagation directions in the parallel plane region, especially when a close spaced array of probes is used. Thus, depending on the pattern of a single driven probe as seen in the two dimensional region, the array could be properly matched to the transmission line yet not to the 2D modes. Total matching of the lens involves a simultaneous meeting of boundary conditions on both sides of the probe. A heuristic argument (based on a requirement for perfect absorption of plane waves falling at an arbitrary angle on an array) is convincing that a $\cos\theta$ behavior of the pattern for each element is required. (This is the pattern of an aperture of a blackbody radiator or the albedo of a perfectly absorbing material.) Following this logic, it is then impossible to obtain simultaneous total matching of a parallel plane lens and beam "orthogonality" where orthogonality implies overlap at the 3 or 4 dB points.

In addition to being used to excite wavefronts from a linear array, two lenses can be used in series (with the element planes attached one to one) to provide a laboratory approximation of an antenna range. Figure II-2 diagrams the concept. A signal attached to one of the input ports couples uniformly to output elements of that lens. These are directly attached to the elements of the second lens. Finally, the space propagation in the second lens excites the output probes and can approximate a sinc(x) distribution. (The sinc function is sampled only at the points where probes exist so only a line spectral approximation to the sinc function will be observed.) In this way, one can obtain a beam combining system for a discrete set of sources which has a time delay behavior.

The rather strong resemblance of Fig. II-2, 3 to the multiplication of matrices is not coincidental. In the back-to-back case the mathematical model would involve the product of an MxN matrix, M_1, times an NxM matrix, M_2, which is mindful of a generalized inverse of M_1. Thus, if the input excitation vector had a 1 in the m^{th} position, at some frequency of operation the output vector would have a single 1 in the m^{th} position and zeros elsewhere. At other frequencies the same excitation vector might yield an output which peaked at the proper place but show non-zero coupling to the other beams. Only at one excitation frequency will the output probe array have the proper periodicity to sample the sinc function exactly at sidelobe nulls.

It was decided to build a set of lenses using a parallel plane air filled medium since this should be relatively easy to build. High dielectric constant material could be used to significantly reduce the physical size of the lens but would probably cause a considerable amount of bulk scattering from inhomogeneities in the dielectric material. A

goal of a port VSWR of better than 2:1 over a 200 MHz band centered at 3.2 GHz was selected. At this match the return loss is sufficient to diminish resonances to an ignorable level and eliminate effects of multiple delays of the signals through the circuit. The feeds were to be chosen to scan to ± 30° from broadside to the effective linear array with good beam quality and to ± 45° with degraded performance.

III. BASIC LENS CONSIDERATIONS

Figure II-1 illustrated the basic structure of a bootlace lens. The goal of the design is to determine the loci $f(x)$ and $e(\xi)$ which yield a plane waves from the element ports e_j, see Fig. III-1. The symbol e_j is used to denote the j^{th} element of the linear array which would be connected to the output ports of the lens. Each of the transmission lines connecting the j^{th} port to the actual linear array would have identical lengths. The M input ports to the system are labeled f_i and occur at a height f_i above the axis of symmetry. This figure strongly resembles a cross section of an eye. The similarity holds further in that the right solid curve constitutes the actual lens and the left one the receptors (transmitters?). It will be assumed herein that an axis of symmetry is required to permit scanning to equal angles from the broadside of the assumed linear array. Peculiar scanning requirements might be devised for which this is not so but such cases will not be discussed in this report. Likewise the output ports are coupled to the parallel plane medium at heights e_j. Since the transmission lines $L(f_i)$ and $L(e_j)$ are not constrained to a plane these lengths may be varied at will without altering the geometry indicated in the figure, where ε denotes the dielectric constant of the parallel plane medium. The total phase length from feed point f to element point e is given by

$$\psi(f,e) = (2\pi/\lambda)[L(f) + \varepsilon D(f,e) + L(e)] \qquad \text{III-1a}$$

with

$$D(f,e) = \text{SQRT}\{(\xi - x)^2 + (e - f)^2\}. \qquad \text{III-1b}$$

For the lens to perform ideally a uniform phase gradient should exist between element probes. The magnitude of the gradient is governed by the selection of f. In equation form this is

$$\partial\psi/\partial e = F(f) \text{ and } \partial F/\partial e = 0. \qquad \text{III-2}$$

To be realistic, the function F will not be an exact constant over the entire range of e. Therefore the more appropriate approach would be to minimize the expression

$$\text{VAR}\ (\partial\psi/\partial e)$$

with

$$\text{ABS}(e) < e_{max} \qquad \text{III-3}$$

It will be noted that there is no hint of the existence of probes in Fig. III-1, only loci. The loci must be measured with respect to the center of phase of the probes. This is a very important aspect of the lens and must be accurately determined. Anticipating results to be obtained later, the central feed probe phase center must lie exactly at

the center of the circular arc $e(\xi)$. Isolated probes in front of a ground plane exhibit a center of phase at the groundplane since this is the center of symmetry for the probe and its image. As additional probes are placed near the test probe the same distance from the groundplane the phase center will migrate away from the wall due to phase shifts introduced by the mutual coupling with nearby probes. In lieu of solving a difficult set of boundary conditions to determine the effective phase center of a probe embedded in a non-uniform array, a direct method is to make the array uniform so that each probe will display an identical shift of phase center. Thus an experimental measurement can determine this shift and the loci can be located at this point relative to the probe itself, i.e., the loci to be determined relate to the phase center, not the wall nor the probes. Non-uniform spacing of probes could be expected to yield differing phase centers and a shift of up to 90° may result.

Now that the technique for the determination of the phase center of a probe embedded in a uniform array has been clarified, we can proceed with the determination of the loci associated with the inputs (feeds) and outputs (elements) of a lens. This entails a determination of the functions $f(x)$ and $e(\xi)$ either from equation III-2 or from III-3. It will be assumed that the $L(f_i)$ and $L(e_j)$ are constants as is the dielectric constant, ϵ. Then we can work only with $D(f,e)$ rather than with the more involved $\psi(f,e)$.

To start, we will investigate the information available from the derivatives of the phase along the locus of $e(\xi)$. Denoting partial derivatives by subscripts one can write

$$D = SQRT\left((f-e)^2 + (x-\xi)^2\right) \qquad \text{III-1b}$$

and

$$D_e = (1/D)\left\{(\xi-x)\xi_e + (e-f)\right\} \qquad \text{III-4}$$

Continuing by taking the second derivative, D_{ee}, and equating to zero allows one to deduce the conditions necessary to obtain zero phase error for any feed point f over the entire range of the element ports e. Due to the algebraic complexity (and also the fact that D_{ee} cannot be identically zero over the entire range of e) we will assume $e(\xi)$ to be the function which by inspection minimizes the dependence of D_e on e yet maintains a dependence on f. Rewriting III-4 as

$$D\,D_e = (\xi\xi_e + e) - x\xi_e - f \qquad \text{III-5}$$

allows us to see that the term in parenthesis can be made identically zero by the choice $\xi_e = -e/\xi$, which happens to be the differential equation for a circle centered at e=0, ξ=0. From the geometry of the problem the radius of that circle is ξ_o, the separation between the feed and element postions on the axis of symmetry. With that geometry the remaining dependence is linear in f as desired but with an error term xe/ξ. This error term is to be small and it will be insofar as x and e are small relative to ξ_o. Continuing then

$$D_{ee} = \left\{1 + (e/\xi)^2\right\}x/\xi D - \left\{ex/\xi - f\right\}^2/D^3 \qquad \text{III-6}$$

This can be cast in the form

$$f^2 + (-2e/\xi)fx + (e^2/\xi^2)x^2 + (-\xi_o + 4/\xi^3)x = 0 \qquad \text{III-7}$$

with $D = \xi$. This is a canonical form for a rotated ellipse of shifted origin but centered on the x axis. Ignoring the rotation term yields an ellipse with a major axis of .56 ξ_o and a minor axis of .44 ξ_o. This curve was graphed and fitted with a circle of radius .63 for f up to .5 (measured in terms of ξ_o). Alternately this can be approached by approximating the equation by

$$f^2 = \xi_o x \qquad \text{III-8}$$

which is an equation for a parabola. Using the Gaussian curvature

$$1/R = f''(x)/[1 + (f''(x))^2]^{3/2} \qquad \text{III-9}$$

the radius of curvature at the axis is $R = .5\xi_o$. This is the expected feed locus for a lens which, without error, feeds a cylindrical array. In conclusion, an examiniation of the derivatives of $D(f,e)$ directly elicits the property that $e(\xi)$ should be a circle of large radius of curvature. The curve $f(x)$ cannot so easily be determined but is found to be an elliptical shape.

IV. DESIGN PROCEDURES

Two major questions remain to be answered in the design of the lens.

a. what is the phase center of the probes, and

b. what are the feed and element probe positions?

To resolve the first question we built a "D" lens for which the final layout is shown in Fig. IV-1. There were 3 major goals of this experimental effort, namely, what are the probe dimensions that yield a good transmission line match, what is the array element pattern, and where is the phase center. An additional factor was whether either the element pattern or the phase center varied if the array were linear or mildly curvilinear. The "D" shape was selected since it bracketed the curvatures expected for the final lens, i.e., the linear side had less curvature and the arc had greater curvature. The experimental assembly used two large sheets of aluminum spaced by sections of X-band waveguide, one such section functioning as the wall for the linear array of input probes. Absorber was placed in an arc away from this wall and a single probe inserted. Access holes in the top plate of the lens provided a means of inserting a field probe to determine field strength. The plan was to measure match and pattern. Once a probe was transmission line matched it would be embedded in a larger array of identical probes. The central probe would then be altered for improved match and all probes modified to that design. This iterative procedure with ever increasing array size should eventually terminate in that no modification of the probe would be required on increasing the number of elements in the array. Finally the absorber would be removed and replaced by a reflecting wall with a similar array of probes to terminate the entire region. Completely enclosing the

perimeter of the lens by the probe array was done primarily to avoid the use of absorbing material within the parallel plane structure.

When the probe array was of size 7 it was determined that there were too few design degrees of freedom available to simultaneously match the probe to the transmission line and obtain a good cosθ element pattern. To provide another degree of freedom, a parasitic stub was placed in front of each probe away from the wall, see Fig. IV-2. A very considerable improvement of the element pattern resulted, Fig. IV-3.

The phase center of a single driven probe embedded in an array was measured by inserting a field probe through the top plate of the cavity through holes drilled in a circle with center at the central probe of the linear side. Figure IV-4 shows the results. The radius of the circle was approximately 3 wavelengths and the size of the array was also about 3 wavelengths. Such near field probing, although providing for considerable phase center location accuracy, suffers from large relative angular changes from the group of probes. Consequently, instead of obtaining a very smooth curve, indicated by the conceptualized curves labeled at wall and 1/2 way in Fig. IV-4, the phase measurements show a growing oscillatory form away from the symmetry axis. This arises from the differences in space attenuation and angle between elements of the array. With parasitic stubs the oscillations seem to have a mean which is centered on the horizontal axis, indicating that the phase center exists at the center of the circle, i.e., exists at the on-axis probe itself. (Looking ahead, after testing of the final assembly this interpretation was confirmed, at least to the accuracy possible in the above measurement. A very minor difference of about 4% closer to the wall was measured.)

The second question which had to be answered was that concerning the ideal loci and positions for the f and e probes. In lieu of actually solving the variational equations a numeric method was used to empirically estimate the desired functions. The numerical procedure has some advantages since amplitudes could be used in computing the sum of the phasors which represents the far field from an array antenna attached one-to-one to the ports e_i. Physically, at some angle from the broadside to the antenna (dependent on the feed port f_i) the phasor sum will reach a maximum. The maximum should have a value proportional to N^2 but will be degraded by phase errors. Thus the difference from N^2 will be measure of the phase error. This could be a useful criterion in selecting the curves f and e, assuming that the phase errors which occur are not periodic. A lens with a fixed separation of the axial intercept points was assumed and different curves used to calculate the phasor sum, or gain. The curve parameters were altered in a multivariable gradient routine using max gain as a performance criterion. Ellipses were chosen for the curve form.

A second empirical approach was used based on the minimization of the variance from a linear dependence of D(e). This was motivated by the examination of the derivatives in section III. A spreadsheet was prepared on an IBM PC which was programmed using a circle for $e(\xi)$. A value of f was chosen and a value of x iteratively entered to find a minimum in the deviation of D(e,x) from a linear dependence on e. This very rapidly yielded the shape of the desired curve f(x) and showed a form very close to a circle for probes near the axis.

Both empirical approaches arrived at the same curve for the feeds over the desired interval in spite of the fact that the gain calculation used an amplitude weighting and the variance procedure used only the phase length. In fact, the curve f(x) was not terribly sensitive to exact contour and a circle of 10λ yielded the best gain and minimum variance for ξ_o=16λ. The approximating circle was used in the construction of the final lenses. The two sets of points needed to locate the probes, (e_i,ξ_i) and (f_j,x_j), were calculated such that there was an element probe and a feed probe on axis and the chord length between adjacent probes was exactly λ/2. To blend these two curves together into a closed surface an ad hoc spline curve was used which was both smooth and of a length which was a multiple of λ/2. The final assembly blueprint is represented in Fig. IV-5.

V. TEST AND EVALUATION

The T&E of the pair of lenses was conducted using an HP 8510 Network Analyzer system. This system provides a very accurate measurement of the scattering matrix for a microwave circuit two ports at a time. Since each of the lenses had more than 100 ports it was necessary to load all ports except the two for which the components of the >100x100 scattering matrix was being evaluated. After each lens was characterized individually they were connected in a back-to-back configuration and the combination similarly characterized. For the back to back case of each transmission line interconnecting element ports was phase trimmed to a standard length. This was done by connecting the central input port and central output port to the network analyzer, loading all other ports save two, connecting those two with a transmission line, and trimming that length of line to a reference electrical phase length. The connecting cables had previously been cut to very nearly the same length such that no 2π error existed. After the trimming that cable was disconnected, the ports loaded and another set of elements treated in the same way.

Figure V-1, 2 show the complex reflection coefficient for one of the lenses. The abscissa for these curves are labeled BOTTOM (UPPER) PORT NUMBER which refer to the lens input ports and element ports, respectively. In these Fig. 67 ports are measured for the input and 51 for the elements. The remaining ports occur in the "corners" of the lenses, in the spline fit region, and are superfluous for this analysis even though they are critical for the performance of the lens. Figure V-1 shows the magnitude of the reflection coefficient at the top and the phase at the bottom. The critical region covers ±24 ports which corresponds to an output scan angle from a linear array attached directly to the elements (±16 ports) of ±45°. It can be seen that the reflection coefficient is less than -20 dB over this region everywhere except for port 0, the on-axis port. This corresponds to VSWR of better than 1.2:1 almost everywhere. The exception, port 0, is unique in that all the mismatch from the opposite surface returns in phase because it occurs on a circle with center at port 0. This peak is almost exactly 3 dB higher than that for the adjacent ports. This implies that the reflection from a given port comes primarily from reflections within the lens rather than from a simple mismatch of the transmission line at port 0. Since the reference phase was that through the lens using input 0 and element 0 (involving the entire inphase reflection from the element surface) the reflection phase

relates to the scattering from the second surface as seen from the input port). The 0 port is self conjugate, meaning that all the reflections combine in phase at the input port. All other ports have their inphase reflections combining at the conjugate port. In our enumeration of the ports the port conjugate to input port 1 would be input port -1, that conjugate to port 10 is port -10, and so forth.

Figure V-2 portrays the same information as Fig. V-1 except that the lens surface ports are used as "inputs" from the Network Analyzer. Again the reflection coefficient is small over the range of interest, ±16 ports. In this case there is no exactly conjugate port corresponding to a given input and the reflections from the second surface nowhere add up entirely inphase. Again, the phase curve shows mainly 360° jumps which is of little importance practically.

Figure V-3 to V-28 shows the magnitude and phase behavior across the array of element ports (labled "UPPER") with the feed (BOTTOM) port as a parameter. For the phase curves the linear trend and mean phase have been eliminated by subtracting the most frequently occuring slope, the mode, and then removing the mean value. The system was designed to be optimized over 33 element ports although 51 ports are associated with that side (the additional ports act as dummy ports to eliminate edge effects). The on-axis ports are labled zero. Figure V-3 shows the data for all 51 ports with the input being BOTTOM port 0. It can be seen that beyond 16 on either side (near the sharpest corners in Fig. IV-5) rather large interference occurs. Within the design range, both the phase and amplitude is well behaved, withing 0.5 dB, and of a cyclic nature. All in all the amplitude and phase variation is well behaved. There is even the semblance of a cosine elemental pattern apparent in the magnitude plot. The fact that the MODE SLOPE of Fig. V-3 is not zero indicates that the center of curvature of the UPPER or element ports is not exactly at input port (BOTTOM) 0. The 1.641 degree trend from port to port is indicative of a center of curvature approximately $\lambda/14$ to the negative side, toward negative port numbers. This corresponds to a 7 mm wedge (over 33 ports) inserted in the two sections of the lens as it was joined together. This linear trend could be taken out when the lenses were configured in a back-to-back configuration although it is so small that it is probably not significant. If a linear array were attached directly to the element ports it would cause the beam to be squinted by 0.5°.

Figure V-29 to V-35 are samples of patterns in the back-to-back configuration. The abscissa is output "feed" ports with input "feed" port as a parameter, these are denoted BOTTOM and BOTTOM(1), respectively. It should be remembered that the back-to-back configuration is very similar to a telescopic arrangement of optical lenses which have the same focal length. In essence the two lenses are positioned so that the back focal plane of the first is coincident with the front focal plane of the second. Ideally, a point source positioned in the front focal plane of the first lens (at the feed point) will focus all the energy to the conjugate point, the inverted image, located in the back focal plane of the second lens (since the wavefronts are collimated between the lenses). The source radiates energy which is not captured by the first lens (the element pattern in this case) so there is some loss in the transfer of energy from object to the image. For the bootlace lenses

approximately half the energy is lost in passing through each lens for a total of 6 dB loss. This loss is evident at the top of Fig. V-29. The impulse response function or pattern in this case should be mindful of a sinc squared function modified slightly due to a cosine aperture weighting. Figure V-29 does resemble a sinc squared for the near in sidelobes but deviates in the far out sidelobes as might be expected.

Figure V-30 shows a similar situation wherein input port -8 is excited. Figure V-31 illustrates input +11, Fig. V-32 for port 16, and Fig. V-33 for port -25. It will be noted that the main beam occurs at the conjugate port in the back-to-back arrangement and second time around effects which would occur at the proper port number are not strong. Figure V-34, 35 illustrate patterns when multiple ports are excited. The first shows ports 8 and 9 equally driven. The second, Fig. V-35, excites ports 7, 9 and 11 with weights 0.5, 1.0, and 0.5. The latter case approximates a Taylor weighted beamformer for 45 dB far out sidelobes.

The last two sets of figures, 36-44 and 45-53, display the frequency response with feed and receive ports as parameters. The first nine are associated with input or feed port 0 whereas the last nine relate to a common feed port 8. These curves essentially illustrate how the peaks and nulls of the back-to-back combination of bootlace lenses change as the frequency is altered. It is to be remembered that this system includes a virtual linear array between the lenses by the interconnecting cables. Although the arrangement is a pure time delay system which implies that the mainbeam direction will not deviate with frequency, the size of the aperture in terms of wavelenghts will change. This alters the sidelobe periodicity. Because the frequency excursion is not great, only 200 MHz, there is less evidence of a frequency sensitivity for the sidelobes than for the nulls. Figure V-36, for example has a null within the frequency range and a near null elsewhere. The 180° phase change as the frequency is swept through the null is apparent. For Fig. V-38 there are apparently two nulls but the first is probably an artifact of the data (also V-47). It can be seen that there is obviously inconsistent data near 3.11 GHz, spikes, and here is a high probability that some system malfunction, transient effect or data dropout introduced these artifacts. Figure V-42 shows much the same type of behavior and should in fact be identical with Fig. V-38, except for the lack of sharpness of the phase transition. This latter property points to both some coma and some spherical aberration in the lens system. Figure V-44 illustrates the effect of spherical aberration more strongly in decreasing the depth of the null at 3.215 GHz and moderating the phase jump at that frequency. Figure 45-53 are similar except that the constant feed port is number 8. Now the spherical aberration completely eliminates the formation of a deep null in the frequency span.

VI. CONCLUSIONS

The main conclusion which can be drawn from this effort is that it is possible to obtain a reasonable quality beamformer using a parallel plane medium for the lens. This is true provided care is taken in the design of the probes so that a reasonable approximation to an ideal element pattern can be achieved. The system being well matched implies that the element pattern even when embedded in the curvilinear arrays used

(10λ and 16λ of curvature) is close to ideal although not perfect. There does not have to be severe resonances nor is it necessary to load the medium with absorber to avoid unwanted modes. It was observed however, that if even one of the ports were opened or shorted, severe degradation of the beamforming resulted. This means that the system is quite unstable to variations of the transmission line match.

VII. REFERENCES

1. W.F. Gabriel, "Adaptive Arrays-An Introduction," Proc. IEEE, Vol. 64, pp. 239-272, Feb 1976.

2. W.F. Gabriel, "Using Spectral Estimation Techniques in Adaptive Processing Antenna Systems," IEEE-AP, AP-34, #3, pp 291-300, Mar 1986.

3. A.M. Vural, "Effects of Perturbations on the Performance of Optimum/Adaptive Arrays," IEEE-AES, Vol. AES-15, #1, pp 76-87 Jan 1979.

4. J. Blass, "Multi-Directional Antenna-A New Approach to Stacked Beams," IRE Natl. Conv. Record, Pt. 1, pp 48-50, 1960.

5. J. Butler and R. Lowe, "Beamforming Matrix Simplifies Design of Electronically Scanned Antennas," Electronic Design Vol. 9, pp 170-173, 1961.

6. H. Gent, "The Bootlace Aerial," Ray. Radar Establishment J., pp 47-57, Oct 1957.

7. J. Ruze, "Wide-Angle Metal-Plate Optics," Proc. IRE, Vol. 38, pp 53-58, Jan 1950.

8. W. Rotman and R.F. Turner, "Wide-Angle Microwave Lens for Line Source Applications," IEEE-AP, Vol. AP-11, #6, pp 623-632, Nov 1963.

9. D. Archer, "Lens-Fed Multiple-Beam Arrays," Microwave J., Vol 18, #10, pp 37-42, Oct 1975.

10. K. Takashi, S. Mano, and S. Sato, "An Improved Design Method of Rotman Lens Antennas," IEEE-AP, Vol AP-32, #5, pp 524-527, May 1984.

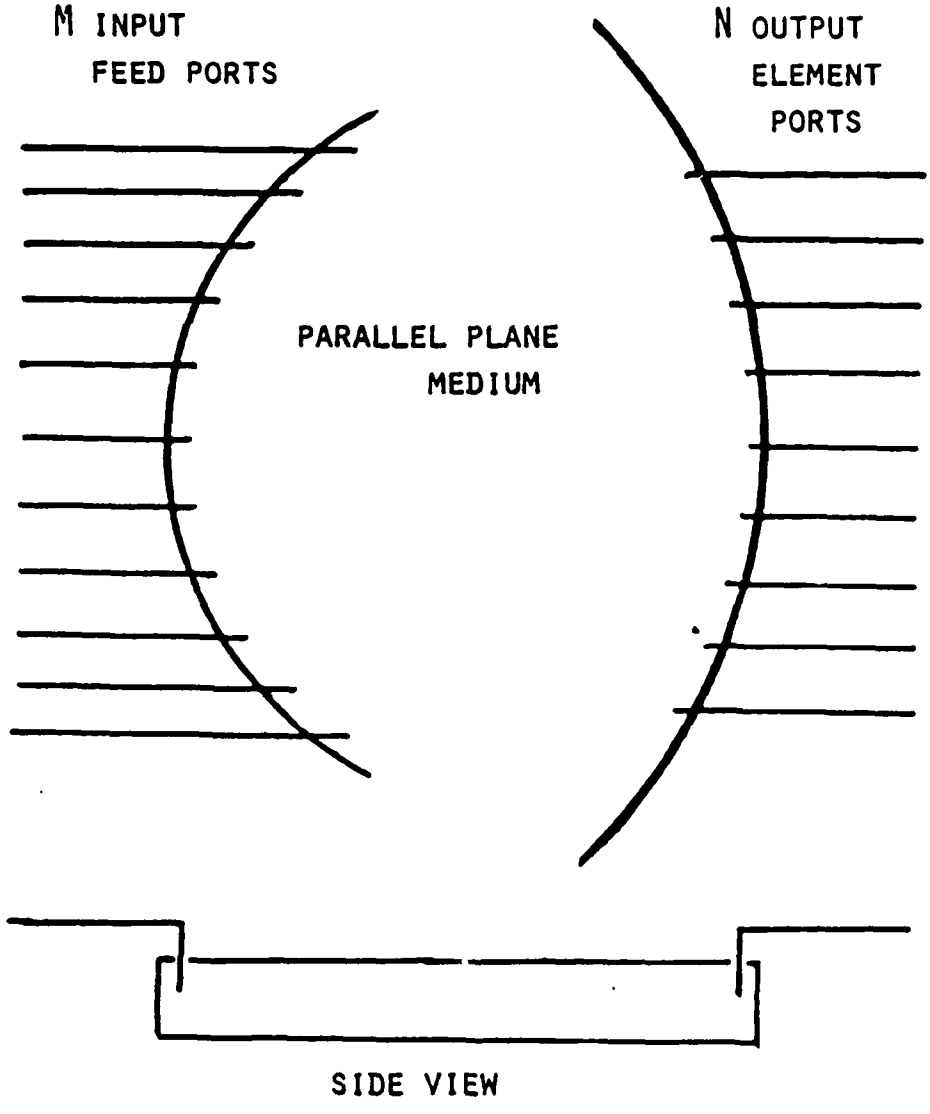

FIGURE II-1 PARALLEL PLANE BOOTLACE LENS

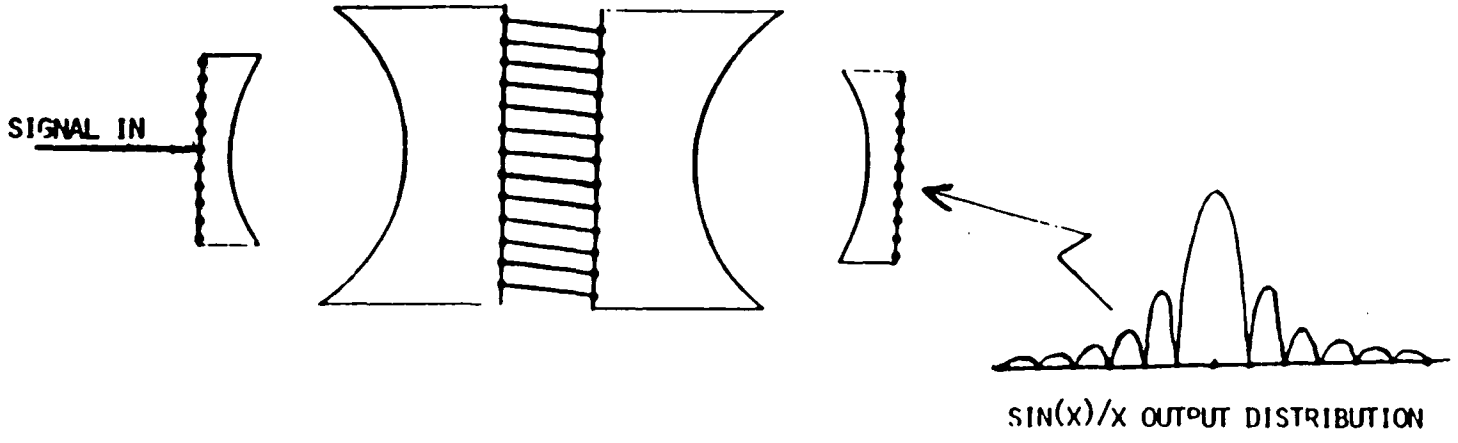

FIGURE II-2 IMPULSE RESPONSE FOR THE DUAL LENS ASSEMBLY

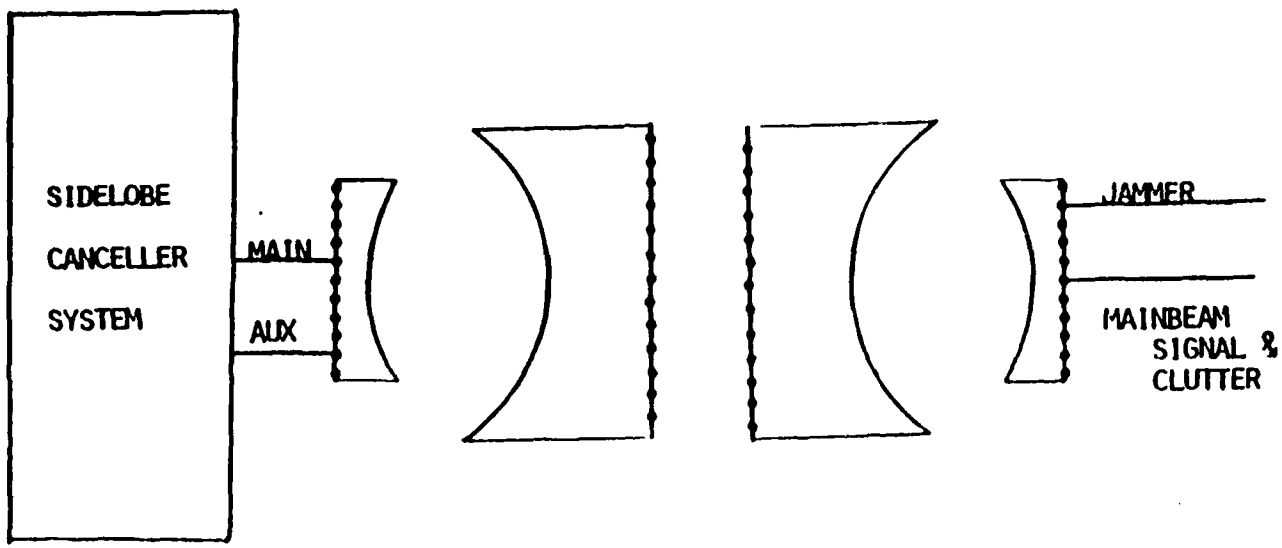

FIGURE II-3 BACK TO BACK FAR FIELD SIMULATOR

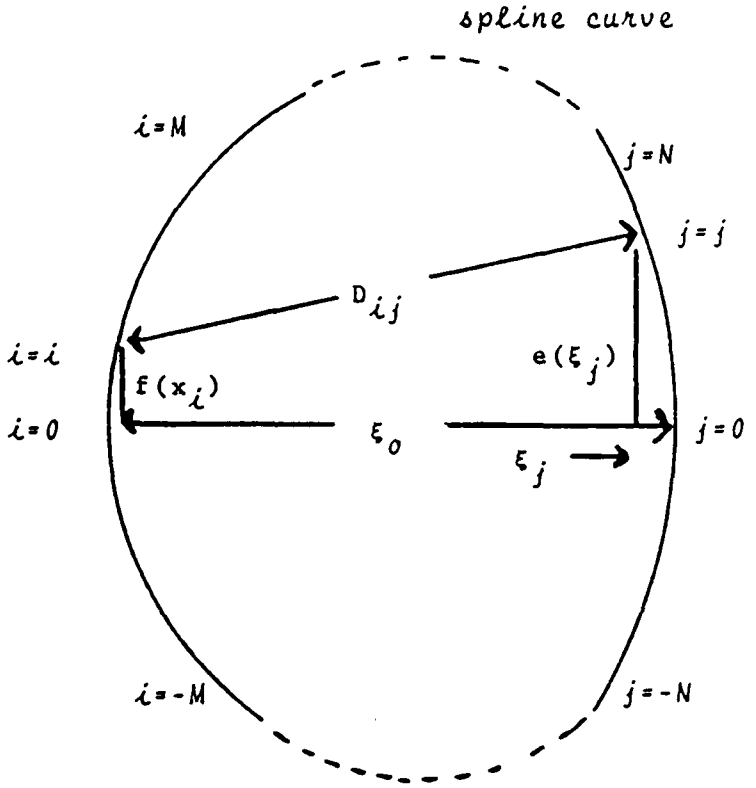

FIGURE III-1 BOOTLACE LENS GEOMETRY

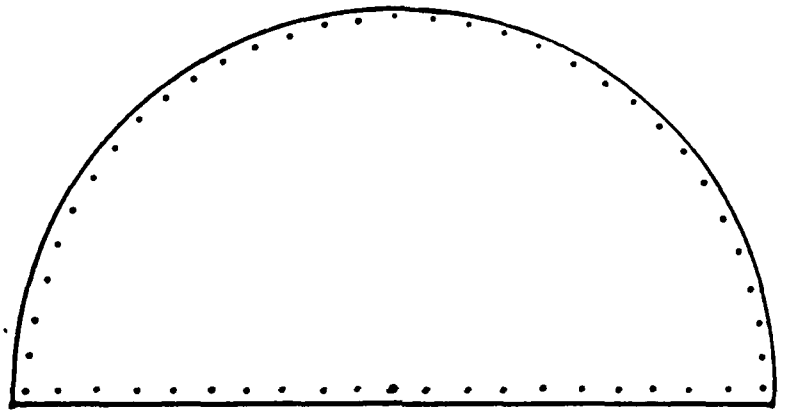

FIGURE IV-1 "D" LENS

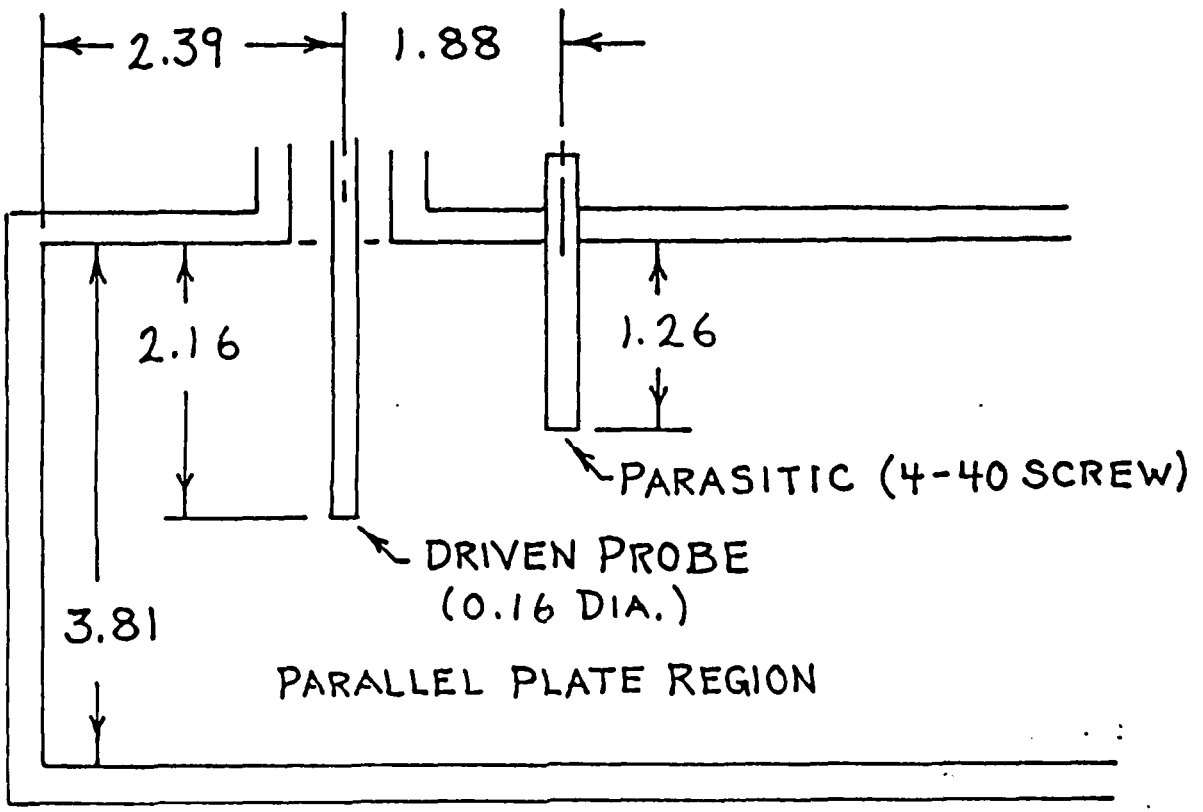

Figure IV-2 - Diagram of lens probe assembly

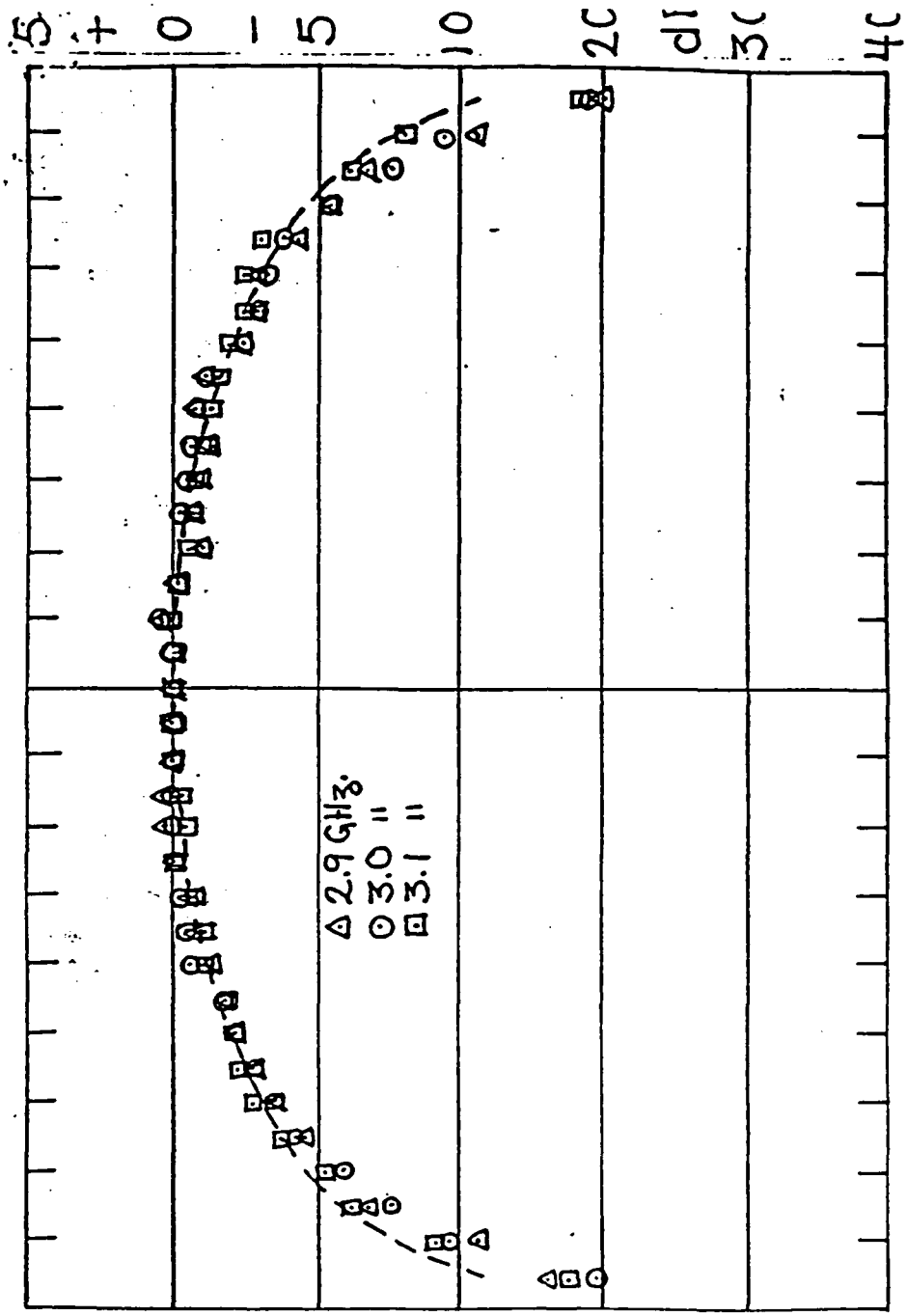

Figure IV-3 Radiation patterns of lens probe assembly 2.9 to 3.1 GHz. --- cos θ power pattern.

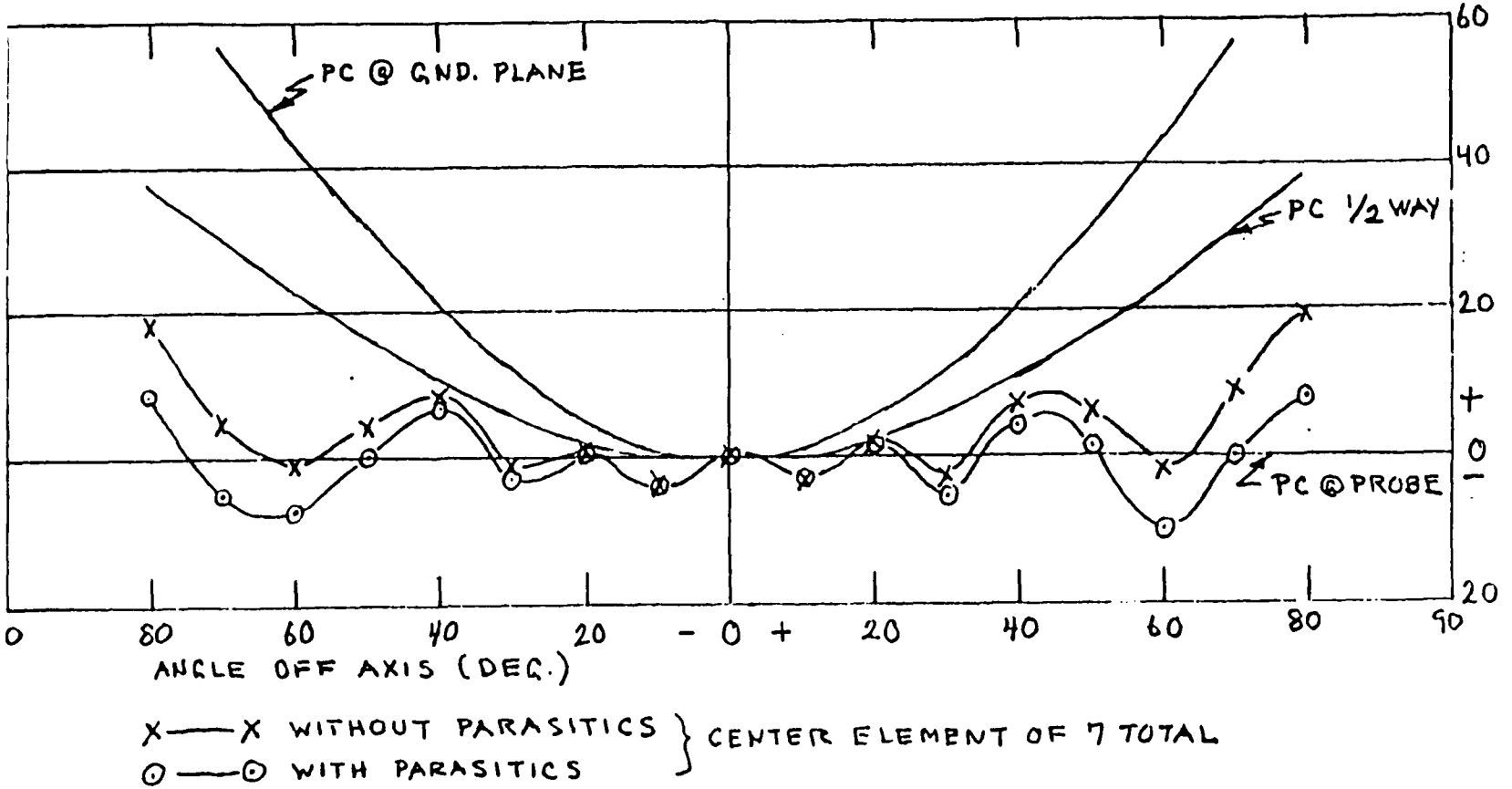
PC @ GND. PLANE
PC 1/2 WAY
PC @ PROBE
60
40
20
+
0
-
20
0
80
60
40
20
- 0 +
20
40
60
80
90
ANGLE OFF AXIS (DEG.)
X—X WITHOUT PARASITICS
O—O WITH PARASITICS
CENTER ELEMENT OF 7 TOTAL

Figure IV-4

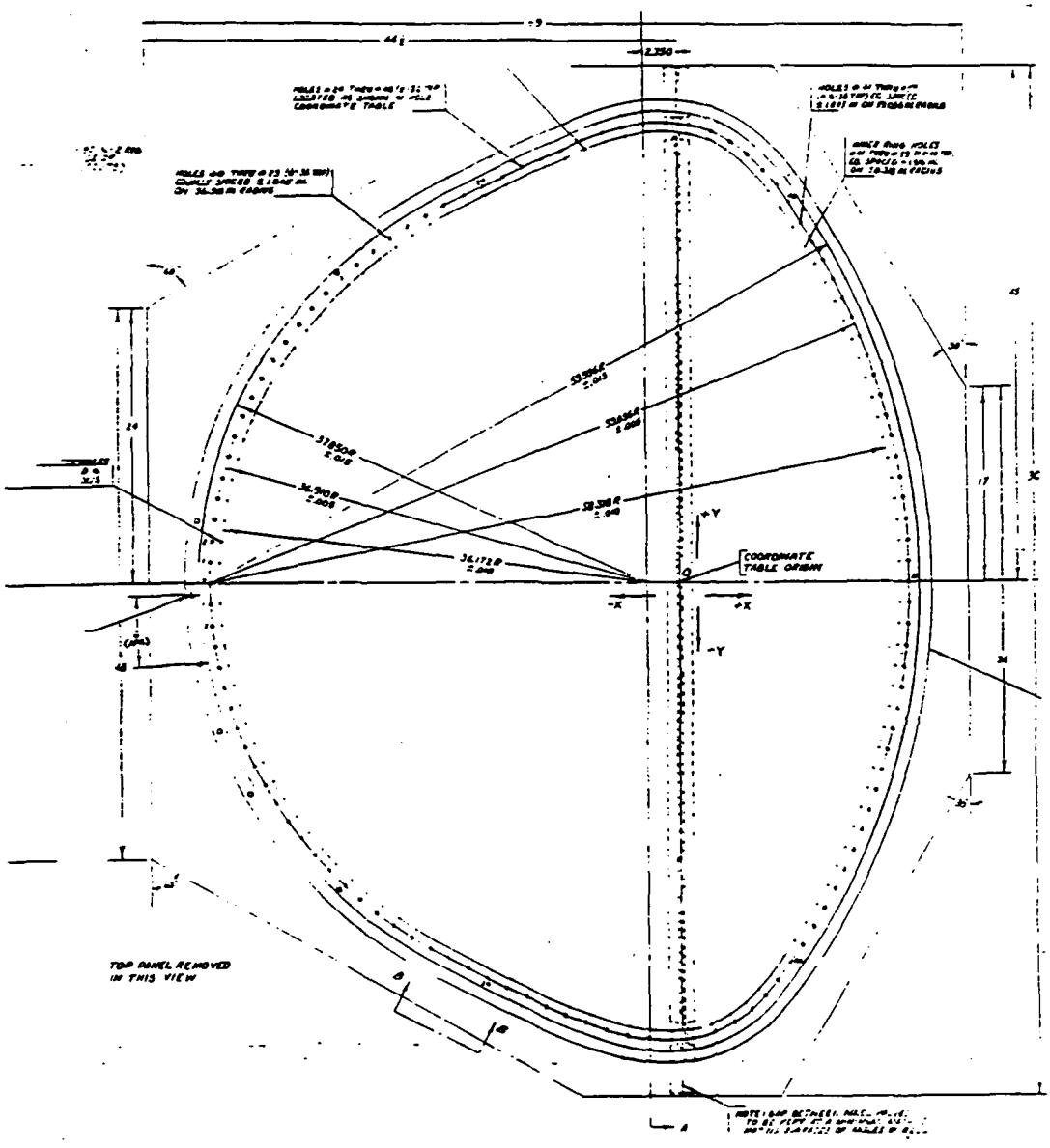

Figure IV-5

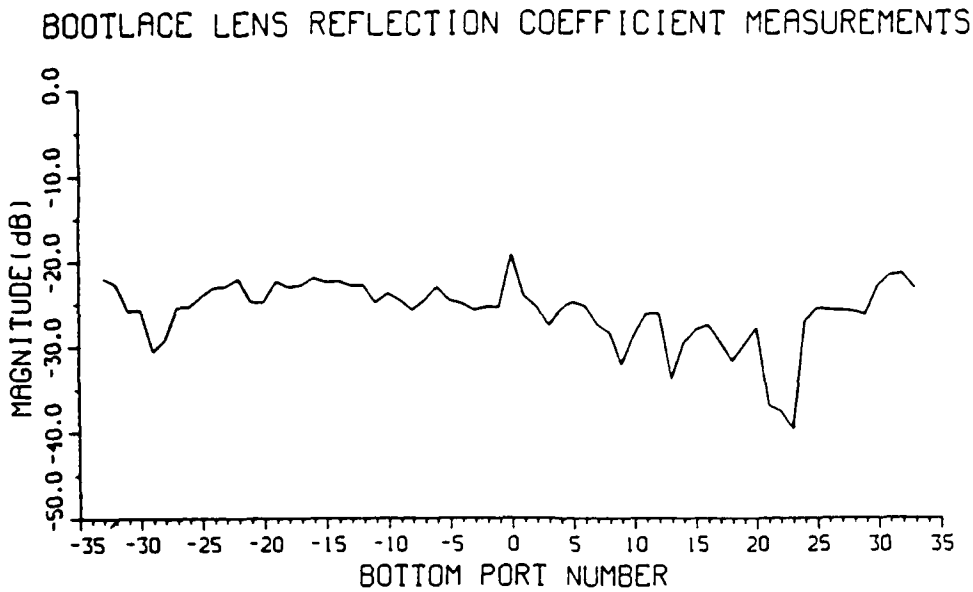

FREQ: 3.20000 GHz

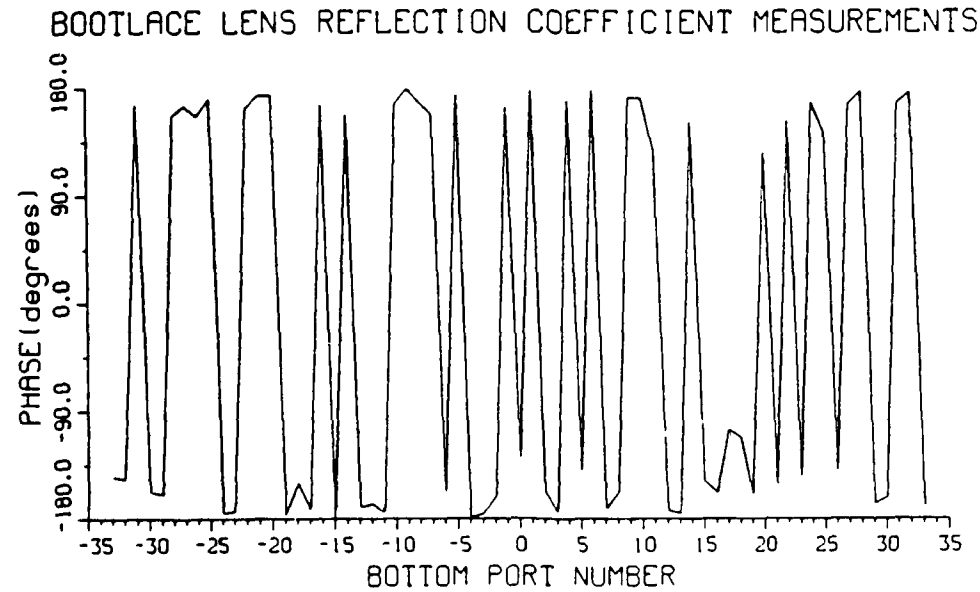

Figure V-1

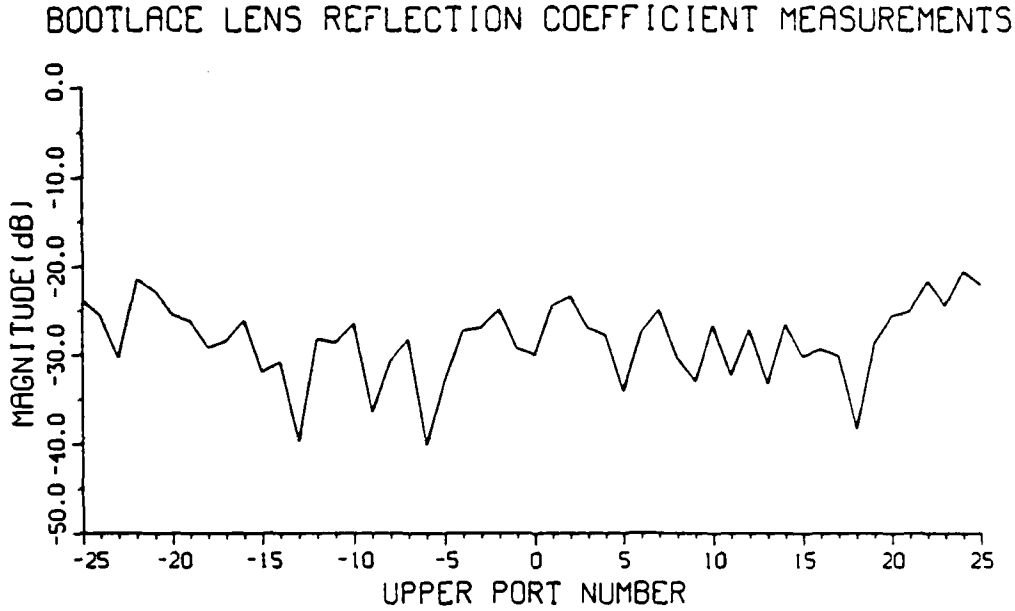

FREQ: 3.20000 GHz

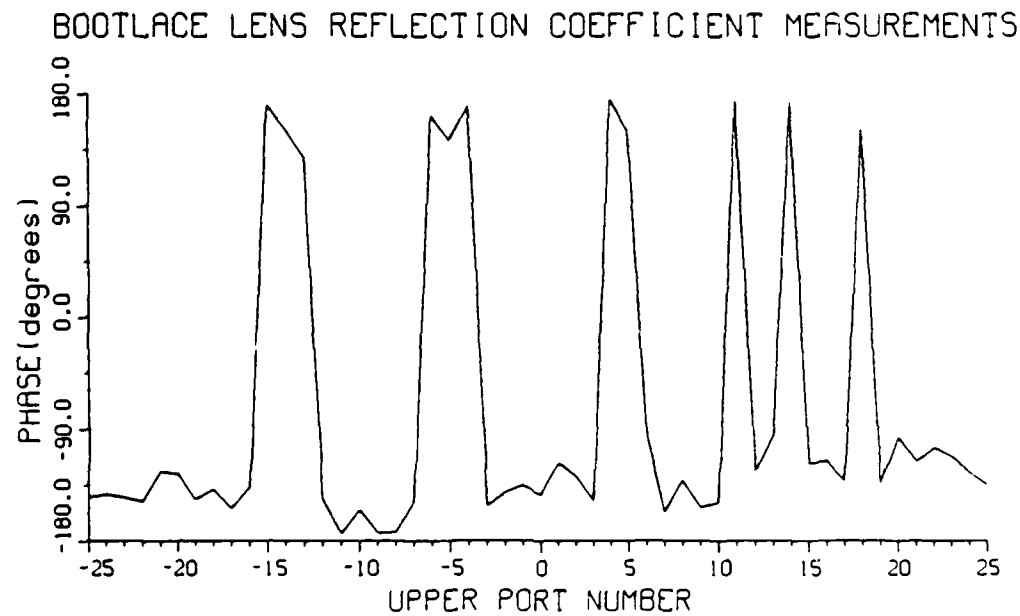

Figure V-2

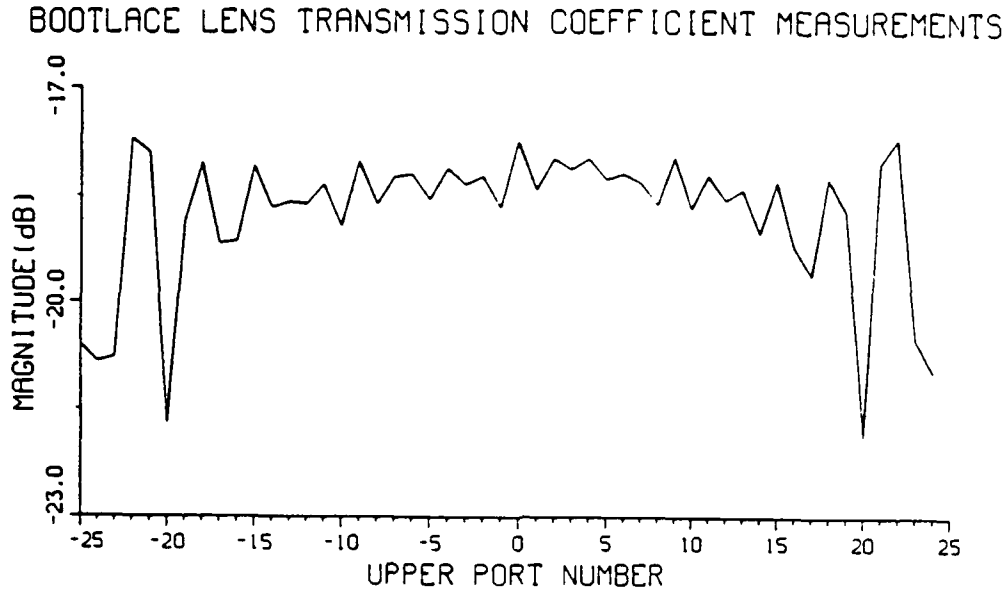
BOOTLACE LENS TRANSMISSION COEFFICIENT MEASUREMENTS
MAGNITUDE(dB)
-17.0
-20.0
-23.0
-25 -20 -15 -10 -5 0 5 10 15 20 25
UPPER PORT NUMBER
FREQ: 3.20000 GHz
PORT NUMBER:
BOTTOM:0

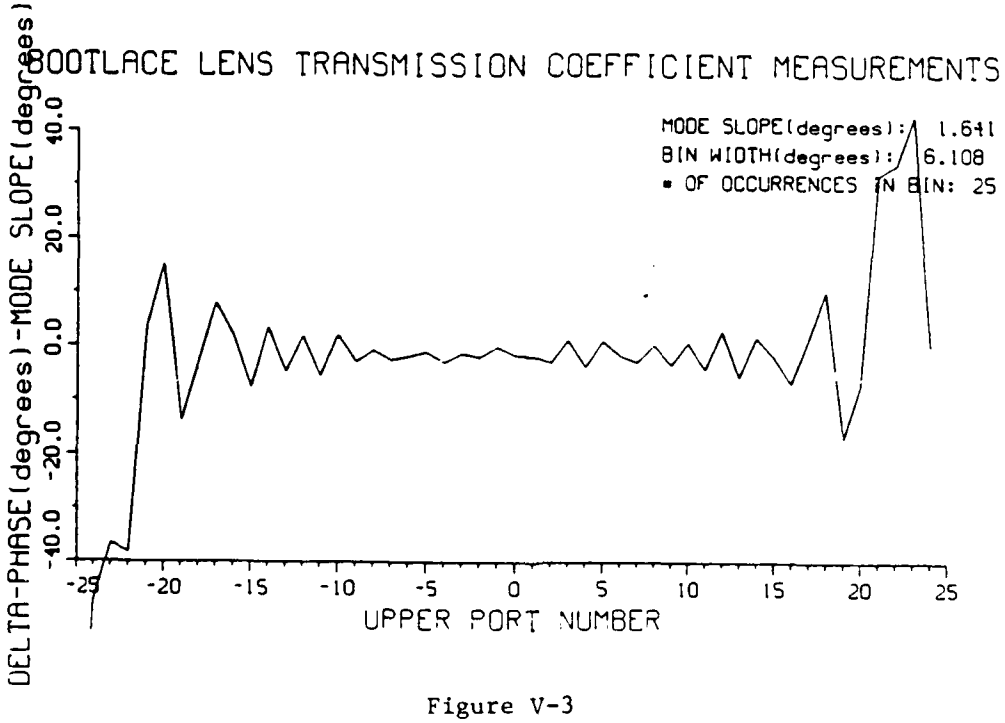
BOOTLACE LENS TRANSMISSION COEFFICIENT MEASUREMENTS
MODE SLOPE(degrees): 1.641
BIN WIDTH(degrees): 6.108
OF OCCURRENCES IN BIN: 25
DELTA-PHASE(degrees)-MODE SLOPE(degrees)
40.0
20.0
0.0
-20.0
-40.0
-25 -20 -15 -10 -5 0 5 10 15 20 25
UPPER PORT NUMBER

Figure V-3

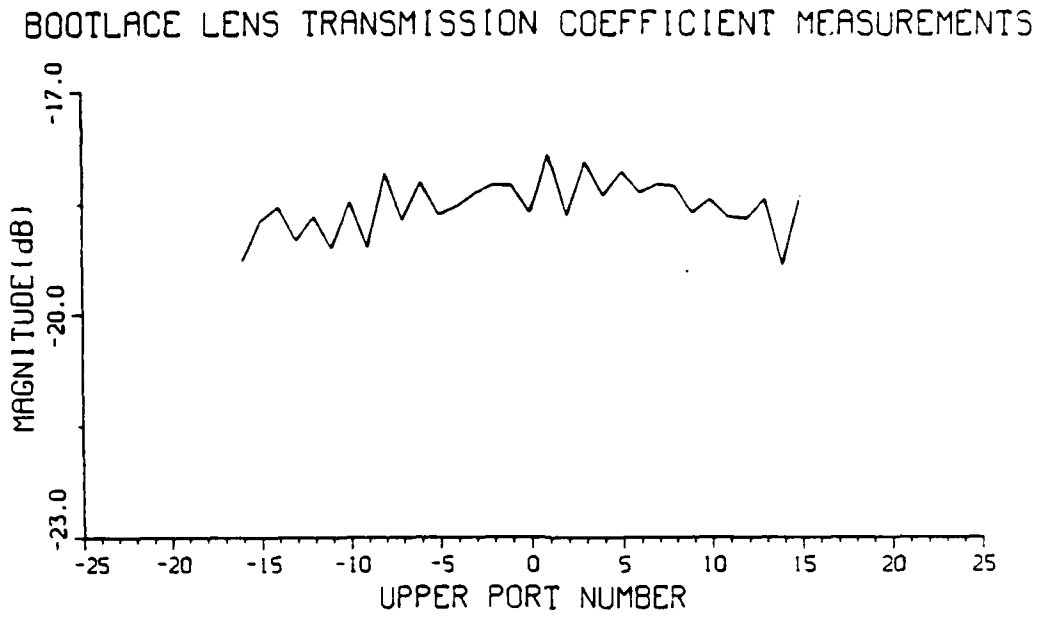
BOOTLACE LENS TRANSMISSION COEFFICIENT MEASUREMENTS
MAGNITUDE(dB)
-17.0
-20.0
-23.0
-25
-20
-15
-10
-5
0
5
10
15
20
25
UPPER PORT NUMBER
FREQ: 3.20000 GHz
PORT NUMBER:
BOTTOM: -1

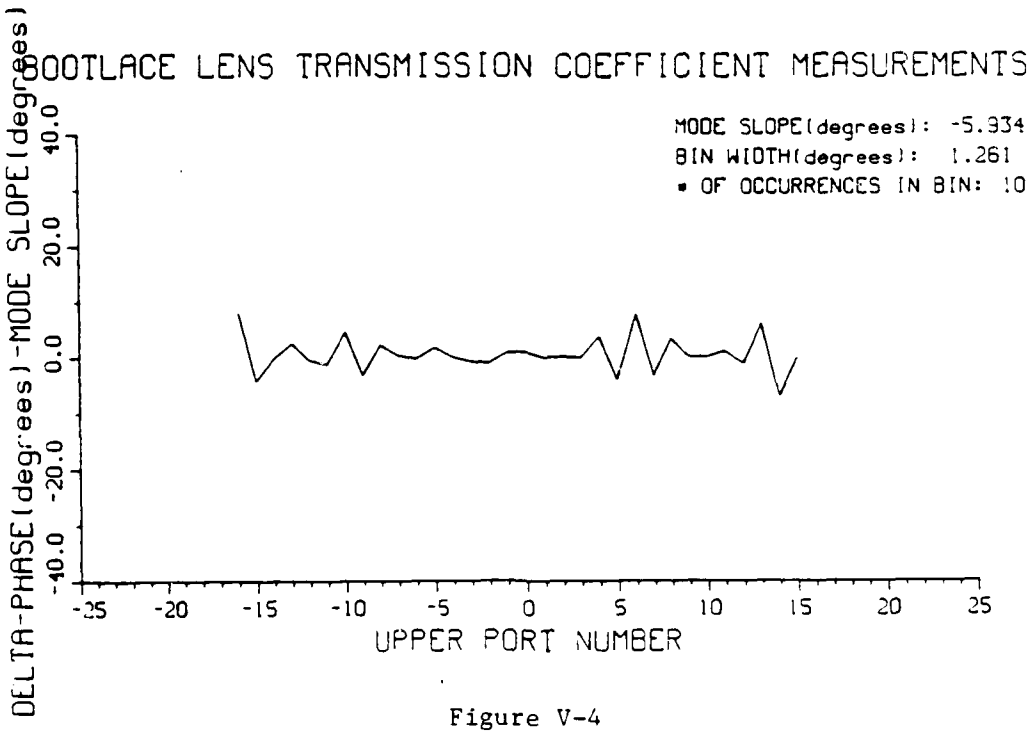
BOOTLACE LENS TRANSMISSION COEFFICIENT MEASUREMENTS
MODE SLOPE(degrees): -5.334
BIN WIDTH(degrees): 1.261
OF OCCURRENCES IN BIN: 10
DELTA-PHASE(degrees)-MODE SLOPE(degrees)
40.0
20.0
0.0
-20.0
-40.0
-25
-20
-15
-10
-5
0
5
10
15
20
25
UPPER PORT NUMBER

Figure V-4

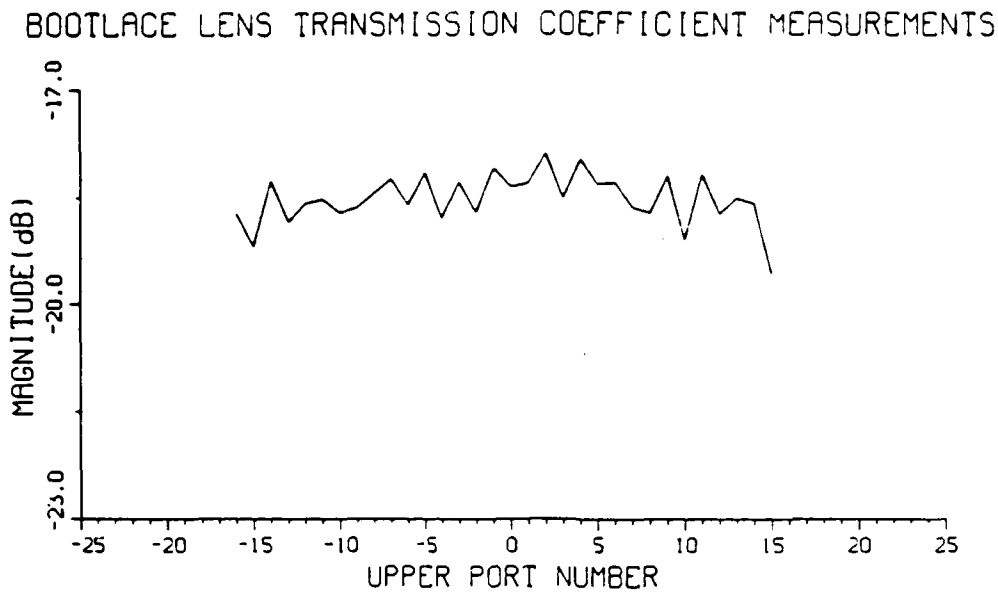
BOOTLACE LENS TRANSMISSION COEFFICIENT MEASUREMENTS
MAGNITUDE(dB)
-17.0
-20.0
-23.0
-25 -20 -15 -10 -5 0 5 10 15 20 25
UPPER PORT NUMBER
FREQ: 3.20000 GHz
PORT NUMBER:
BOTTOM: -2

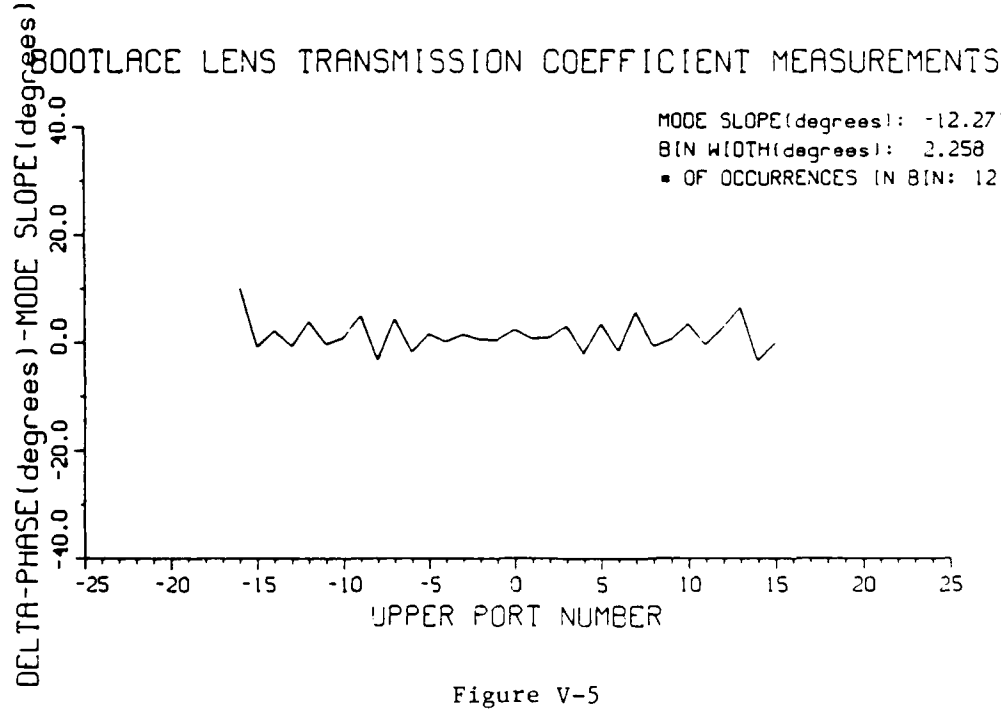
BOOTLACE LENS TRANSMISSION COEFFICIENT MEASUREMENTS
MODE SLOPE(degrees): -12.271
BIN WIDTH(degrees): 2.258
OF OCCURRENCES IN BIN: 12
DELTA-PHASE(degrees)-MODE SLOPE(degrees)
40.0
20.0
0.0
-20.0
-40.0
-25 -20 -15 -10 -5 0 5 10 15 20 25
UPPER PORT NUMBER

Figure V-5

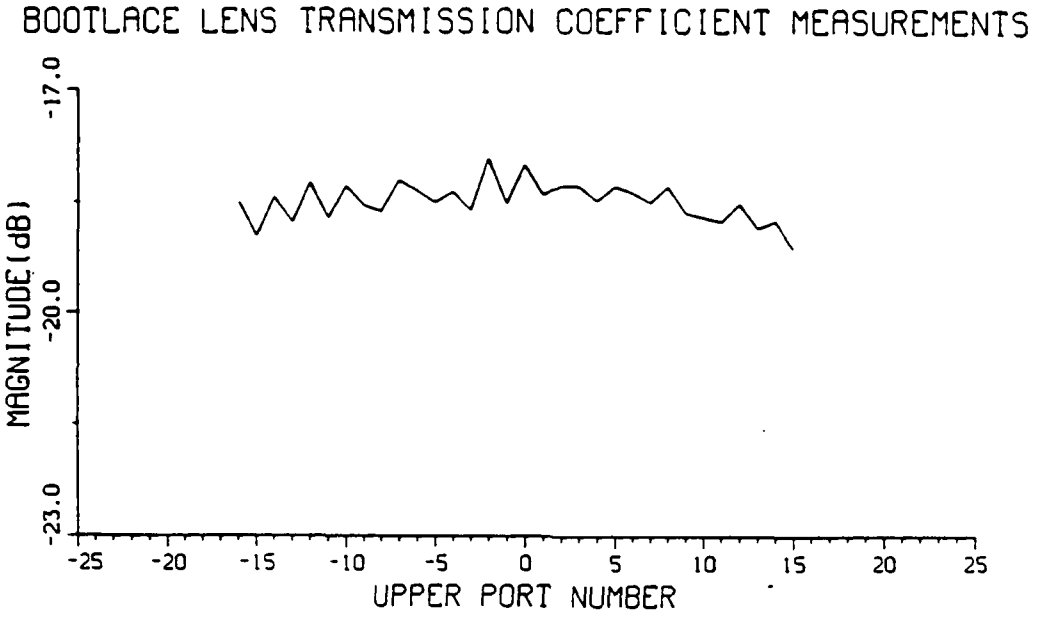
BOOTLACE LENS TRANSMISSION COEFFICIENT MEASUREMENTS
MAGNITUDE(dB)
-17.0
-20.0
-23.0
-25
-20
-15
-10
-5
0
5
10
15
20
25
UPPER PORT NUMBER
FREQ: 3.20000 GHz
PORT NUMBER:
BOTTOM: -3

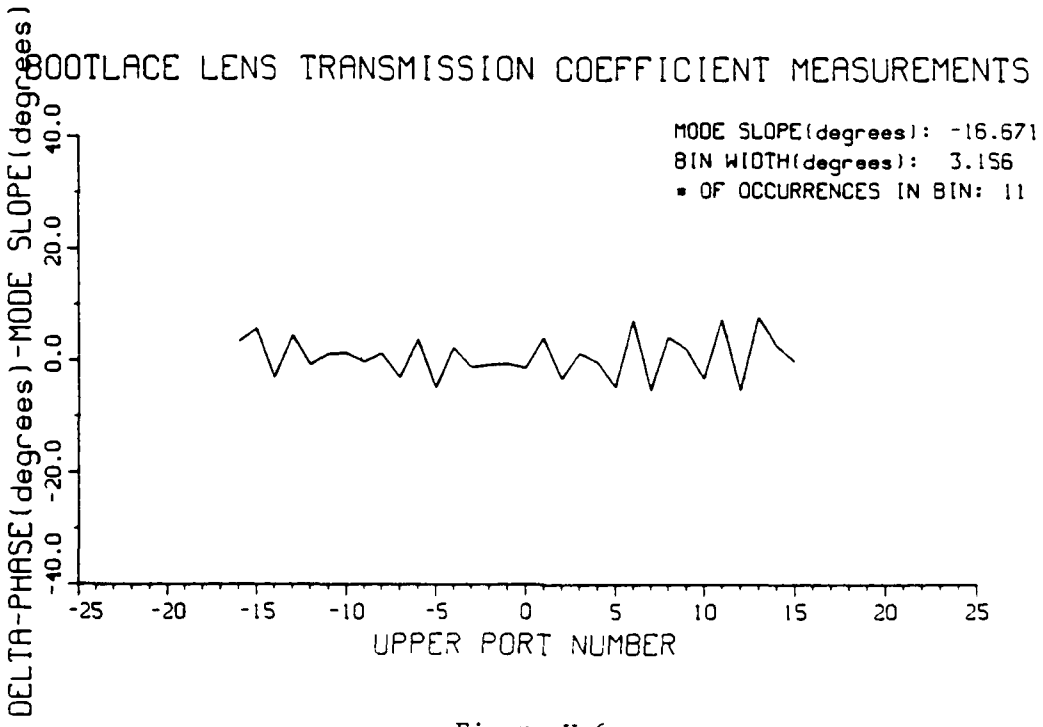
BOOTLACE LENS TRANSMISSION COEFFICIENT MEASUREMENTS
MODE SLOPE(degrees): -16.671
BIN WIDTH(degrees): 3.156
OF OCCURRENCES IN BIN: 11
DELTA-PHASE(degrees)-MODE SLOPE(degrees)
40.0
20.0
0.0
-20.0
-40.0
-25
-20
-15
-10
-5
0
5
10
15
20
25
UPPER PORT NUMBER

Figure V-6

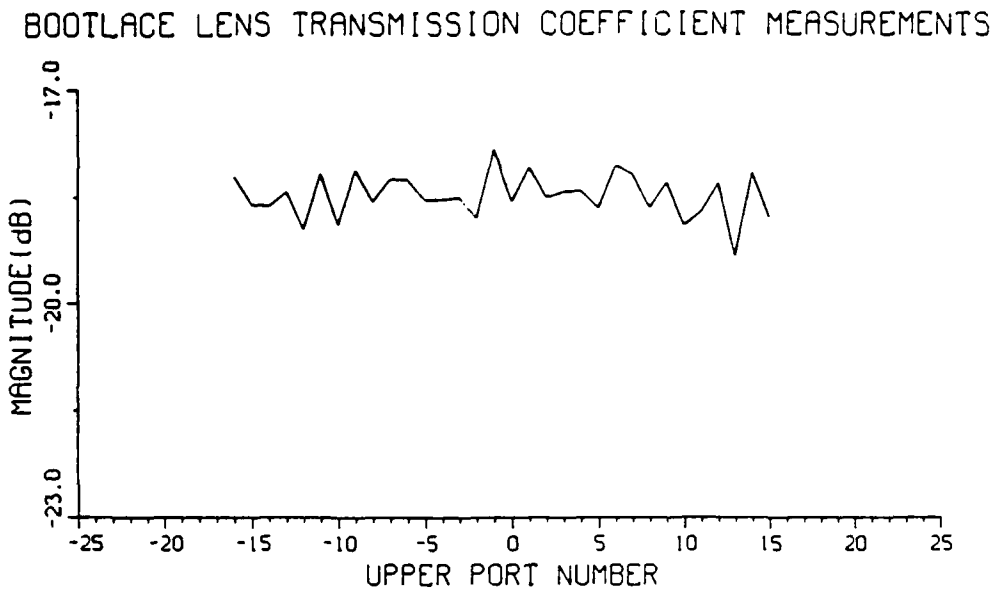
BOOTLACE LENS TRANSMISSION COEFFICIENT MEASUREMENTS
MAGNITUDE(dB)
-17.0
-20.0
-23.0
-25
-20
-15
-10
-5
0
5
10
15
20
25
UPPER PORT NUMBER
FREQ: 3.20000 GHz
PORT NUMBER:
BOTTOM: -4

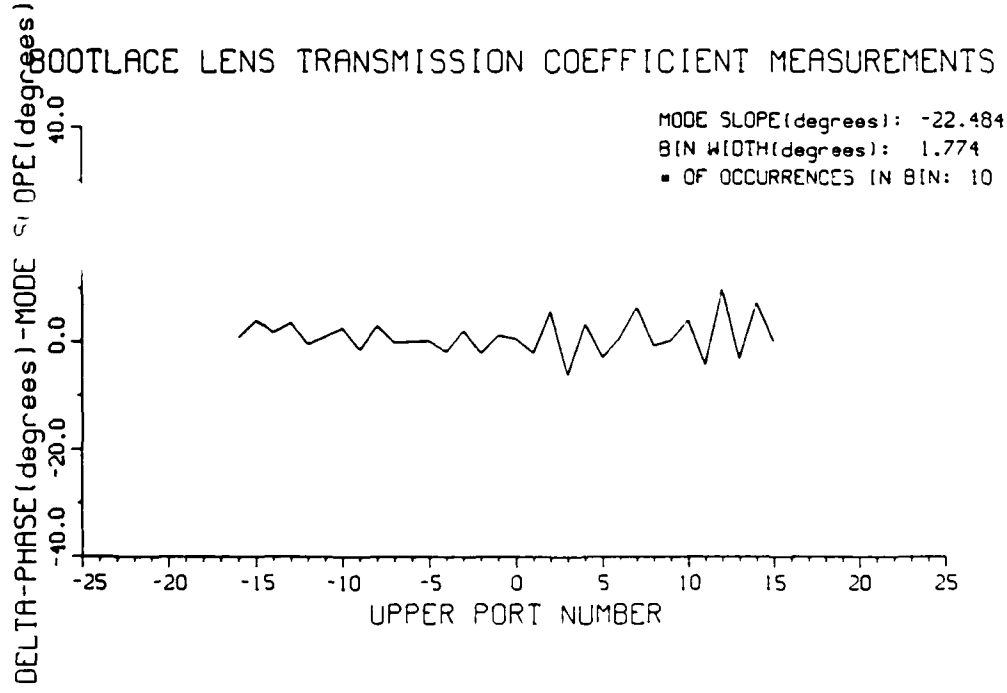
BOOTLACE LENS TRANSMISSION COEFFICIENT MEASUREMENTS
MODE SLOPE(degrees): -22.484
BIN WIDTH(degrees): 1.774
OF OCCURRENCES IN BIN: 10
DELTA-PHASE(degrees)-MODE SLOPE(degrees)
40.0
0.0
-20.0
-40.0
-25
-20
-15
-10
-5
0
5
10
15
20
25
UPPER PORT NUMBER

Figure V-7

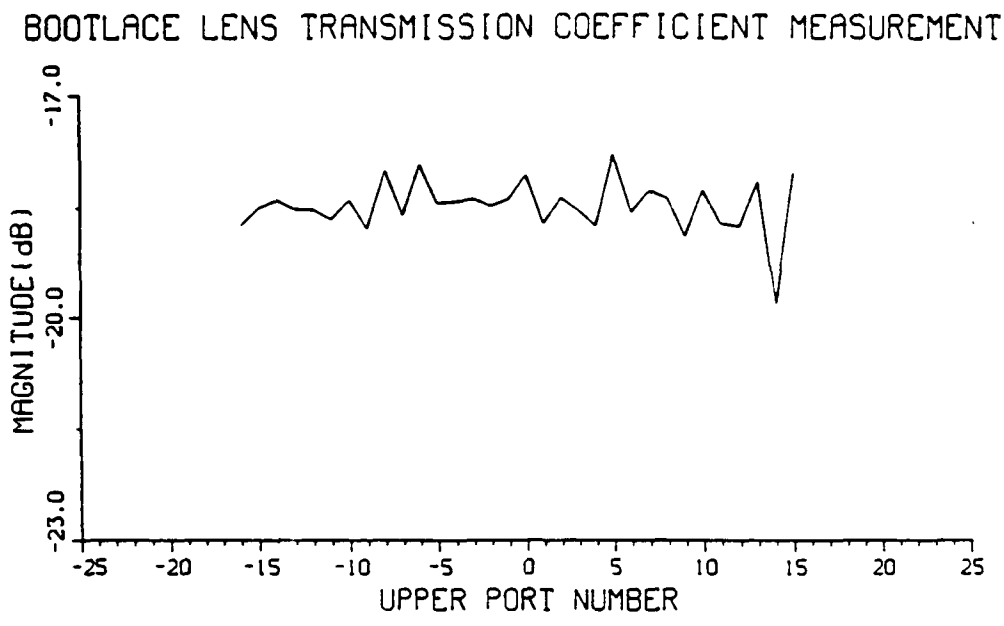
BOOTLACE LENS TRANSMISSION COEFFICIENT MEASUREMENTS
MAGNITUDE(dB)
-17.0
-20.0
-23.0
-25
-20
-15
-10
-5
0
5
10
15
20
25
UPPER PORT NUMBER
FREQ: 3.20000 GHz
PORT NUMBER:
BOTTOM: -5

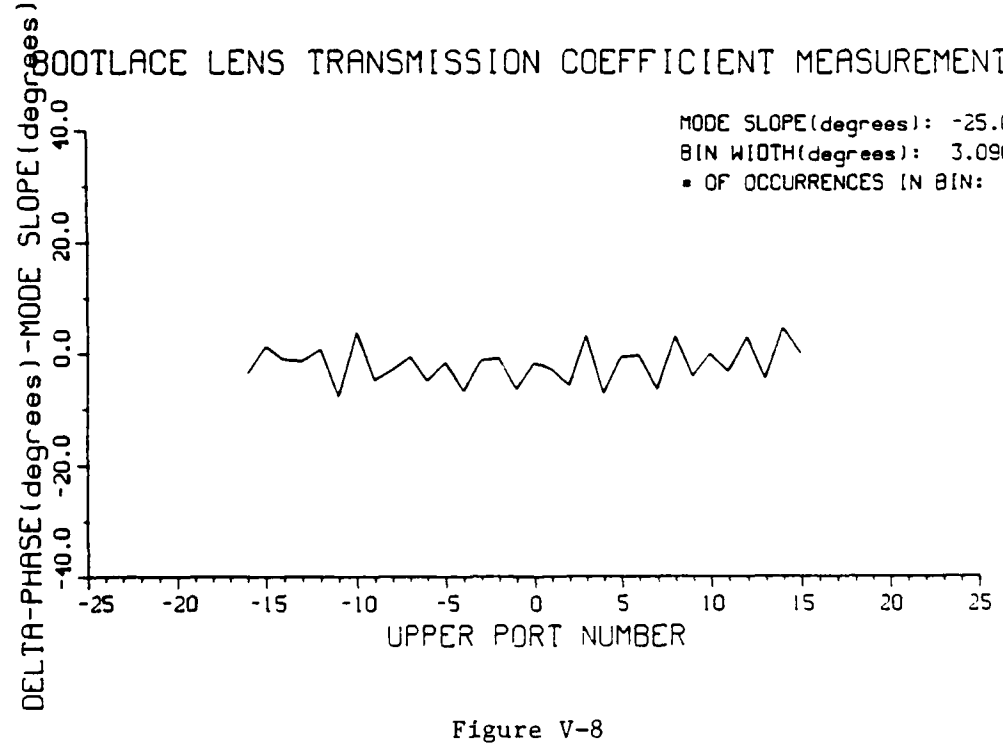
BOOTLACE LENS TRANSMISSION COEFFICIENT MEASUREMENTS
MODE SLOPE(degrees): -25.051
BIN WIDTH(degrees): 3.090
OF OCCURRENCES IN BIN: 10
DELTA-PHASE(degrees)-MODE SLOPE(degrees)
40.0
20.0
0.0
-20.0
-40.0
-25
-20
-15
-10
-5
0
5
10
15
20
25
UPPER PORT NUMBER

Figure V-8

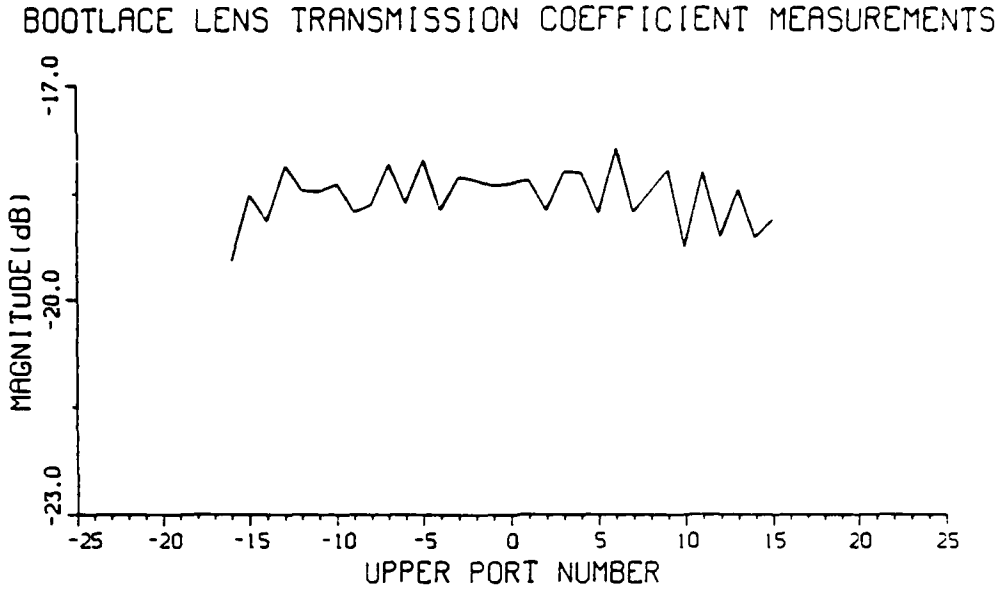
BOOTLACE LENS TRANSMISSION COEFFICIENT MEASUREMENTS
MAGNITUDE(dB)
-17.0
-20.0
-23.0
-25
-20
-15
-10
-5
0
5
10
15
20
25
UPPER PORT NUMBER
FREQ: 3.20000 GHz
PORT NUMBER:
BOTTOM: -6

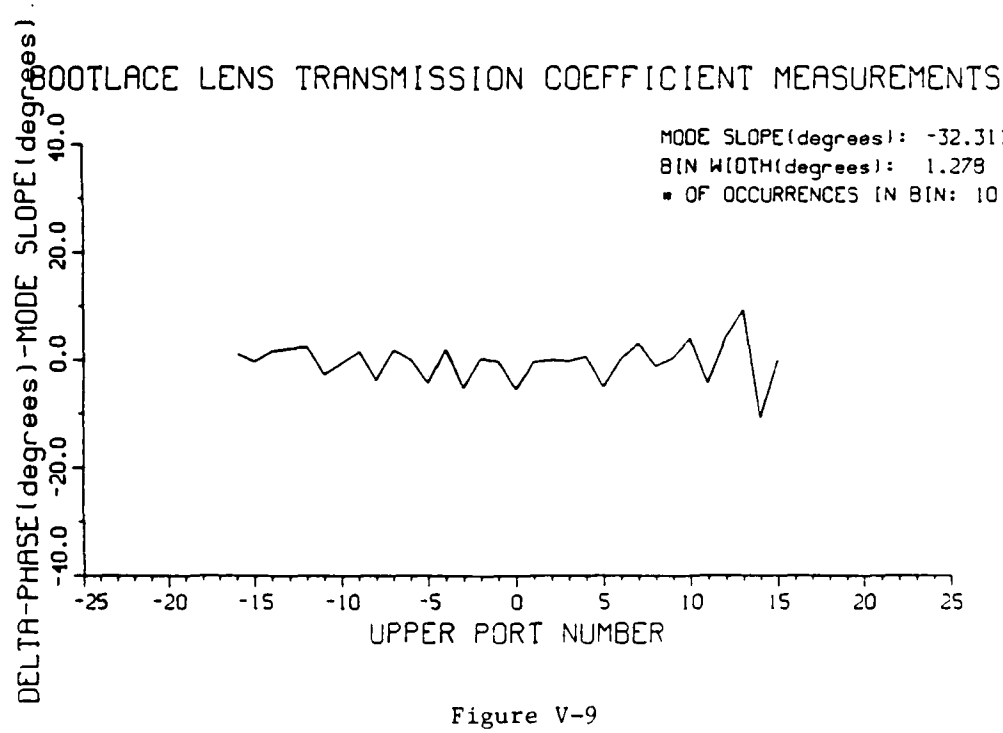
BOOTLACE LENS TRANSMISSION COEFFICIENT MEASUREMENTS
MODE SLOPE(degrees): -32.311
BIN WIDTH(degrees): 1.278
OF OCCURRENCES IN BIN: 10
DELTA-PHASE(degrees)-MODE SLOPE(degrees)
40.0
20.0
0.0
-20.0
-40.0
-25
-20
-15
-10
-5
0
5
10
15
20
25
UPPER PORT NUMBER

Figure V-9

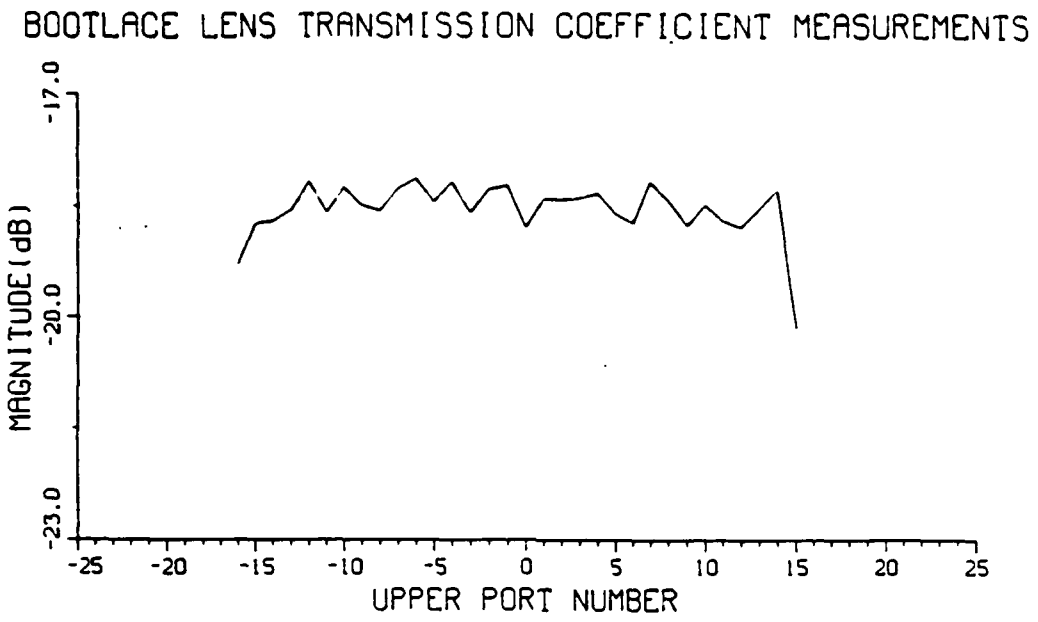
BOOTLACE LENS TRANSMISSION COEFFICIENT MEASUREMENTS
MAGNITUDE(dB)
-17.0
-20.0
-23.0
-25
-20
-15
-10
-5
0
5
10
15
20
25
UPPER PORT NUMBER
FREQ: 3.20000 GHz
PORT NUMBER:
BOTTOM: -7

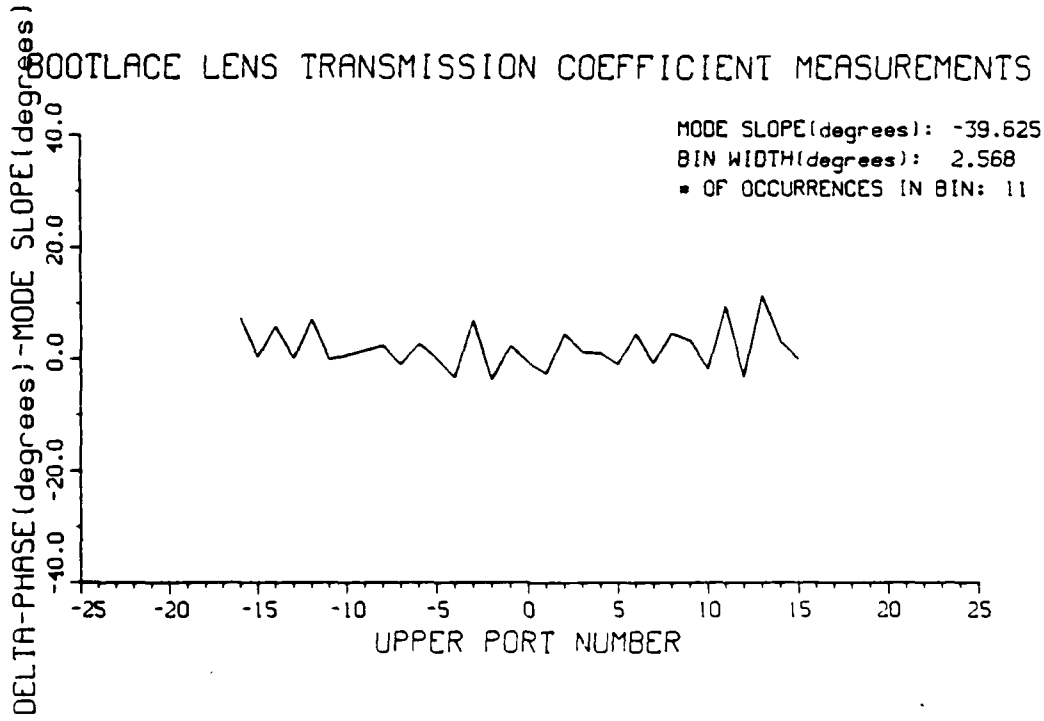
BOOTLACE LENS TRANSMISSION COEFFICIENT MEASUREMENTS
DELTA-PHASE(degrees)-MODE SLOPE(degrees)
MODE SLOPE(degrees): -39.625
BIN WIDTH(degrees): 2.568
OF OCCURRENCES IN BIN: 11
40.0
20.0
0.0
-20.0
-40.0
-25
-20
-15
-10
-5
0
5
10
15
20
25
UPPER PORT NUMBER

Figure V-10

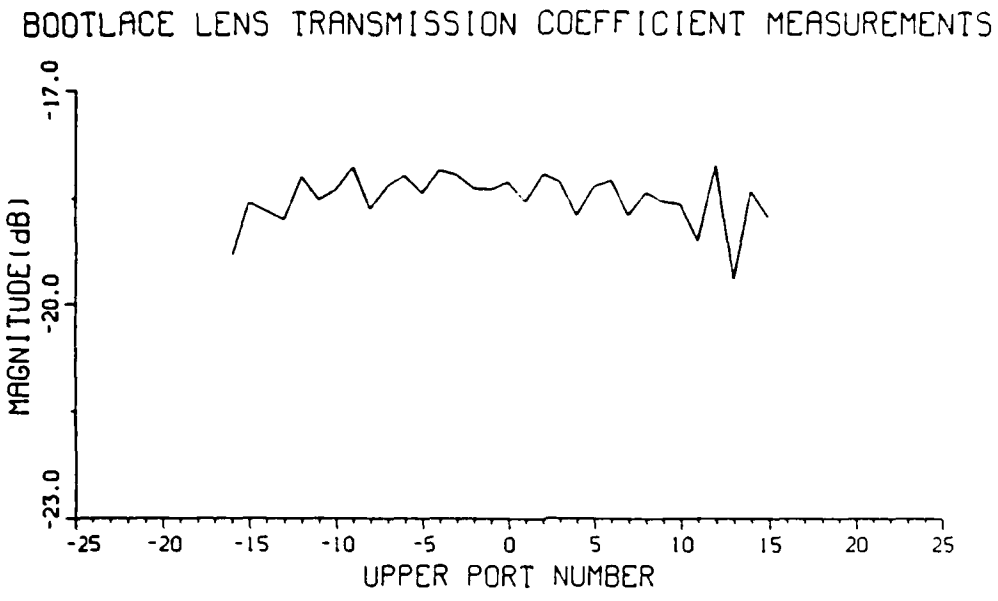
BOOTLACE LENS TRANSMISSION COEFFICIENT MEASUREMENTS
MAGNITUDE(dB)
-17.0
-20.0
-23.0
-25
-20
-15
-10
-5
0
5
10
15
20
25
UPPER PORT NUMBER
FREQ: 3.20000 GHz
PORT NUMBER:
BOTTOM: -8

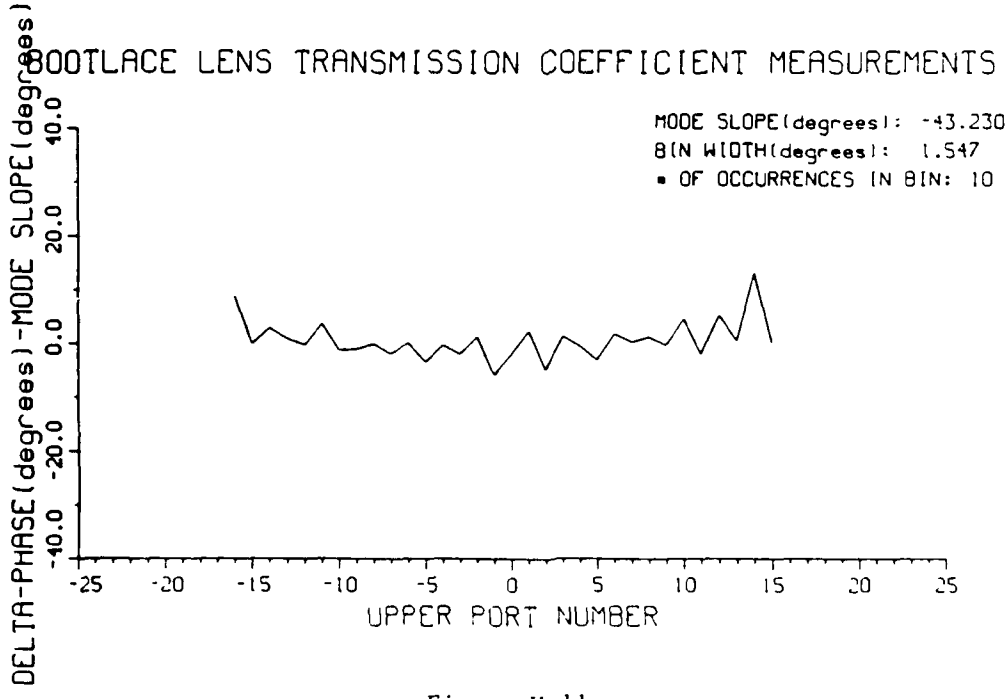
BOOTLACE LENS TRANSMISSION COEFFICIENT MEASUREMENTS
MODE SLOPE(degrees): -43.230
BIN WIDTH(degrees): 1.547
OF OCCURRENCES IN BIN: 10
DELTA-PHASE(degrees)-MODE SLOPE(degrees)
40.0
20.0
0.0
-20.0
-40.0
-25
-20
-15
-10
-5
0
5
10
15
20
25
UPPER PORT NUMBER

Figure V-11

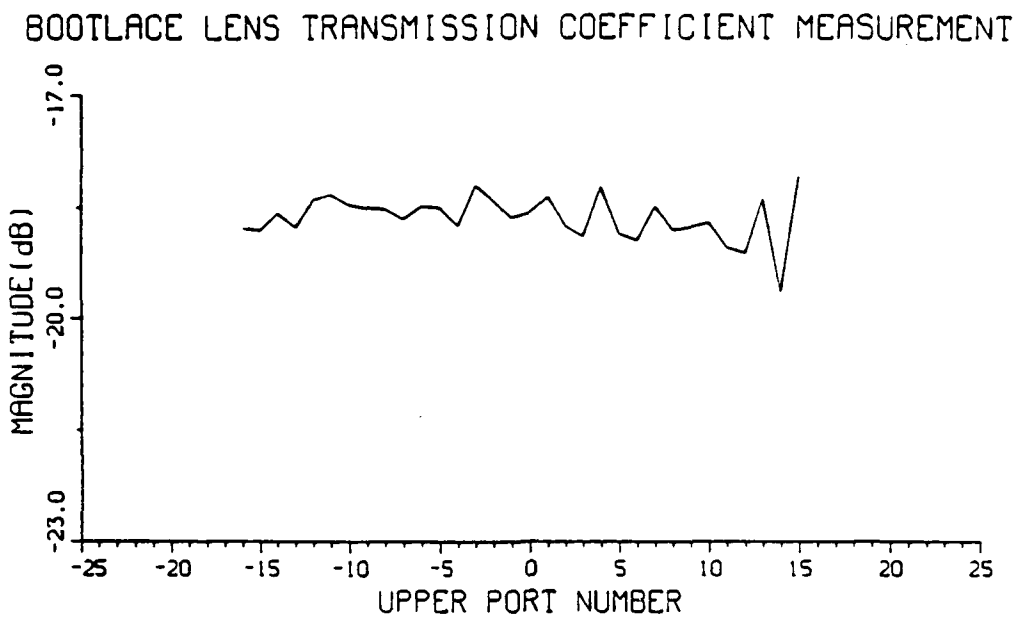
BOOTLACE LENS TRANSMISSION COEFFICIENT MEASUREMENTS
MAGNITUDE(dB)
-17.0
-20.0
-23.0
-25 -20 -15 -10 -5 0 5 10 15 20 25
UPPER PORT NUMBER
FREQ: 3.20000 GHz
PORT NUMBER:
BOTTOM: -9

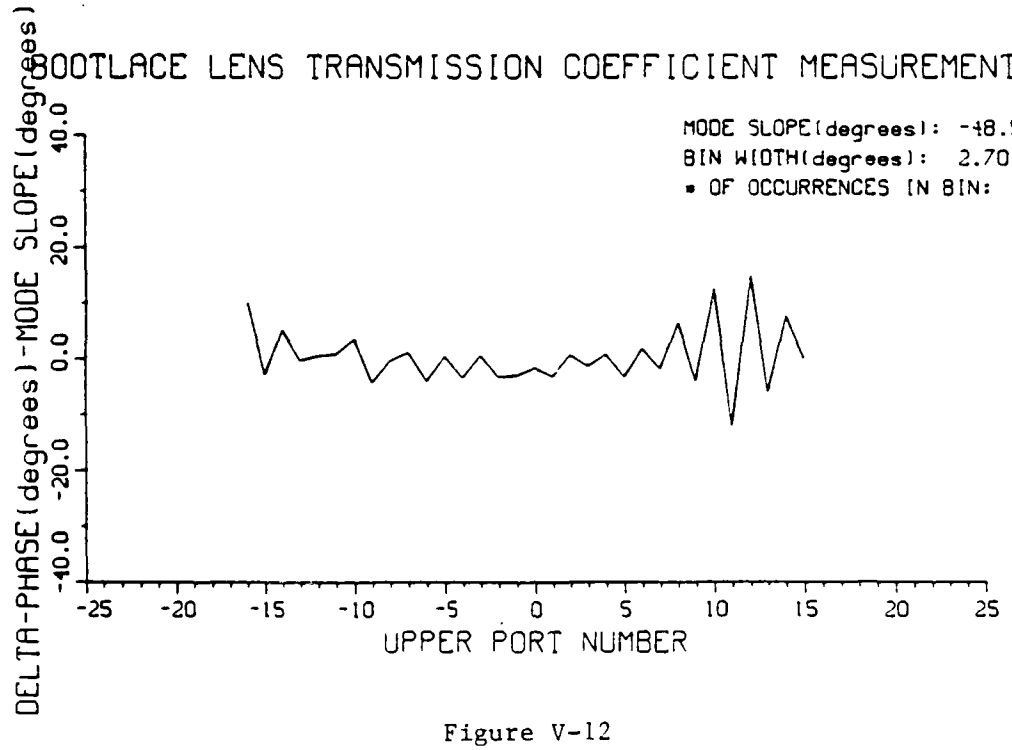
BOOTLACE LENS TRANSMISSION COEFFICIENT MEASUREMENTS
MODE SLOPE(degrees): -48.543
BIN WIDTH(degrees): 2.701
OF OCCURRENCES IN BIN: 10
DELTA-PHASE(degrees)-MODE SLOPE(degrees)
40.0
20.0
0.0
-20.0
-40.0
-25 -20 -15 -10 -5 0 5 10 15 20 25
UPPER PORT NUMBER

Figure V-12

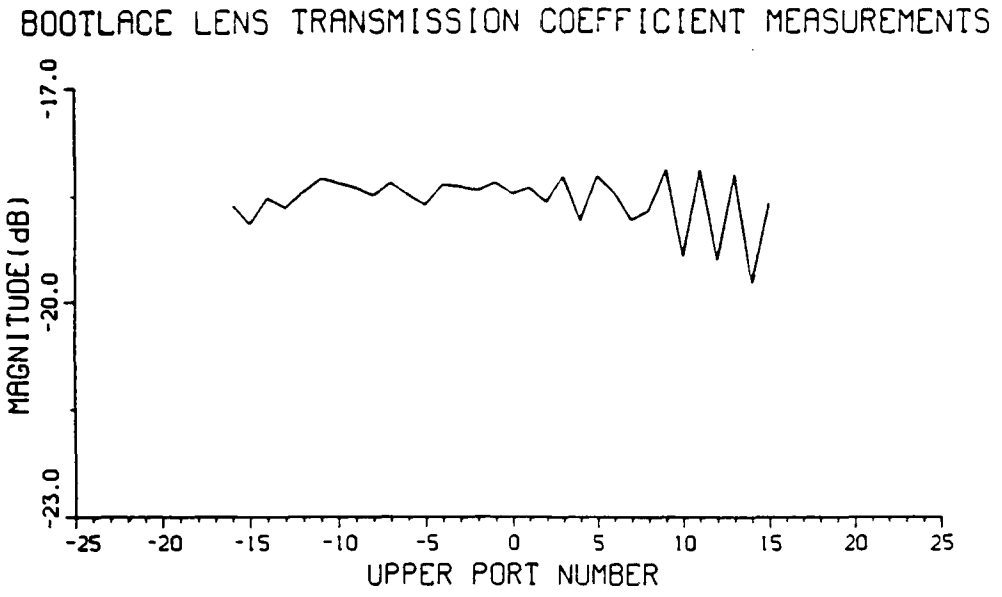
BOOTLACE LENS TRANSMISSION COEFFICIENT MEASUREMENTS
MAGNITUDE(dB)
-17.0
-20.0
-23.0
-25 -20 -15 -10 -5 0 5 10 15 20 25
UPPER PORT NUMBER
FREQ: 3.20000 GHz
PORT NUMBER:
BOTTOM: -10

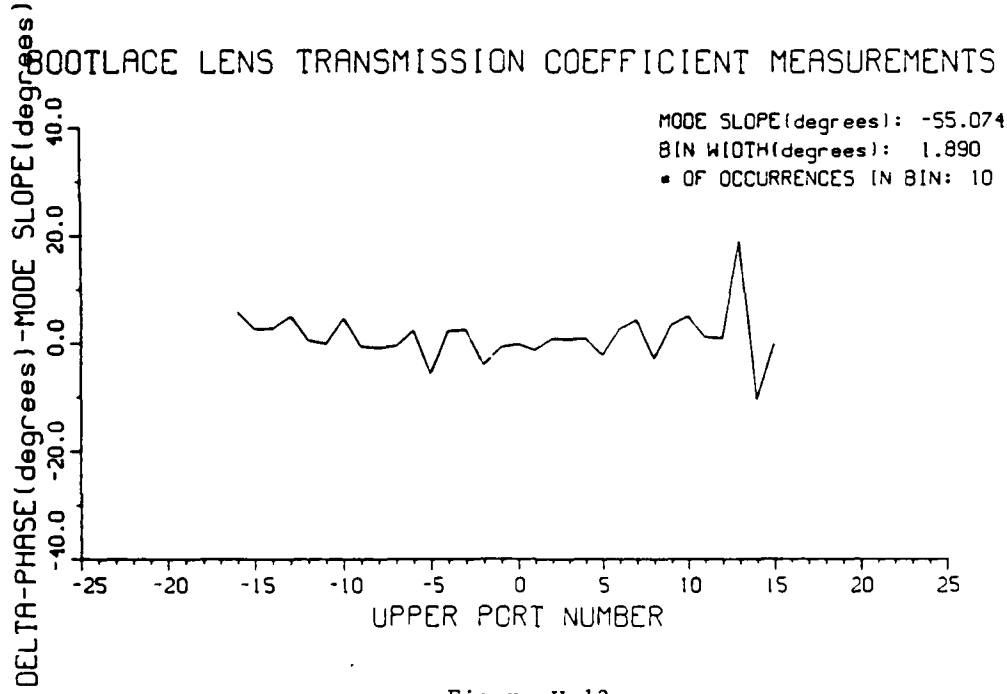
BOOTLACE LENS TRANSMISSION COEFFICIENT MEASUREMENTS
MODE SLOPE(degrees): -55.074
BIN WIDTH(degrees): 1.890
OF OCCURRENCES IN BIN: 10
DELTA-PHASE(degrees)-MODE SLOPE(degrees)
40.0
20.0
0.0
-20.0
-40.0
-25 -20 -15 -10 -5 0 5 10 15 20 25
UPPER PORT NUMBER

Figure V-13

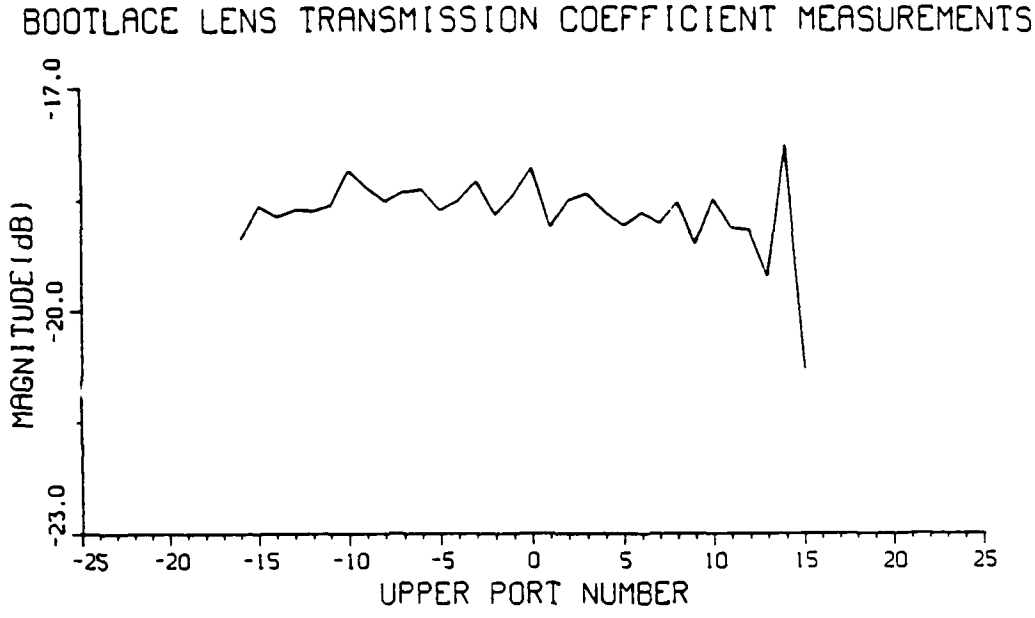
BOOTLACE LENS TRANSMISSION COEFFICIENT MEASUREMENTS
MAGNITUDE(dB)
-17.0
-20.0
-23.0
-25
-20
-15
-10
-5
0
5
10
15
20
25
UPPER PORT NUMBER
FREQ: 3.20000 GHz
PORT NUMBER:
BOTTOM: -11

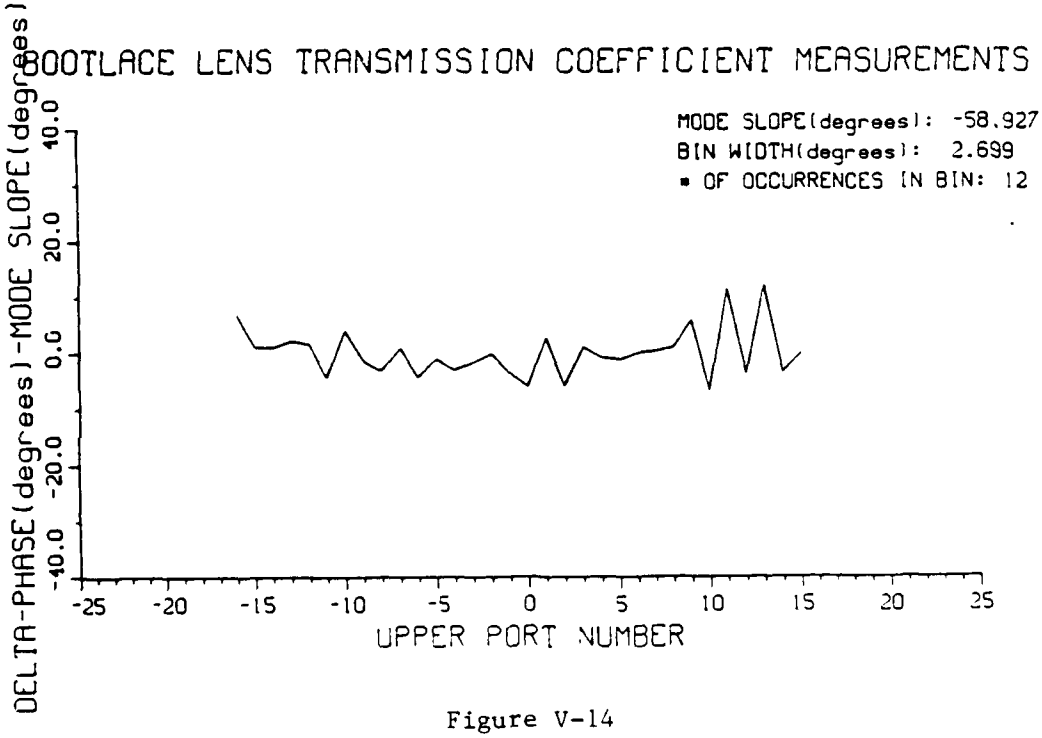
BOOTLACE LENS TRANSMISSION COEFFICIENT MEASUREMENTS
DELTA-PHASE(degrees)-MODE SLOPE(degrees)
MODE SLOPE(degrees): -58.927
BIN WIDTH(degrees): 2.699
OF OCCURRENCES IN BIN: 12
40.0
20.0
0.0
-20.0
-40.0
-25
-20
-15
-10
-5
0
5
10
15
20
25
UPPER PORT NUMBER

Figure V-14

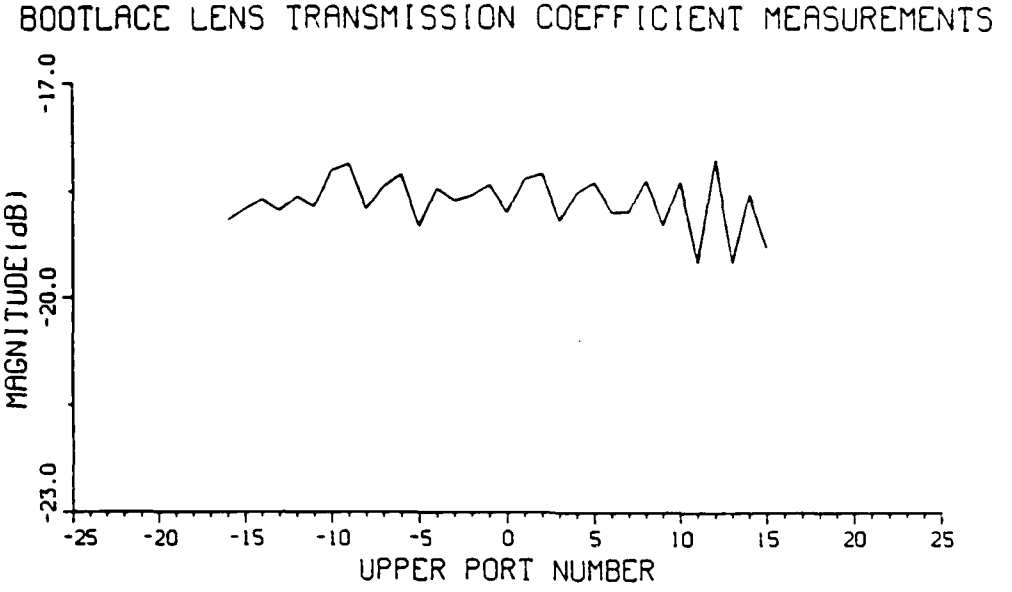
BOOTLACE LENS TRANSMISSION COEFFICIENT MEASUREMENTS
MAGNITUDE(dB)
-17.0
-20.0
-23.0
-25 -20 -15 -10 -5 0 5 10 15 20 25
UPPER PORT NUMBER
FREQ: 3.20000 GHz
PORT NUMBER:
BOTTOM: -12

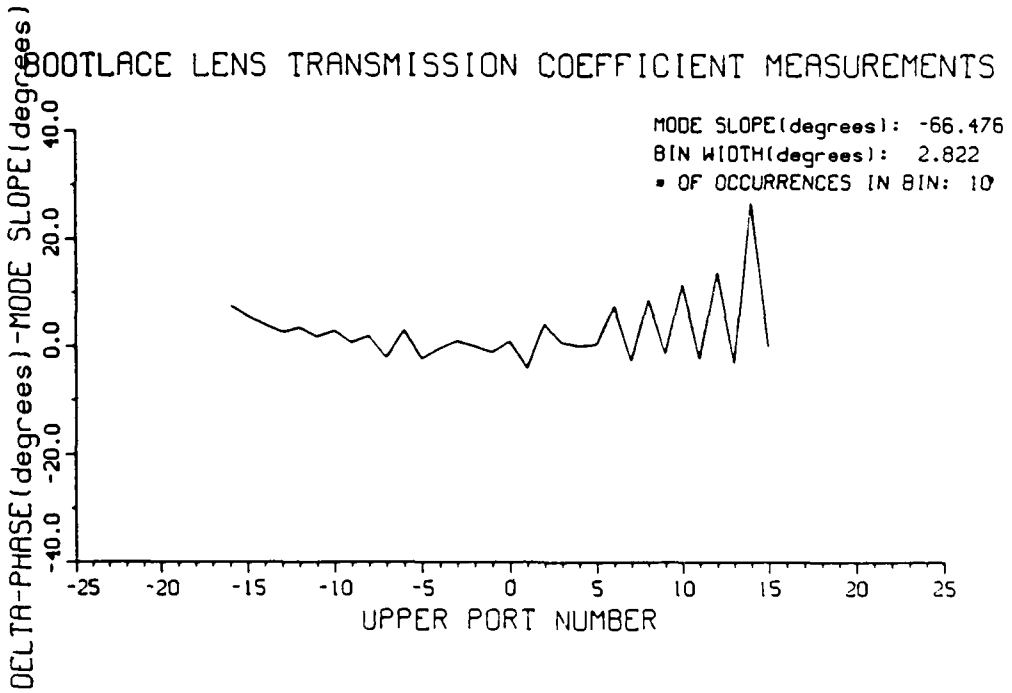
BOOTLACE LENS TRANSMISSION COEFFICIENT MEASUREMENTS
MODE SLOPE(degrees): -66.476
BIN WIDTH(degrees): 2.822
OF OCCURRENCES IN BIN: 10
DELTA-PHASE(degrees)-MODE SLOPE(degrees)
40.0
20.0
0.0
-20.0
-40.0
-25 -20 -15 -10 -5 0 5 10 15 20 25
UPPER PORT NUMBER

Figure V-15

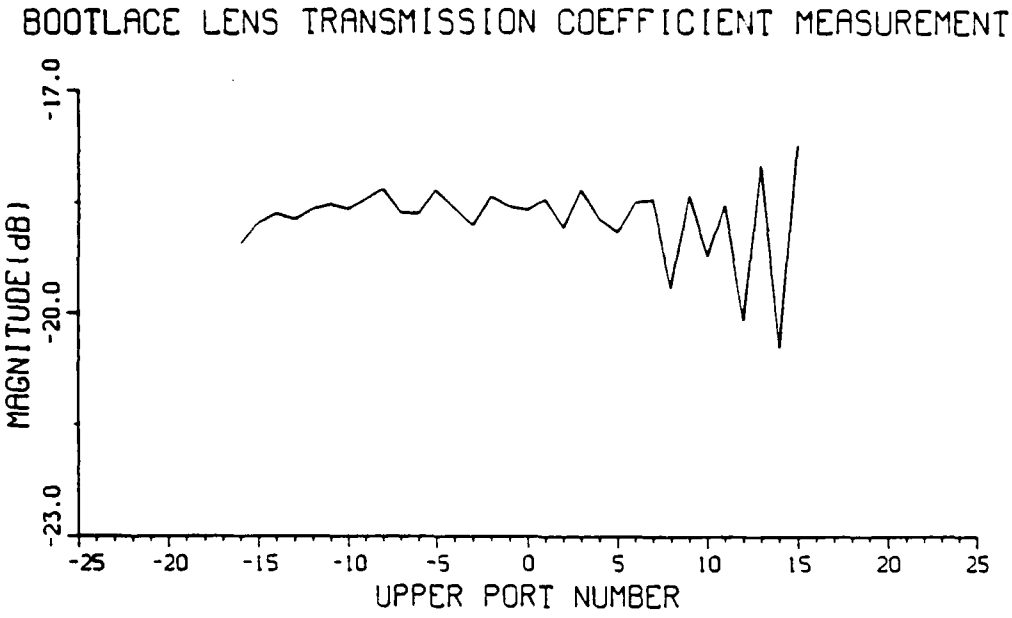
BOOTLACE LENS TRANSMISSION COEFFICIENT MEASUREMENTS
MAGNITUDE(dB)
-17.0
-20.0
-23.0
-25
-20
-15
-10
-5
0
5
10
15
20
25
UPPER PORT NUMBER
FREQ: 3.20000 GHz
PORT NUMBER:
BOTTOM: -13

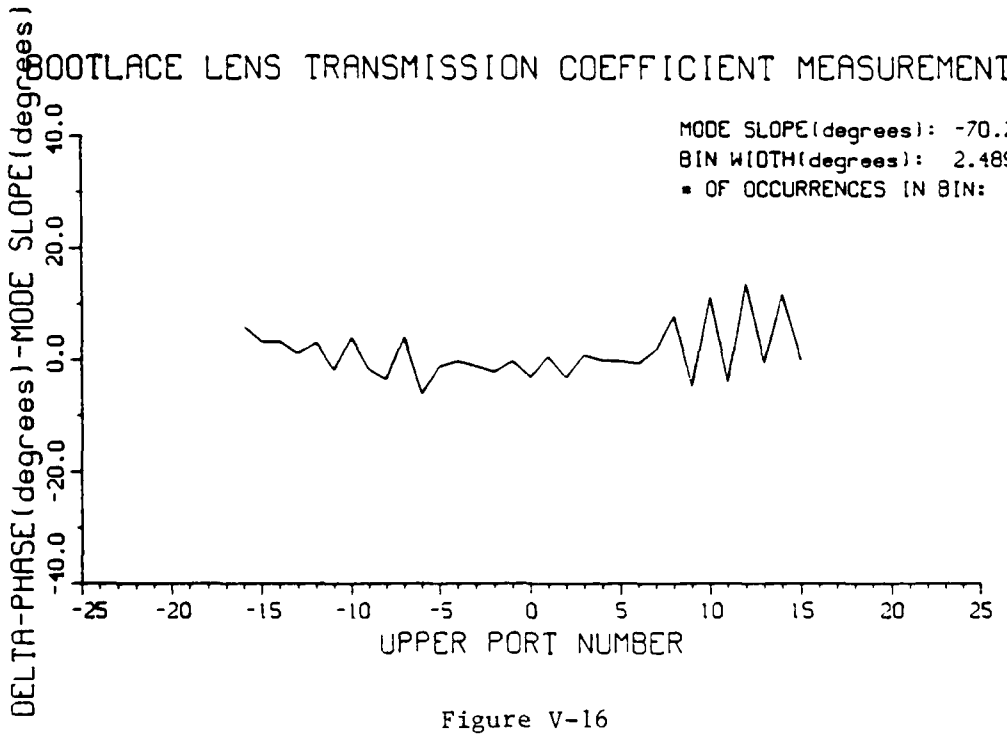
BOOTLACE LENS TRANSMISSION COEFFICIENT MEASUREMENTS
MODE SLOPE(degrees): -70.252
BIN WIDTH(degrees): 2.489
OF OCCURRENCES IN BIN: 11
DELTA-PHASE(degrees)-MODE SLOPE(degrees)
40.0
20.0
0.0
-20.0
-40.0
-25
-20
-15
-10
-5
0
5
10
15
20
25
UPPER PORT NUMBER

Figure V-16

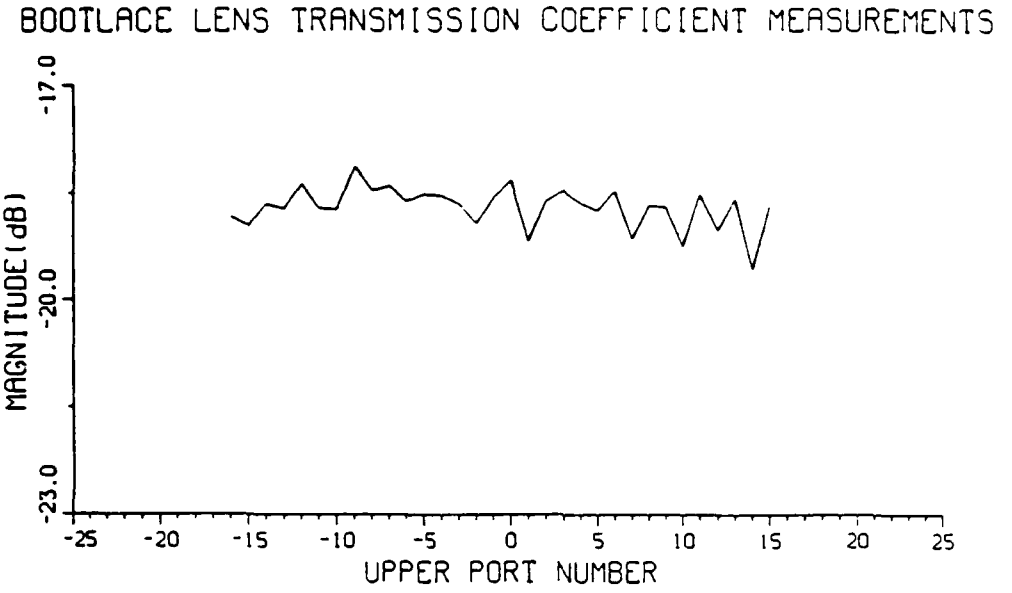
BOOTLACE LENS TRANSMISSION COEFFICIENT MEASUREMENTS
MAGNITUDE(dB)
-17.0
-20.0
-23.0
-25 -20 -15 -10 -5 0 5 10 15 20 25
UPPER PORT NUMBER
FREQ: 3.20000 GHz
PORT NUMBER:
BOTTOM: -14

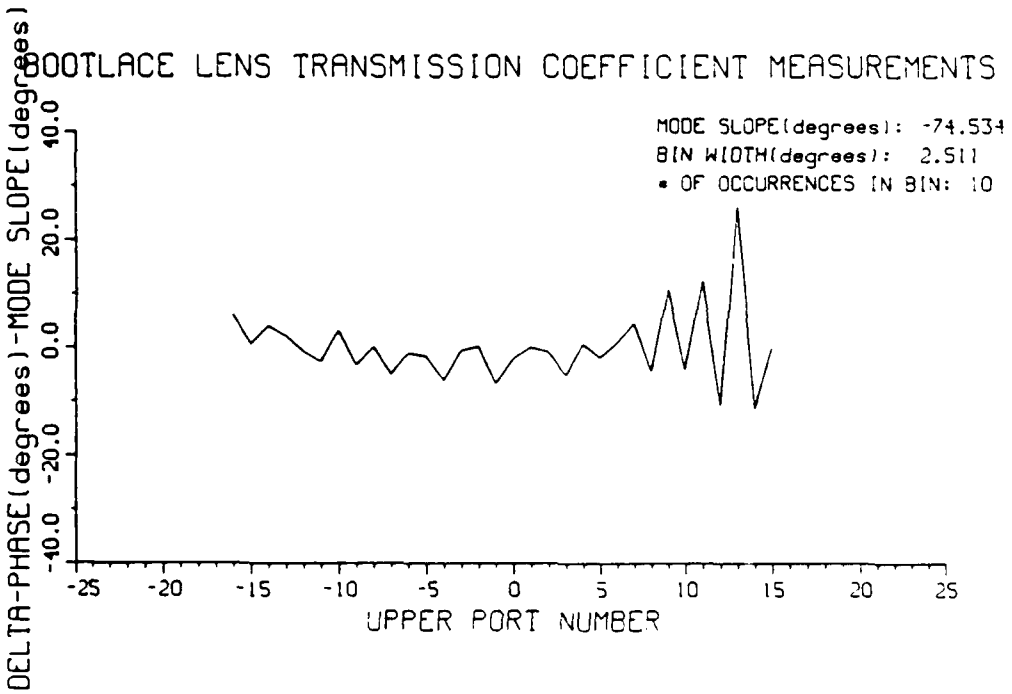
BOOTLACE LENS TRANSMISSION COEFFICIENT MEASUREMENTS
MODE SLOPE(degrees): -74.534
BIN WIDTH(degrees): 2.511
OF OCCURRENCES IN BIN: 10
DELTA-PHASE(degrees)-MODE SLOPE(degrees)
40.0
20.0
0.0
-20.0
-40.0
-25 -20 -15 -10 -5 0 5 10 15 20 25
UPPER PORT NUMBER

Figure V-17

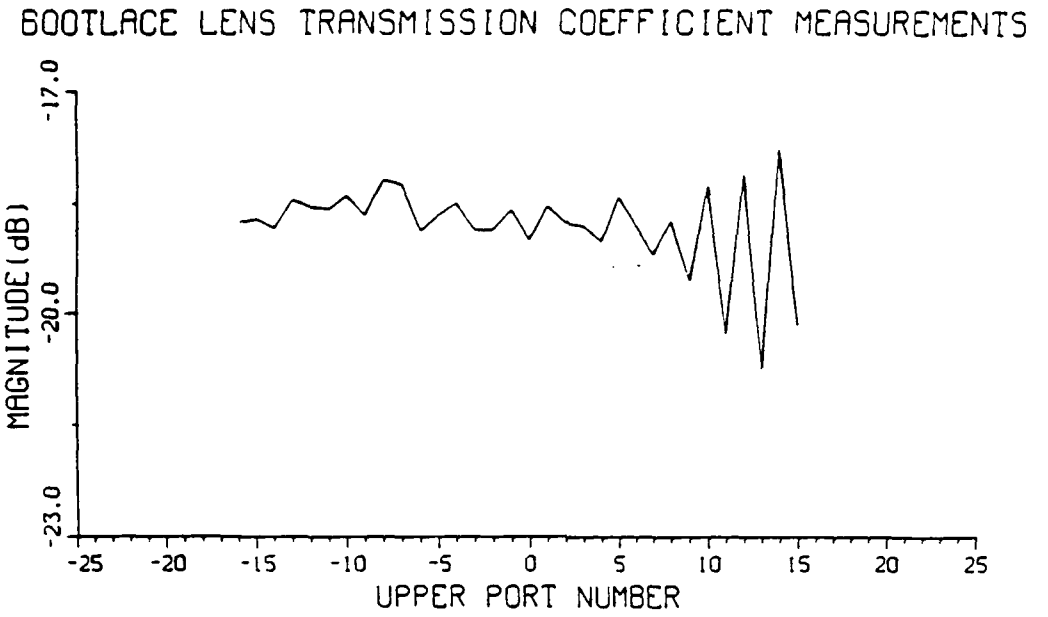
BOOTLACE LENS TRANSMISSION COEFFICIENT MEASUREMENTS
MAGNITUDE(dB)
-17.0
-20.0
-23.0
-25
-20
-15
-10
-5
0
5
10
15
20
25
UPPER PORT NUMBER
FREQ: 3.20000 GHz
PORT NUMBER:
BOTTOM: -15

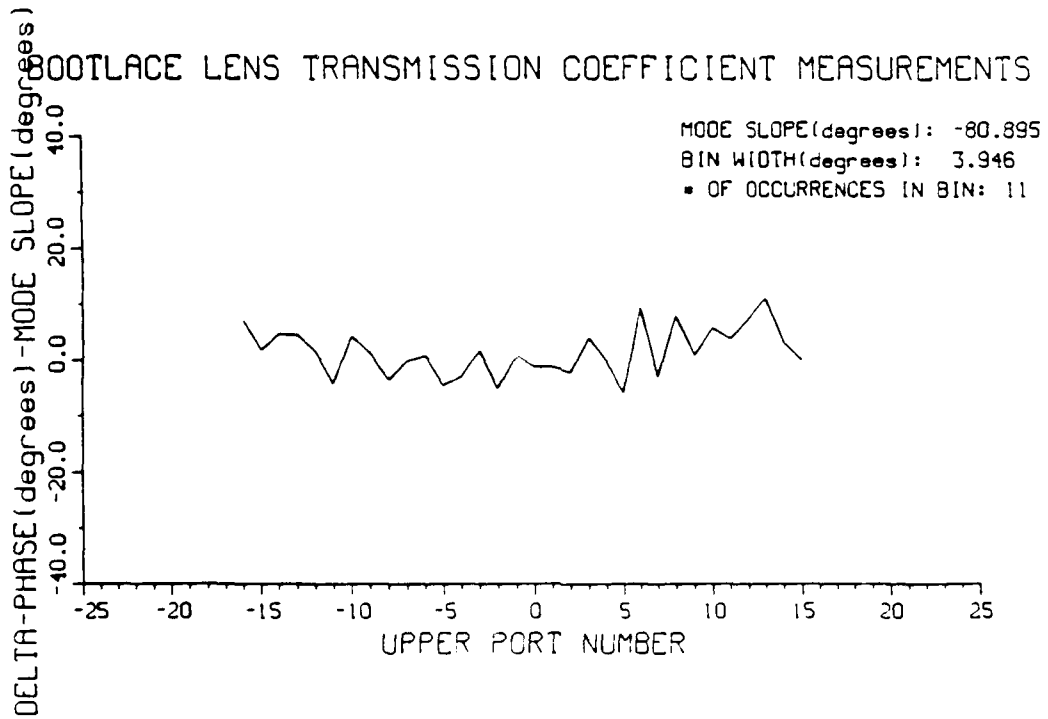
BOOTLACE LENS TRANSMISSION COEFFICIENT MEASUREMENTS
MODE SLOPE(degrees): -80.895
BIN WIDTH(degrees): 3.946
OF OCCURRENCES IN BIN: 11
DELTA-PHASE(degrees)-MODE SLOPE(degrees)
40.0
20.0
0.0
-20.0
-40.0
-25
-20
-15
-10
-5
0
5
10
15
20
25
UPPER PORT NUMBER

Figure V-18

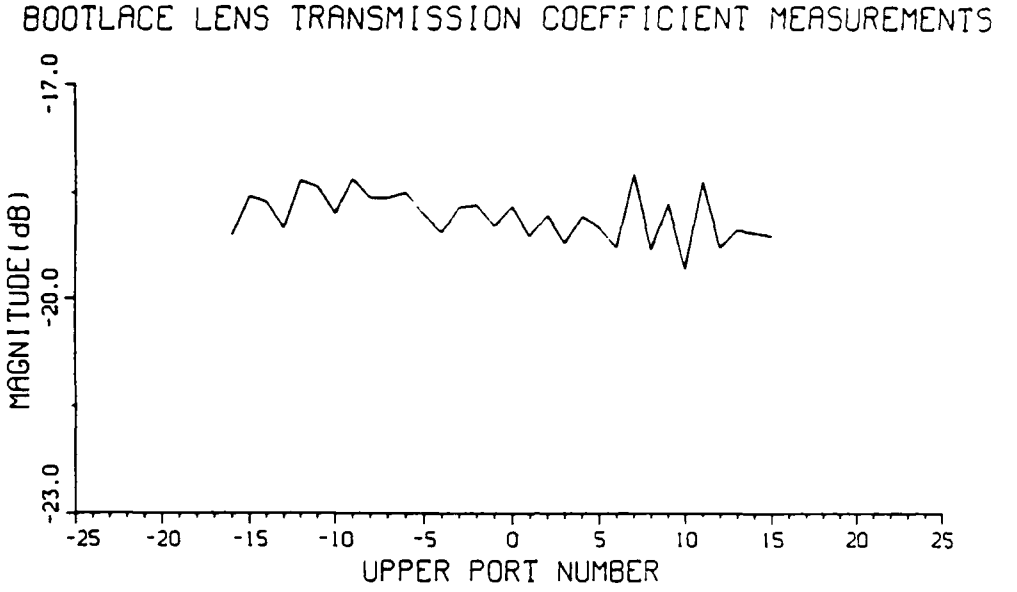
BOOTLACE LENS TRANSMISSION COEFFICIENT MEASUREMENTS
MAGNITUDE(dB)
-17.0
-20.0
-23.0
-25 -20 -15 -10 -5 0 5 10 15 20 25
UPPER PORT NUMBER
FREQ: 3.20000 GHz
PORT NUMBER:
BOTTOM: -16

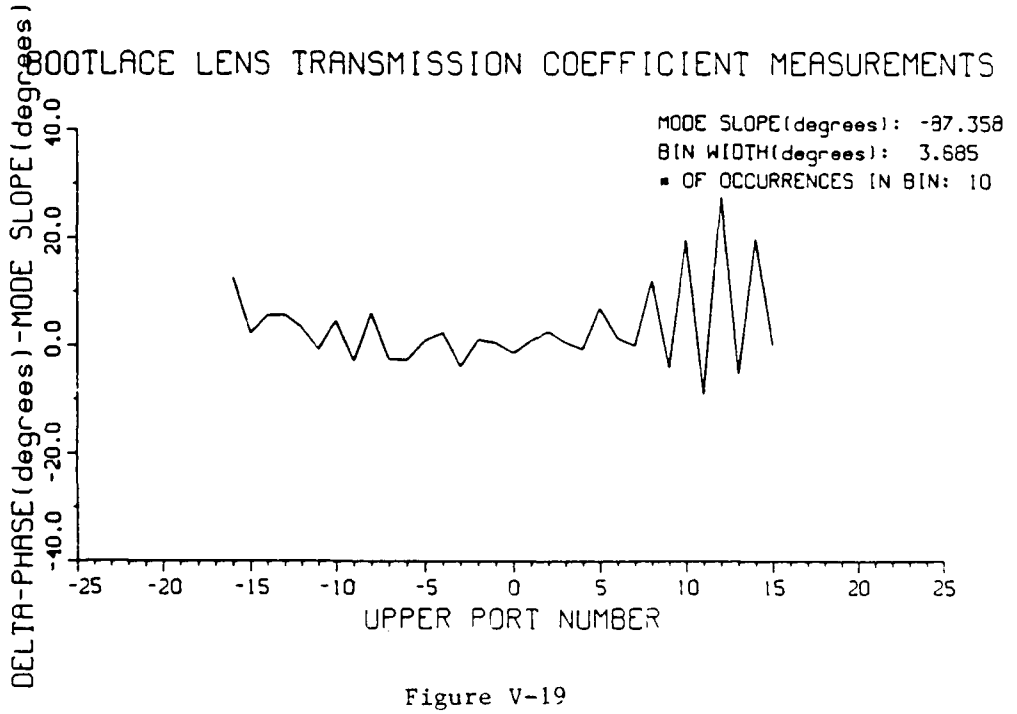
BOOTLACE LENS TRANSMISSION COEFFICIENT MEASUREMENTS
MODE SLOPE(degrees): -87.358
BIN WIDTH(degrees): 3.685
OF OCCURRENCES IN BIN: 10
DELTA-PHASE(degrees)-MODE SLOPE(degrees)
40.0
20.0
0.0
-20.0
-40.0
-25 -20 -15 -10 -5 0 5 10 15 20 25
UPPER PORT NUMBER

Figure V-19

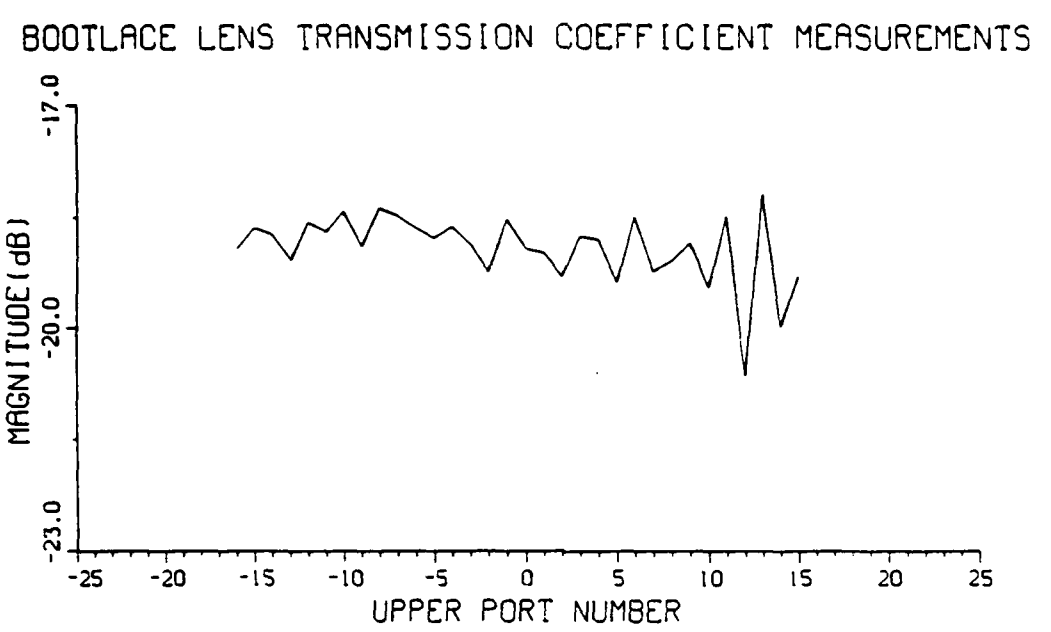
BOOTLACE LENS TRANSMISSION COEFFICIENT MEASUREMENTS
MAGNITUDE(dB)
-17.0
-20.0
-23.0
-25 -20 -15 -10 -5 0 5 10 15 20 25
UPPER PORT NUMBER
FREQ: 3.20000 GHz
PORT NUMBER:
BOTTOM: -17

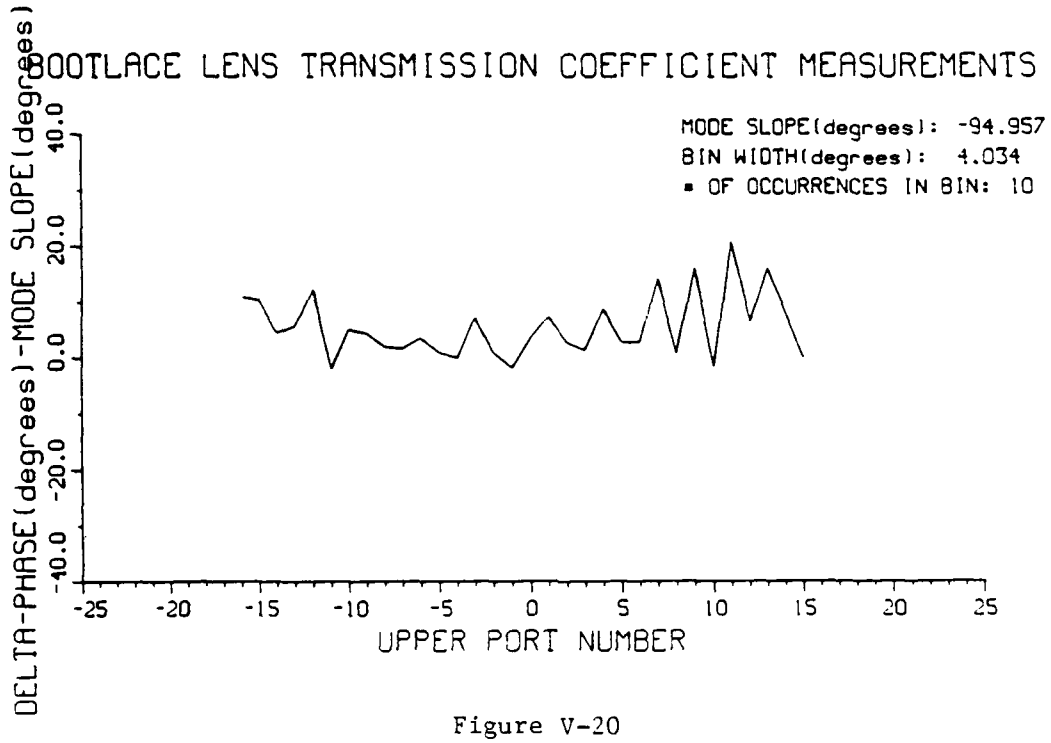
BOOTLACE LENS TRANSMISSION COEFFICIENT MEASUREMENTS
MODE SLOPE(degrees): -94.957
BIN WIDTH(degrees): 4.034
OF OCCURRENCES IN BIN: 10
DELTA-PHASE(degrees)-MODE SLOPE(degrees)
40.0
20.0
0.0
-20.0
-40.0
-25 -20 -15 -10 -5 0 5 10 15 20 25
UPPER PORT NUMBER

Figure V-20

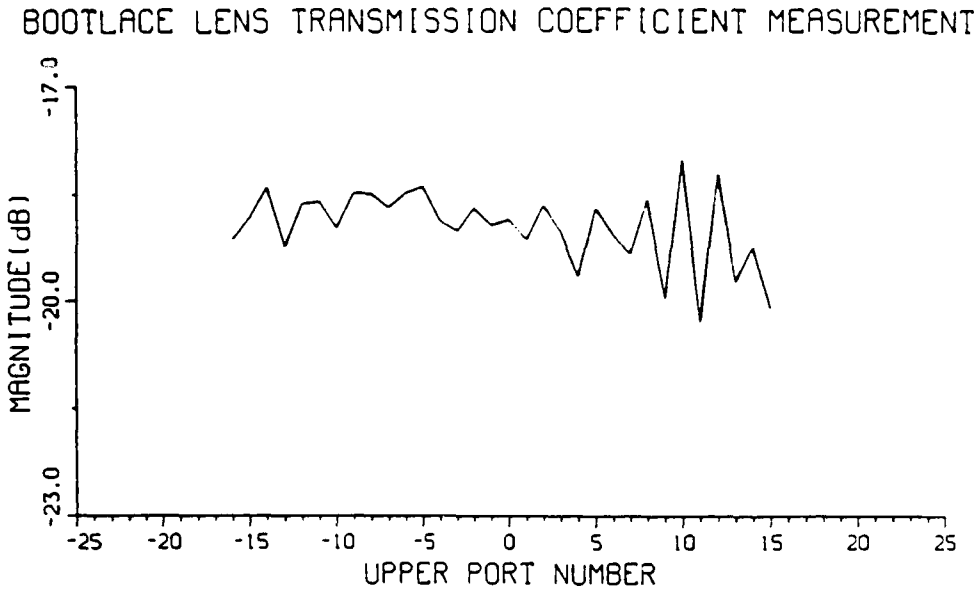
BOOTLACE LENS TRANSMISSION COEFFICIENT MEASUREMENTS
MAGNITUDE(dB)
-17.0
-20.0
-23.0
-25 -20 -15 -10 -5 0 5 10 15 20 25
UPPER PORT NUMBER
FREQ: 3.20000 GHz
PORT NUMBER:
BOTTOM: -18

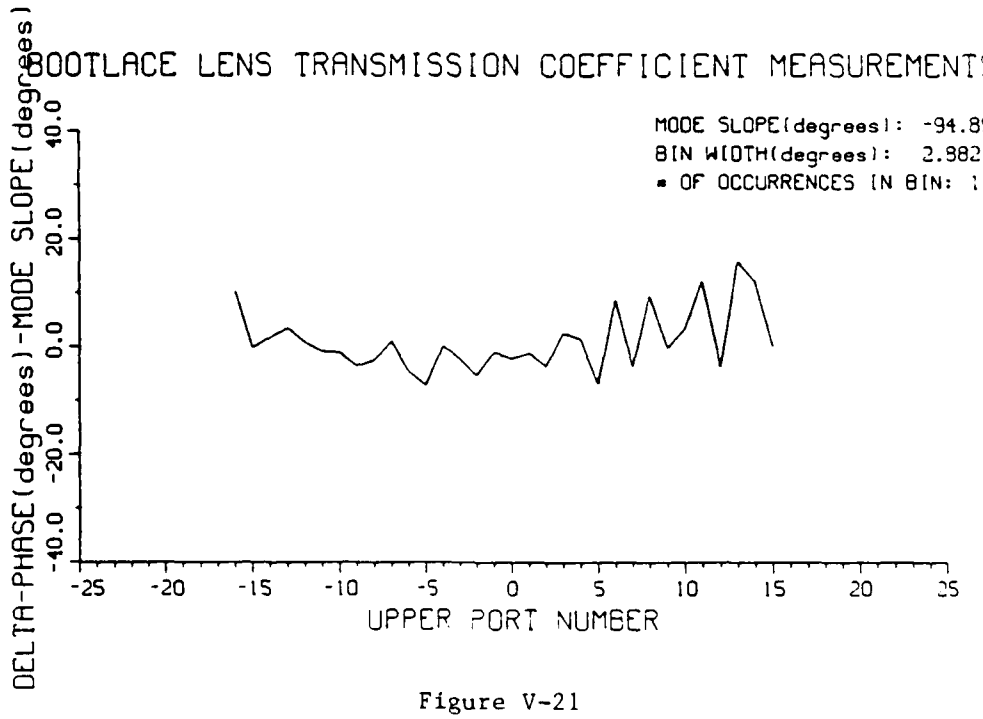
BOOTLACE LENS TRANSMISSION COEFFICIENT MEASUREMENTS
MODE SLOPE(degrees): -94.897
BIN WIDTH(degrees): 2.882
OF OCCURRENCES IN BIN: 11
DELTA-PHASE(degrees)-MODE SLOPE(degrees)
40.0
20.0
0.0
-20.0
-40.0
-25 -20 -15 -10 -5 0 5 10 15 20 25
UPPER PORT NUMBER

Figure V-21

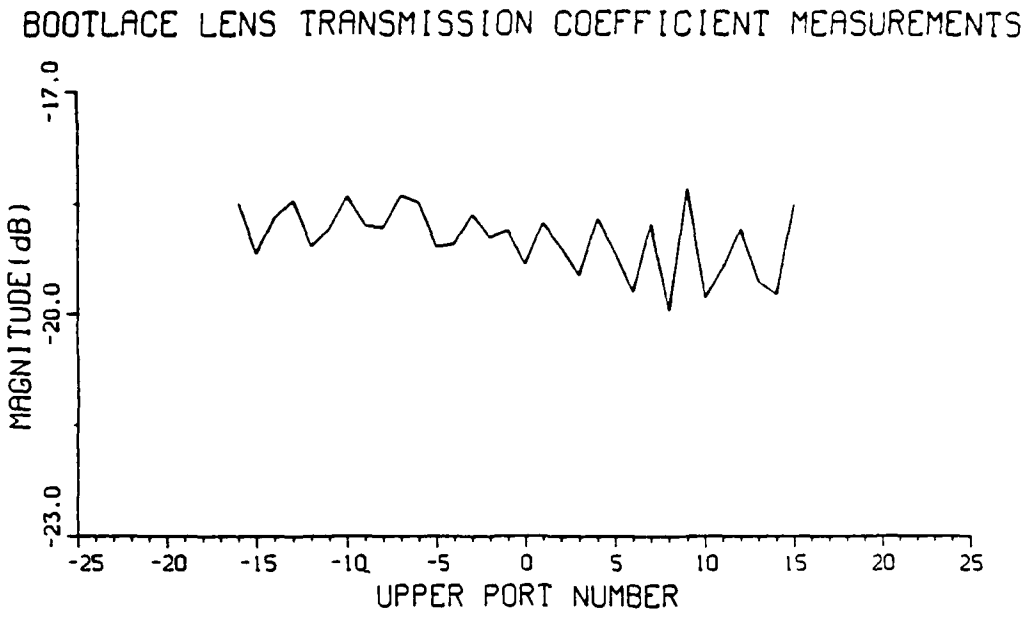
BOOTLACE LENS TRANSMISSION COEFFICIENT MEASUREMENTS
MAGNITUDE(dB)
-17.0
-20.0
-23.0
-25 -20 -15 -10 -5 0 5 10 15 20 25
UPPER PORT NUMBER
FREQ: 3.20000 GHz
PORT NUMBER:
BOTTOM: -19

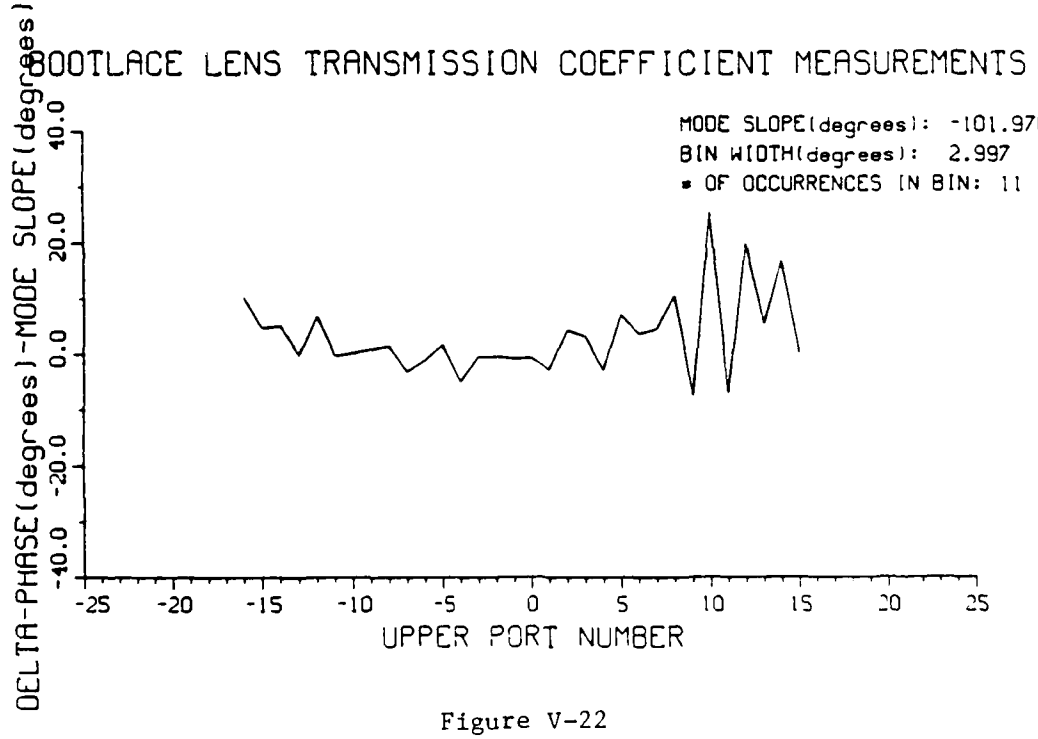
BOOTLACE LENS TRANSMISSION COEFFICIENT MEASUREMENTS
MODE SLOPE(degrees): -101.976
BIN WIDTH(degrees): 2.997
OF OCCURRENCES IN BIN: 11
DELTA-PHASE(degrees)-MODE SLOPE(degrees)
40.0
20.0
0.0
-20.0
-40.0
-25 -20 -15 -10 -5 0 5 10 15 20 25
UPPER PORT NUMBER

Figure V-22

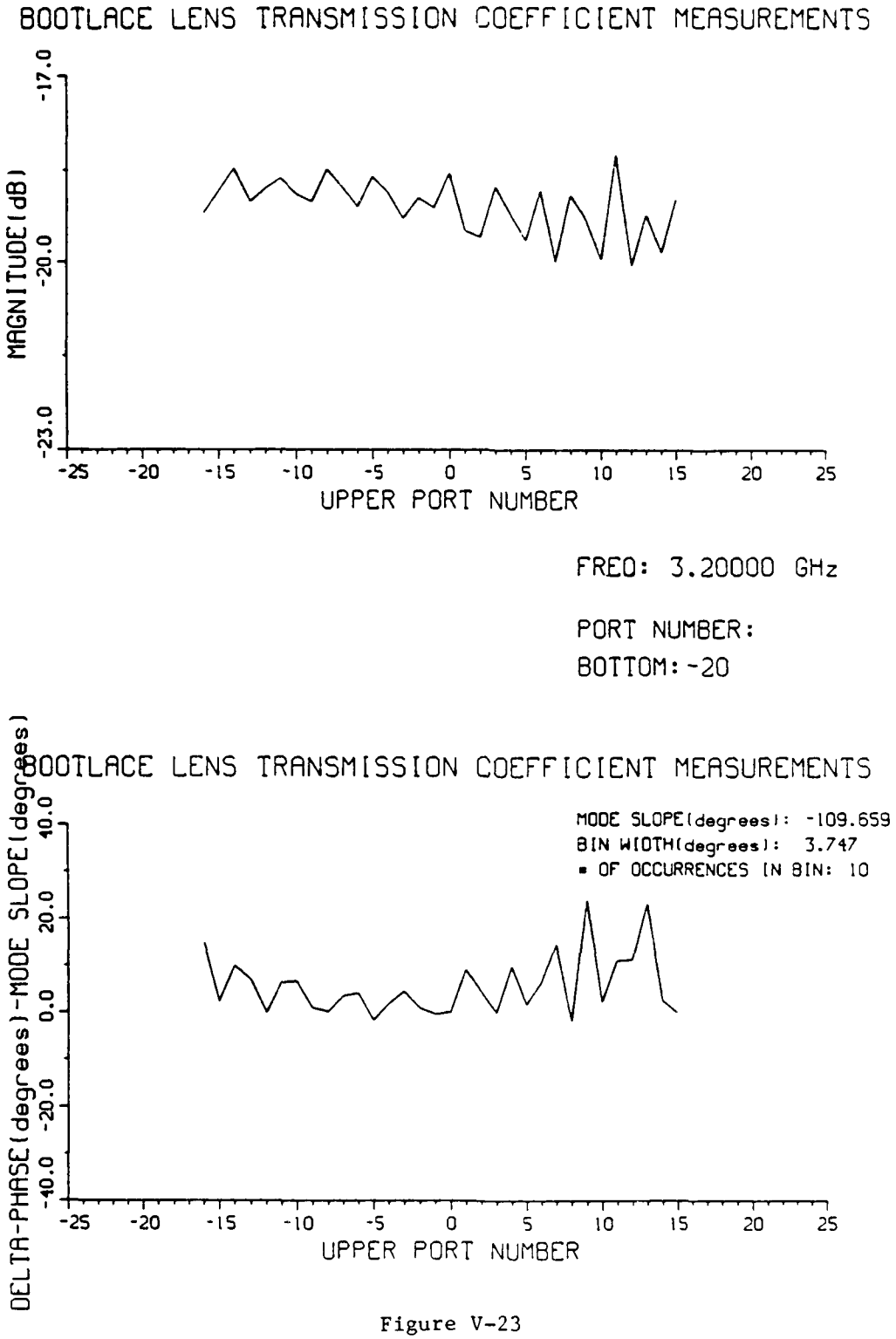
BOOTLACE LENS TRANSMISSION COEFFICIENT MEASUREMENTS
MAGNITUDE(dB)
-17.0
-20.0
-23.0
-25
-20
-15
-10
-5
0
5
10
15
20
25
UPPER PORT NUMBER
FREQ: 3.20000 GHz
PORT NUMBER:
BOTTOM: -20
BOOTLACE LENS TRANSMISSION COEFFICIENT MEASUREMENTS
MODE SLOPE(degrees): -109.659
BIN WIDTH(degrees): 3.747
OF OCCURRENCES IN BIN: 10
DELTA-PHASE(degrees)-MODE SLOPE(degrees)
40.0
20.0
0.0
-20.0
-40.0
-25
-20
-15
-10
-5
0
5
10
15
20
25
UPPER PORT NUMBER

Figure V-23

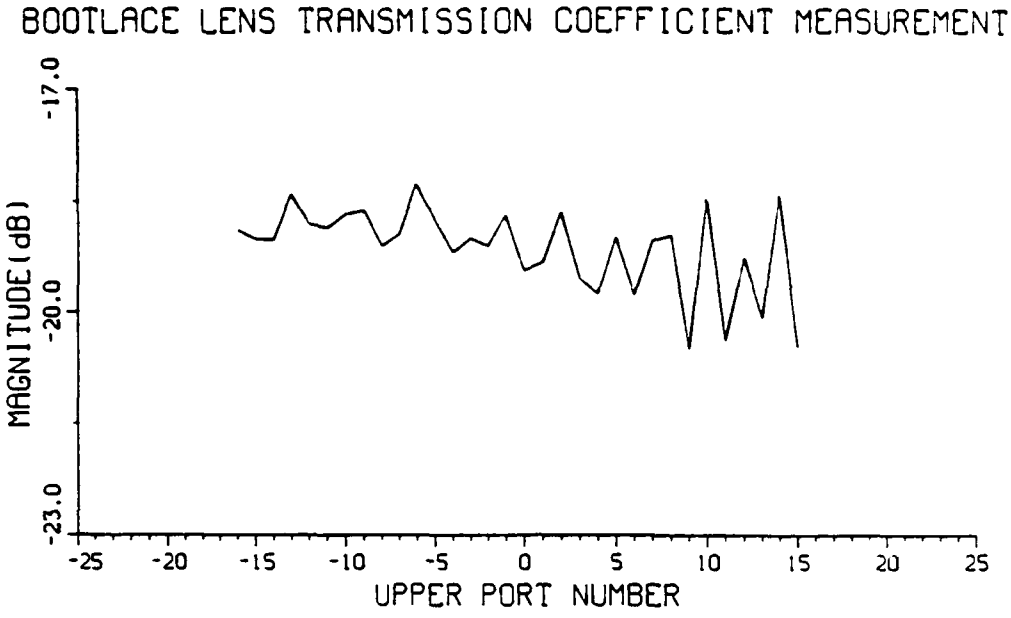
BOOTLACE LENS TRANSMISSION COEFFICIENT MEASUREMENTS
MAGNITUDE(dB)
-17.0
-20.0
-23.0
-25 -20 -15 -10 -5 0 5 10 15 20 25
UPPER PORT NUMBER
FREQ: 3.20000 GHz
PORT NUMBER:
BOTTOM: -21

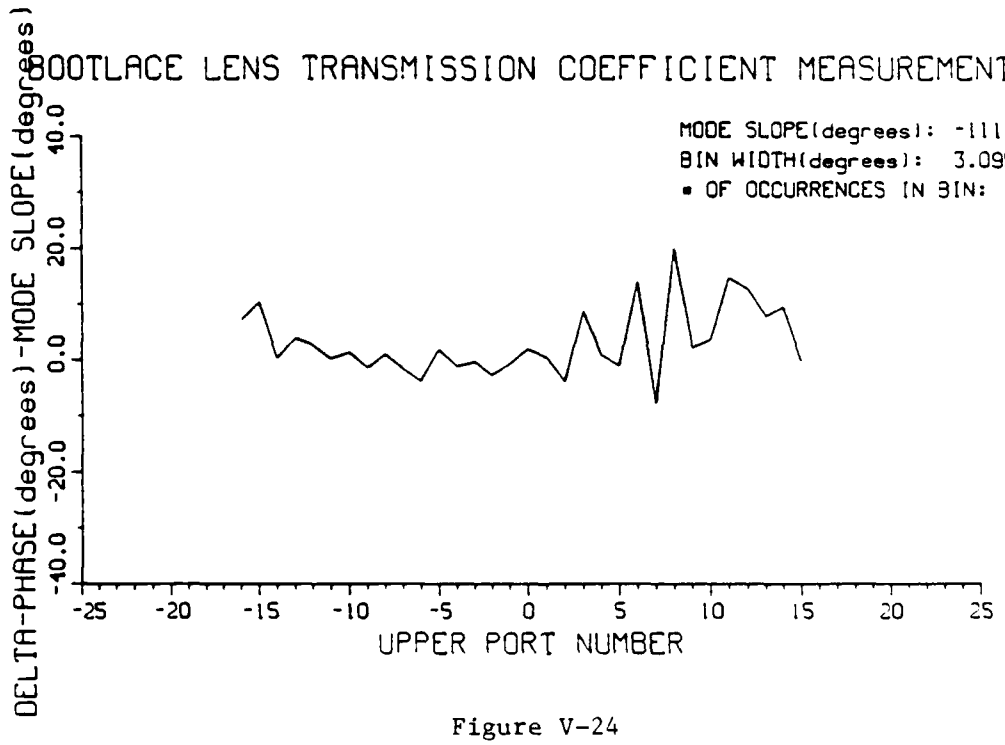
BOOTLACE LENS TRANSMISSION COEFFICIENT MEASUREMENTS
MODE SLOPE(degrees): -111.788
BIN WIDTH(degrees): 3.095
OF OCCURRENCES IN BIN: 12
DELTA-PHASE(degrees)-MODE SLOPE(degrees)
40.0
20.0
0.0
-20.0
-40.0
-25 -20 -15 -10 -5 0 5 10 15 20 25
UPPER PORT NUMBER

Figure V-24

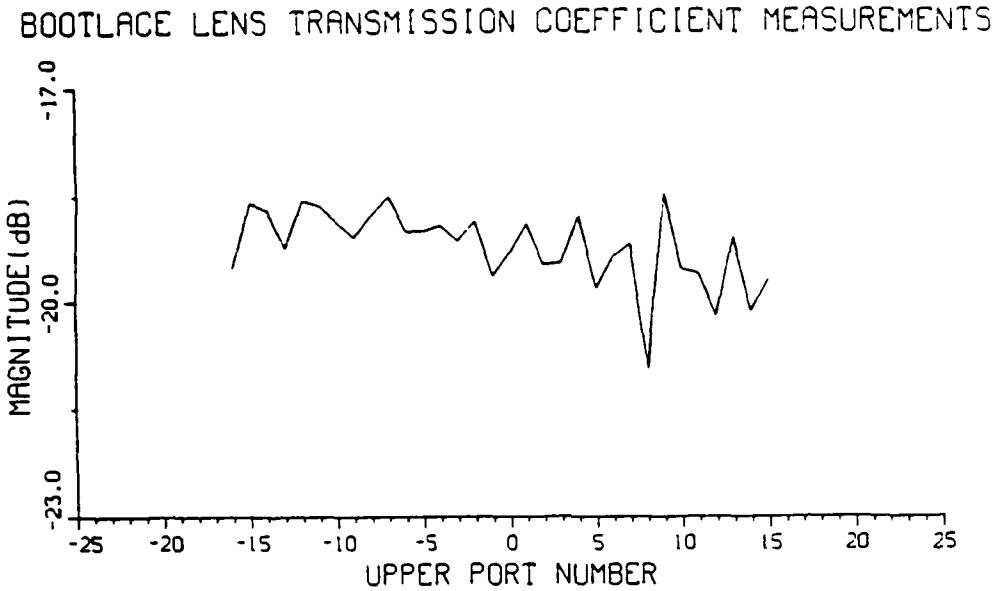
BOOTLACE LENS TRANSMISSION COEFFICIENT MEASUREMENTS
MAGNITUDE(dB)
-17.0
-20.0
-23.0
-25
-20
-15
-10
-5
0
5
10
15
20
25
UPPER PORT NUMBER
FREQ: 3.20000 GHz
PORT NUMBER:
BOTTOM: -22

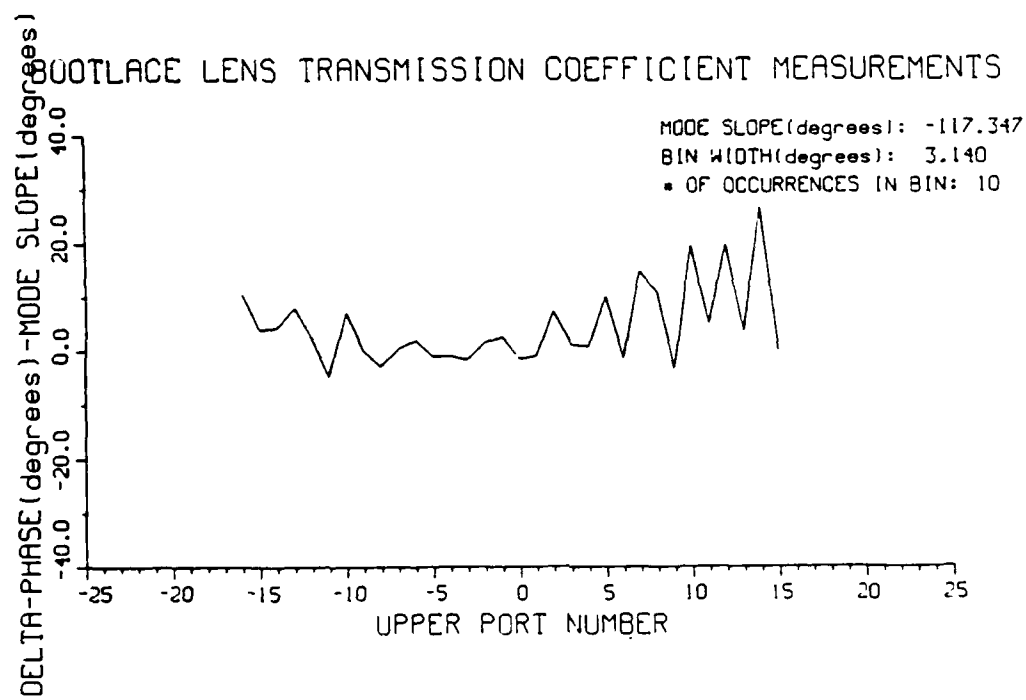
BOOTLACE LENS TRANSMISSION COEFFICIENT MEASUREMENTS
MODE SLOPE(degrees): -117.347
BIN WIDTH(degrees): 3.140
OF OCCURRENCES IN BIN: 10
DELTA-PHASE(degrees)-MODE SLOPE(degrees)
40.0
20.0
0.0
-20.0
-40.0
-25
-20
-15
-10
-5
0
5
10
15
20
25
UPPER PORT NUMBER

Figure V-25

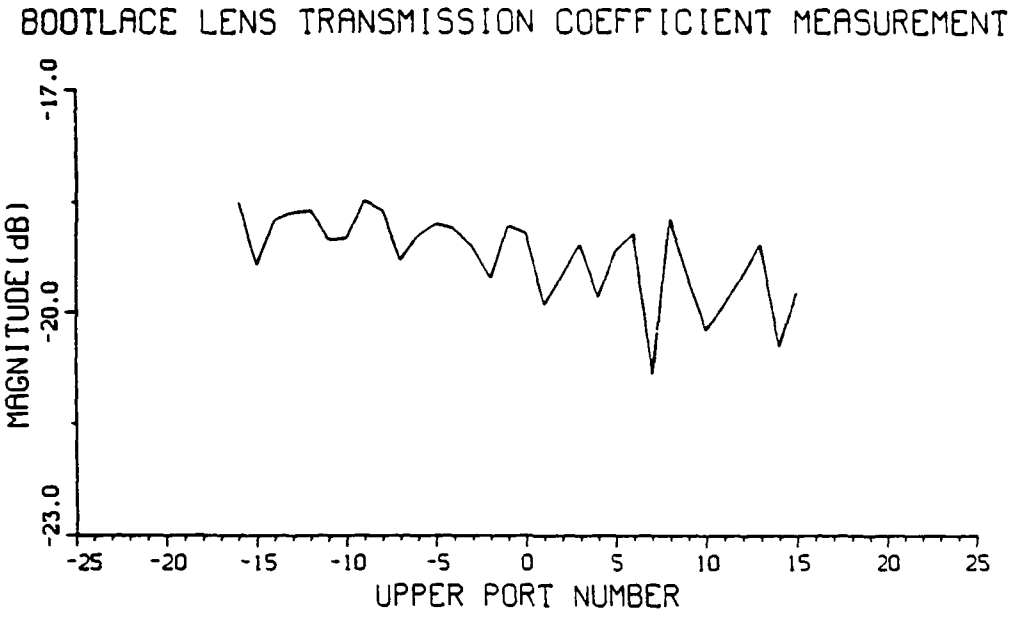
BOOTLACE LENS TRANSMISSION COEFFICIENT MEASUREMENTS
MAGNITUDE(dB)
-17.0
-20.0
-23.0
-25 -20 -15 -10 -5 0 5 10 15 20 25
UPPER PORT NUMBER
FREQ: 3.20000 GHz
PORT NUMBER:
BOTTOM: -23

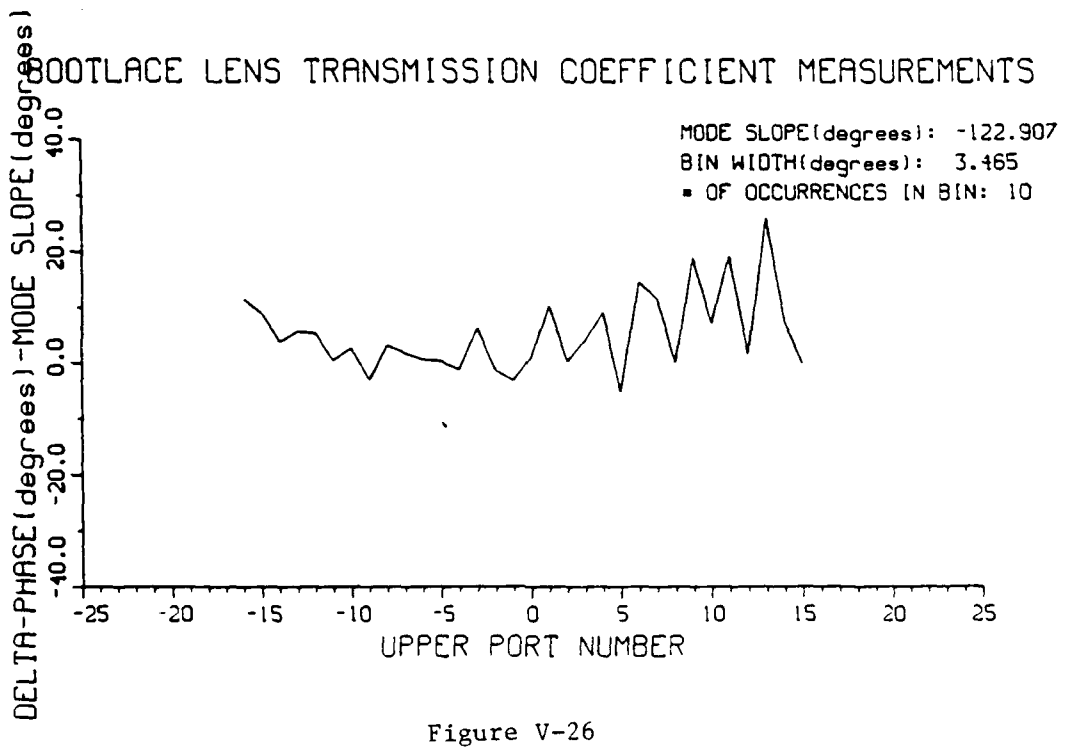
BOOTLACE LENS TRANSMISSION COEFFICIENT MEASUREMENTS
MODE SLOPE(degrees): -122.907
BIN WIDTH(degrees): 3.465
OF OCCURRENCES IN BIN: 10
DELTA-PHASE(degrees)-MODE SLOPE(degrees)
40.0
20.0
0.0
-20.0
-40.0
-25 -20 -15 -10 -5 0 5 10 15 20 25
UPPER PORT NUMBER

Figure V-26

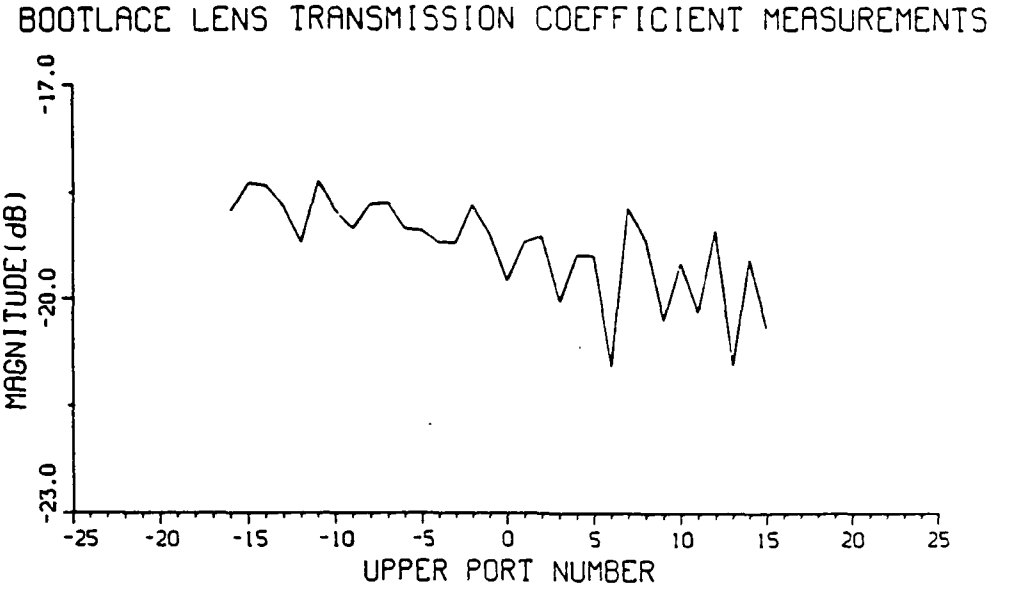
BOOTLACE LENS TRANSMISSION COEFFICIENT MEASUREMENTS
MAGNITUDE(dB)
-17.0
-20.0
-23.0
-25
-20
-15
-10
-5
0
5
10
15
20
25
UPPER PORT NUMBER
FREQ: 3.20000 GHz
PORT NUMBER:
BOTTOM: -24

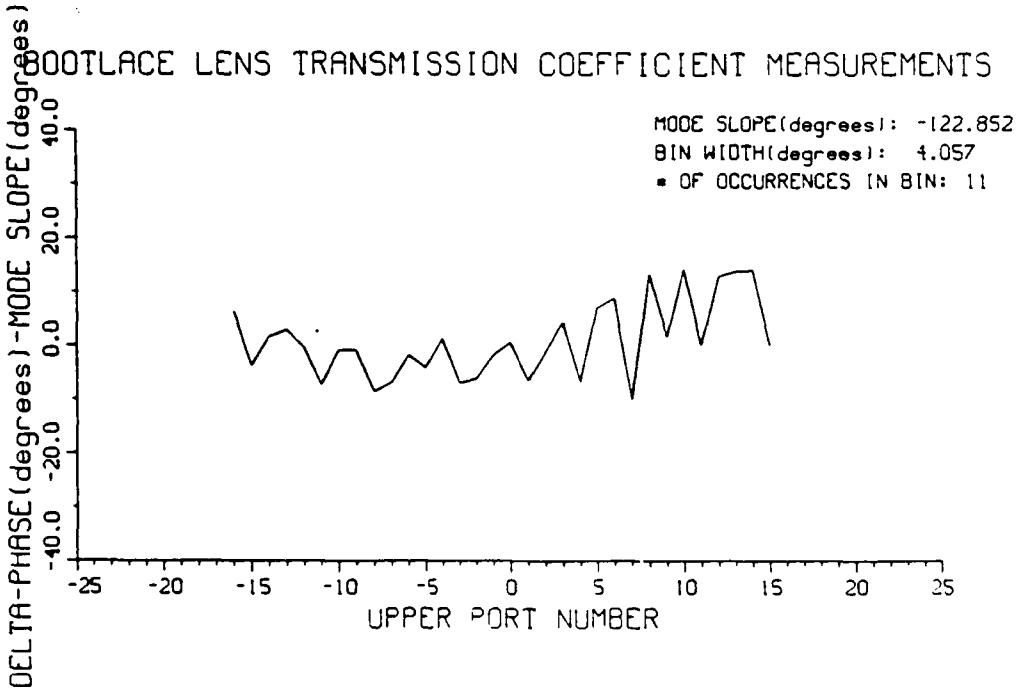
BOOTLACE LENS TRANSMISSION COEFFICIENT MEASUREMENTS
MODE SLOPE(degrees): -122.852
BIN WIDTH(degrees): 4.057
OF OCCURRENCES IN BIN: 11
DELTA-PHASE(degrees)-MODE SLOPE(degrees)
40.0
20.0
0.0
-20.0
-40.0
-25
-20
-15
-10
-5
0
5
10
15
20
25
UPPER PORT NUMBER

Figure V-27

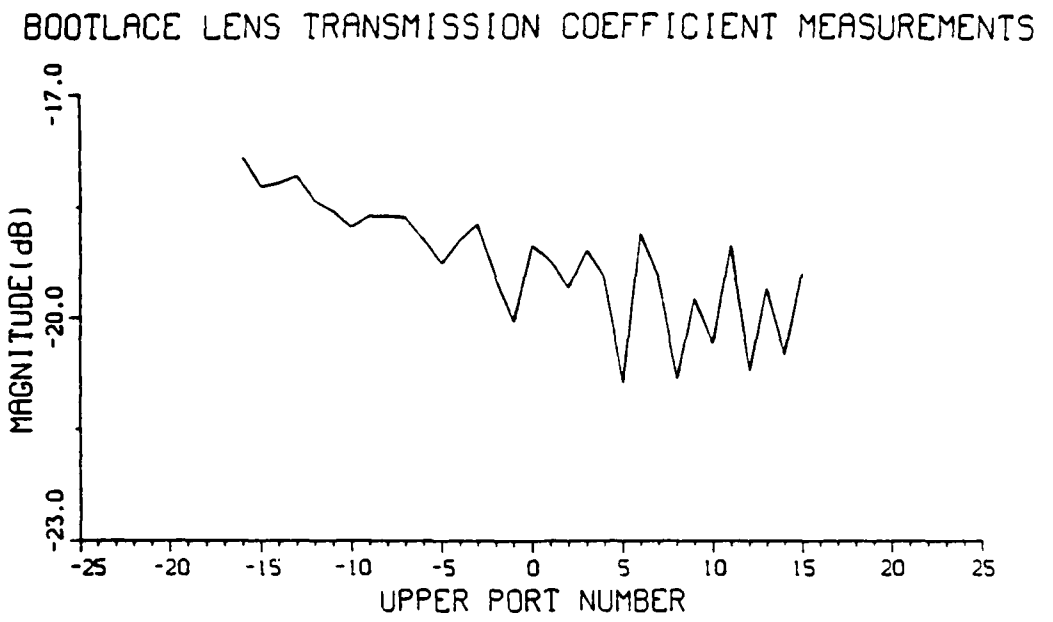
BOOTLACE LENS TRANSMISSION COEFFICIENT MEASUREMENTS
MAGNITUDE(dB)
-17.0
-20.0
-23.0
-25
-20
-15
-10
-5
0
5
10
15
20
25
UPPER PORT NUMBER
FREQ: 3.20000 GHz
PORT NUMBER:
BOTTOM: -25

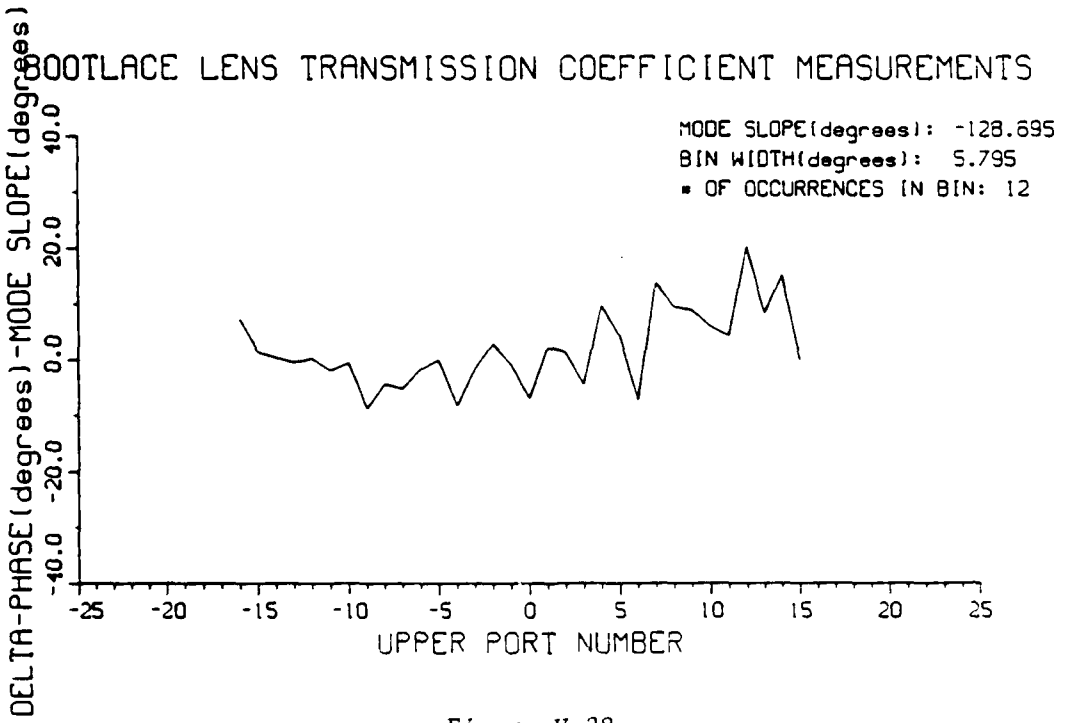
BOOTLACE LENS TRANSMISSION COEFFICIENT MEASUREMENTS
MODE SLOPE(degrees): -128.695
BIN WIDTH(degrees): 5.795
OF OCCURRENCES IN BIN: 12
DELTA-PHASE(degrees)-MODE SLOPE(degrees)
40.0
20.0
0.0
-20.0
-40.0
-25
-20
-15
-10
-5
0
5
10
15
20
25
UPPER PORT NUMBER

Figure V-28

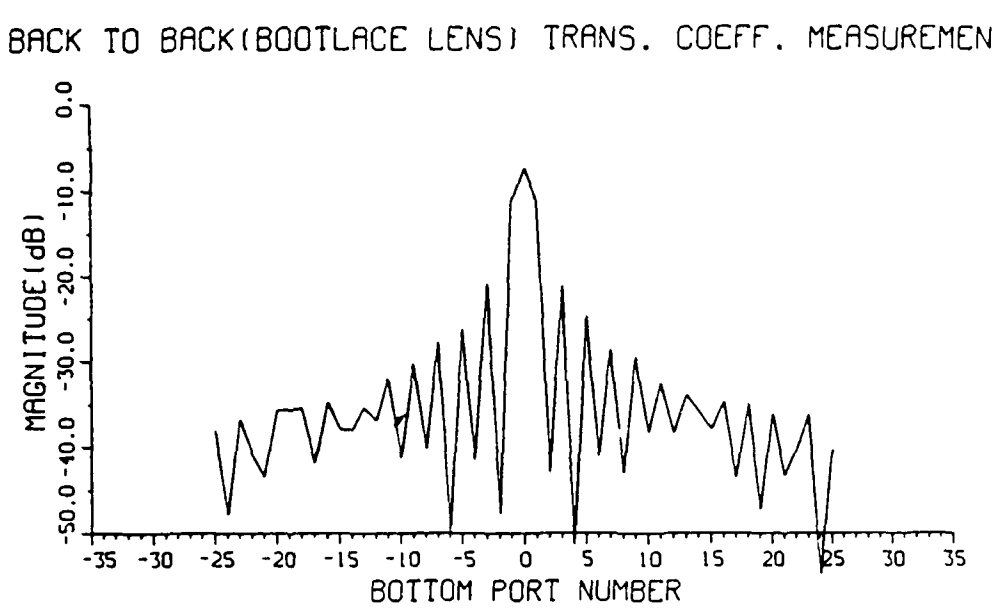
BACK TO BACK(BOOTLACE LENS) TRANS. COEFF. MEASUREMENTS
MAGNITUDE(dB)
0.0
-10.0
-20.0
-30.0
-40.0
-50.0
-35 -30 -25 -20 -15 -10 -5 0 5 10 15 20 25 30 35
BOTTOM PORT NUMBER
FREQ: 3.20000 GHz
PORT NUMBER
BOTTOM(1):0

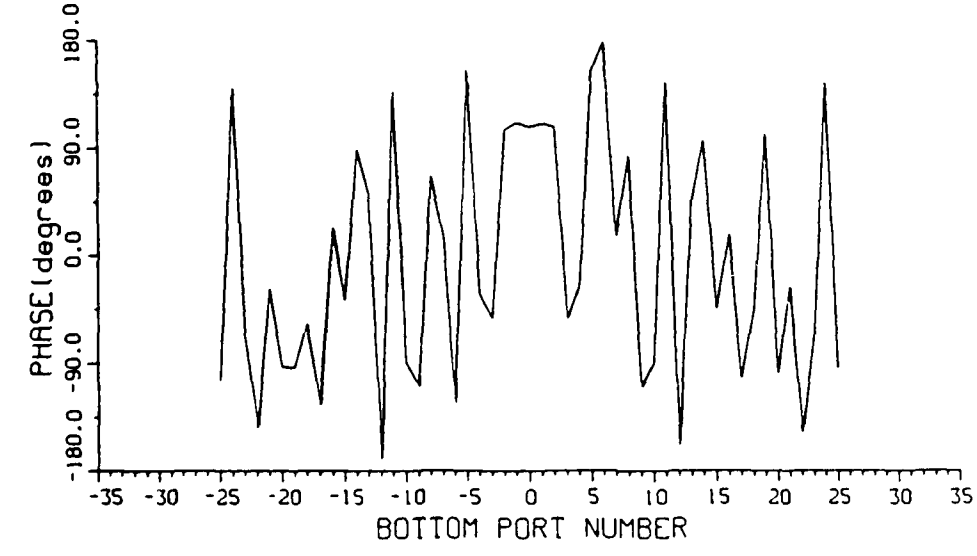
BACK TO BACK(BOOTLACE LENS) TRANS. COEFF. MEASUREMENTS
PHASE(degrees)
180.0
90.0
0.0
-90.0
-180.0
-35 -30 -25 -20 -15 -10 -5 0 5 10 15 20 25 30 35
BOTTOM PORT NUMBER

Figure V-29

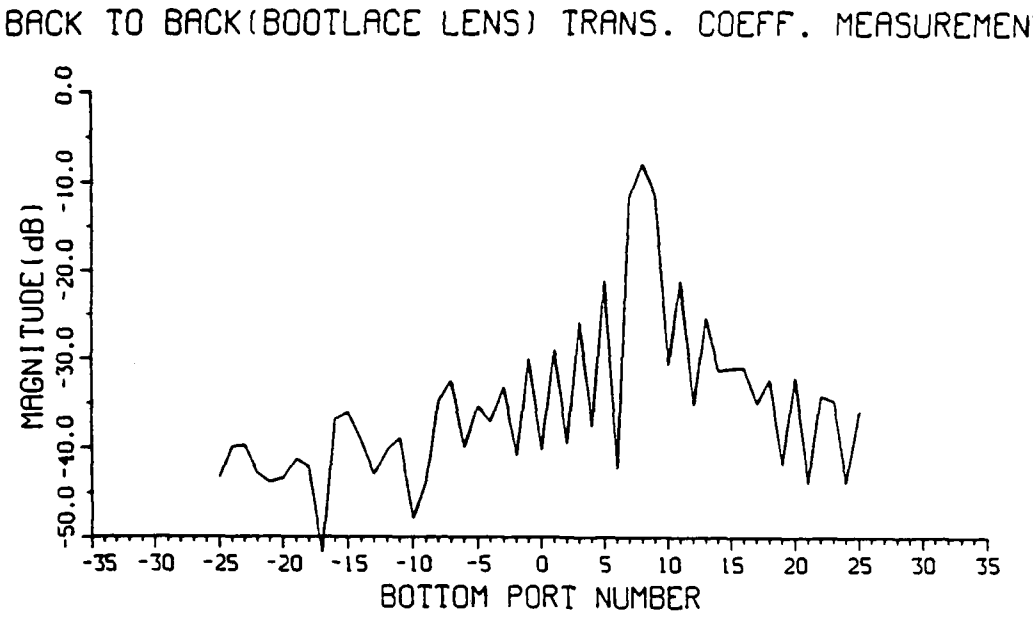
BACK TO BACK(BOOTLACE LENS) TRANS. COEFF. MEASUREMENTS
MAGNITUDE(dB)
0.0
-10.0
-20.0
-30.0
-40.0
-50.0
-35 -30 -25 -20 -15 -10 -5 0 5 10 15 20 25 30 35
BOTTOM PORT NUMBER
FREQ: 3.20000 GHz
PORT NUMBER
BOTTOM(1):8

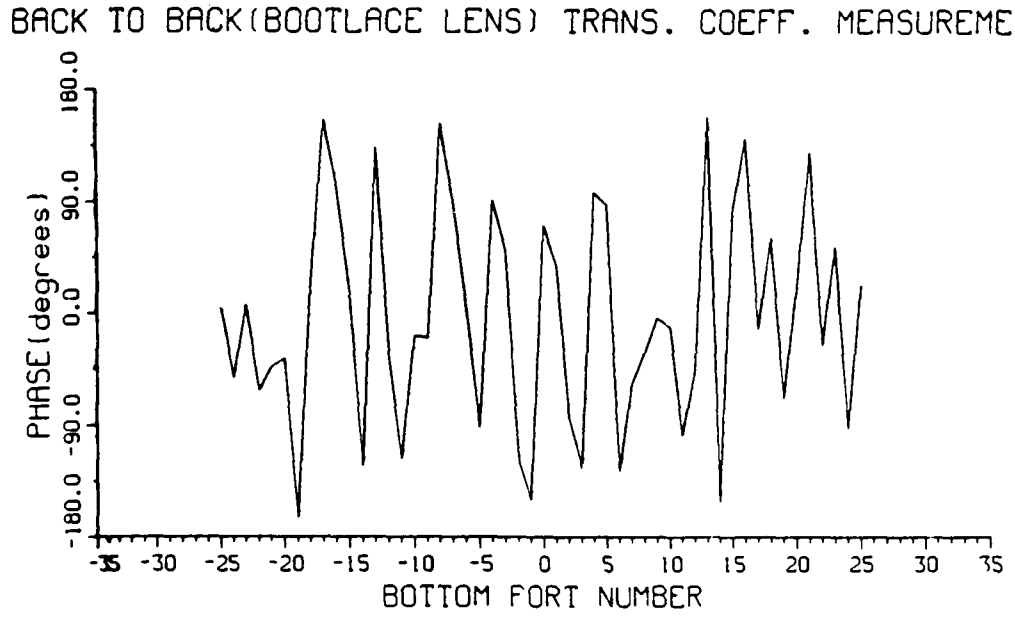
BACK TO BACK(BOOTLACE LENS) TRANS. COEFF. MEASUREMENTS
PHASE(degrees)
180.0
90.0
0.0
-90.0
-180.0
-35 -30 -25 -20 -15 -10 -5 0 5 10 15 20 25 30 35
BOTTOM PORT NUMBER

Figure V-30

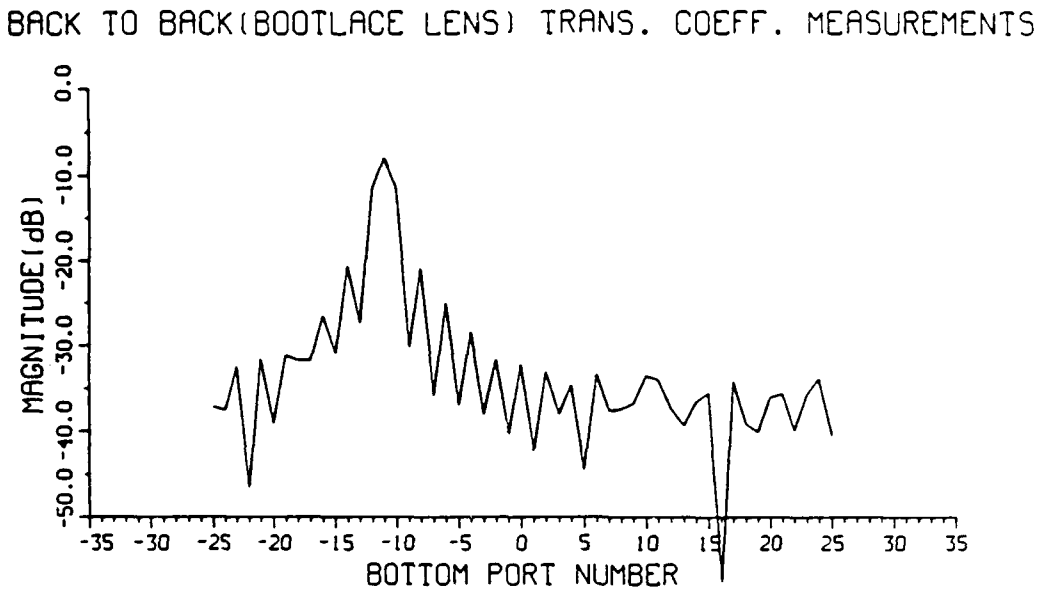
BACK TO BACK(BOOTLACE LENS) TRANS. COEFF. MEASUREMENTS
MAGNITUDE(dB)
0.0
-10.0
-20.0
-30.0
-40.0
-50.0
-35 -30 -25 -20 -15 -10 -5 0 5 10 15 20 25 30 35
BOTTOM PORT NUMBER
FREQ: 3.20000 GHz
PORT NUMBER
BOTTOM(1): -11

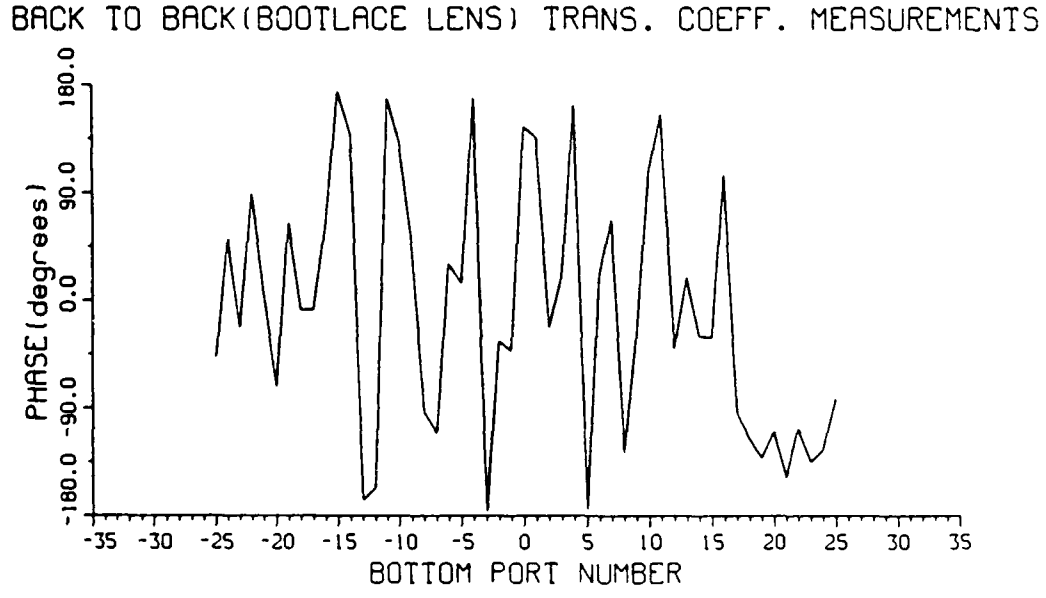
BACK TO BACK(BOOTLACE LENS) TRANS. COEFF. MEASUREMENTS
PHASE(degrees)
180.0
90.0
0.0
-90.0
-180.0
-35 -30 -25 -20 -15 -10 -5 0 5 10 15 20 25 30 35
BOTTOM PORT NUMBER

Figure V-31

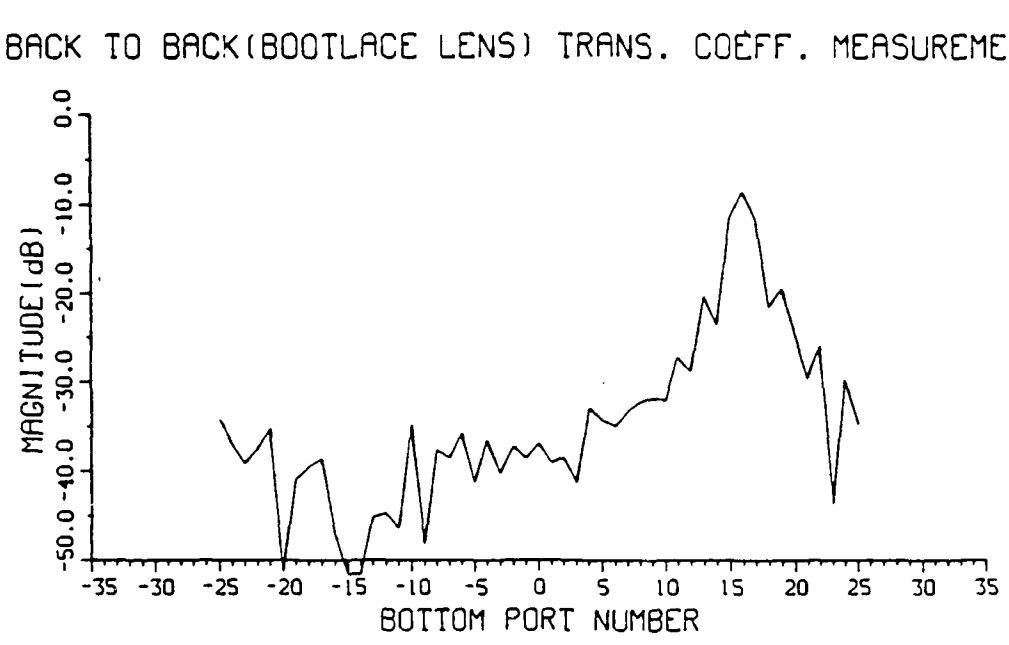
BACK TO BACK(BOOTLACE LENS) TRANS. COEFF. MEASUREMENTS
MAGNITUDE(dB)
0.0
-10.0
-20.0
-30.0
-40.0
-50.0
-35 -30 -25 -20 -15 -10 -5 0 5 10 15 20 25 30 35
BOTTOM PORT NUMBER
FREQ: 3.20000 GHz
PORT NUMBER
BOTTOM(1):16

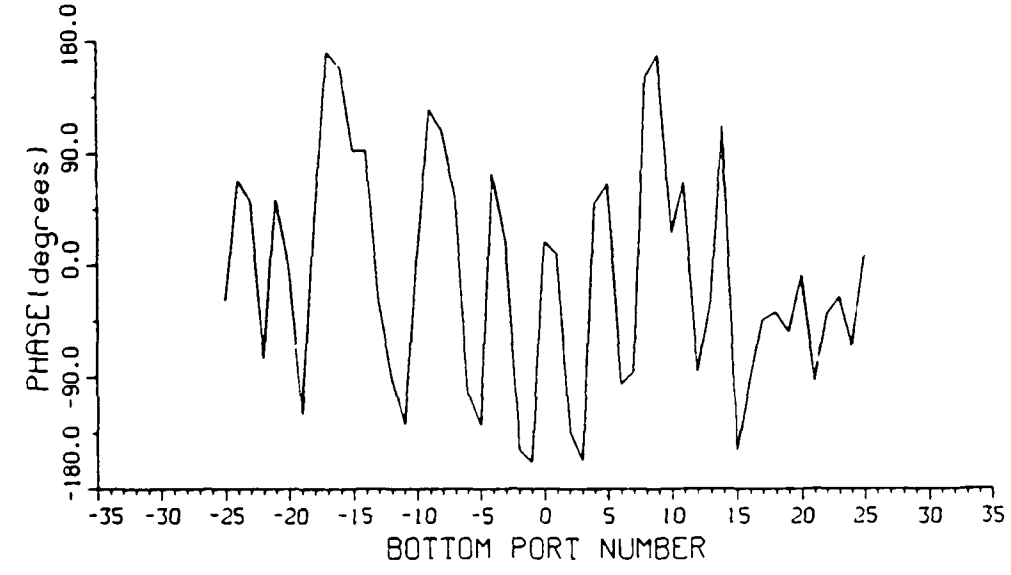
BACK TO BACK(BOOTLACE LENS) TRANS. COEFF. MEASUREMENTS
PHASE(degrees)
180.0
90.0
0.0
-90.0
-180.0
-35 -30 -25 -20 -15 -10 -5 0 5 10 15 20 25 30 35
BOTTOM PORT NUMBER

Figure V-32

BACK TO BACK(BOOTLACE LENS) TRANS. COEFF. MEASUREMENTS

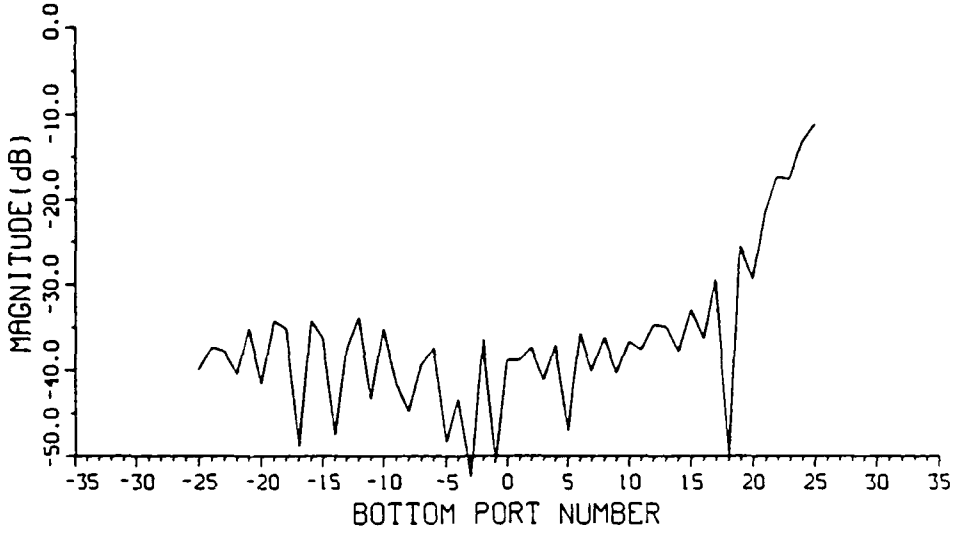

FREQ: 3.20000 GHz
PORT NUMBER
BOTTOM(1): -25

BACK TO BACK(BOOTLACE LENS) TRANS. COEFF. MEASUREMENTS

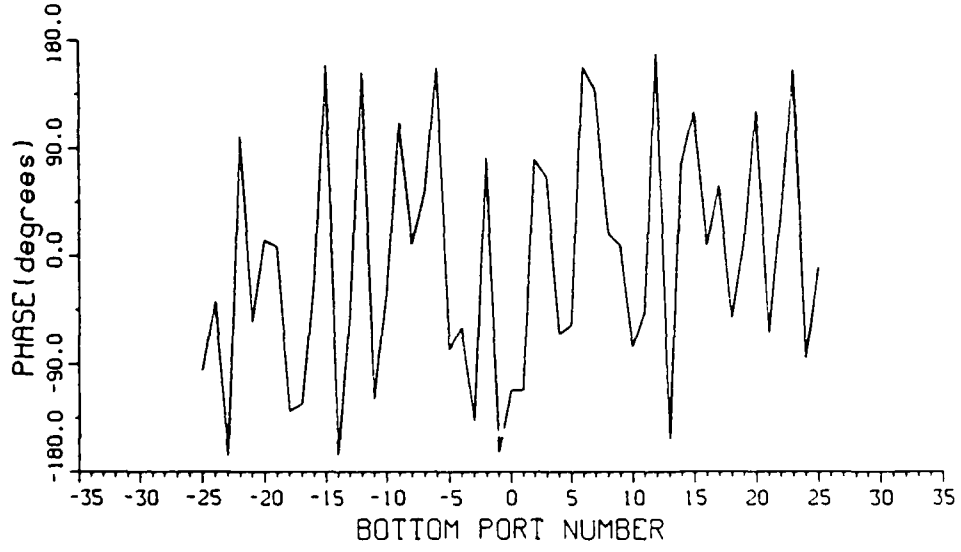

Figure V-33

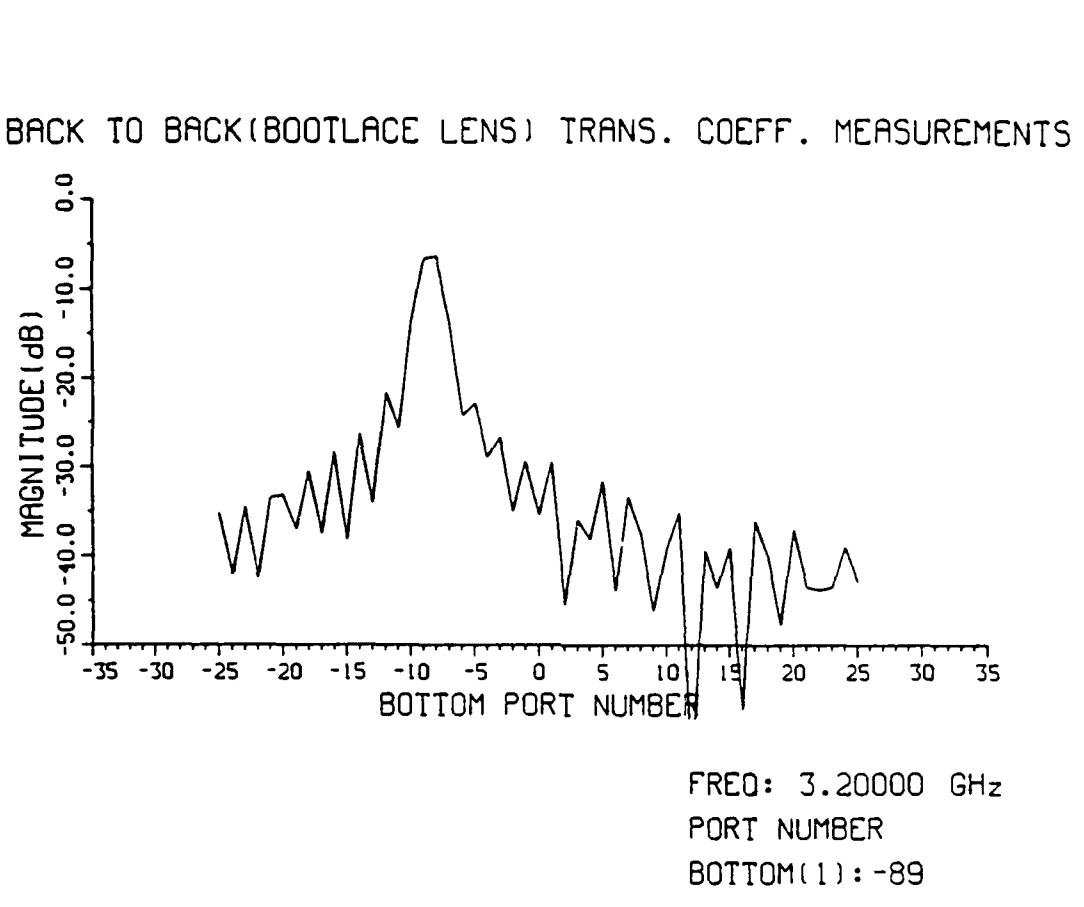
BACK TO BACK(BOOTLACE LENS) TRANS. COEFF. MEASUREMENTS
MAGNITUDE(dB)
0.0
-10.0
-20.0
-30.0
-40.0
-50.0
-35 -30 -25 -20 -15 -10 -5 0 5 10 15 20 25 30 35
BOTTOM PORT NUMBER
FREQ: 3.20000 GHz
PORT NUMBER
BOTTOM(1):-89

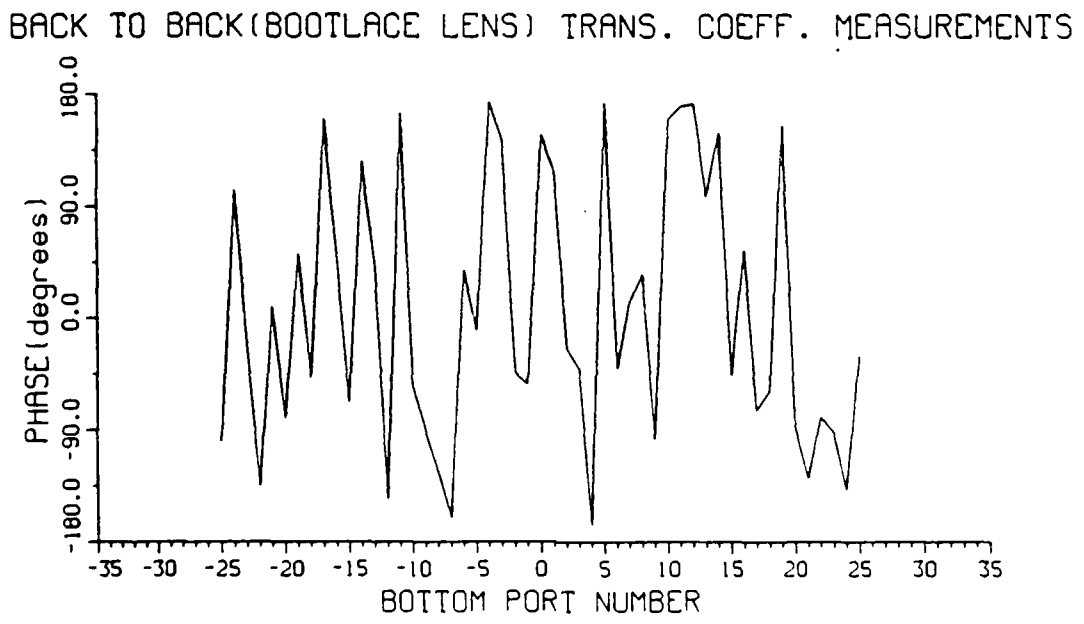
BACK TO BACK(BOOTLACE LENS) TRANS. COEFF. MEASUREMENTS
PHASE(degrees)
180.0
90.0
0.0
-90.0
-180.0
-35 -30 -25 -20 -15 -10 -5 0 5 10 15 20 25 30 35
BOTTOM PORT NUMBER

Figure V-34

BACK TO BACK(BOOTLACE LENS) TRANS. COEFF. MEASUREMENTS

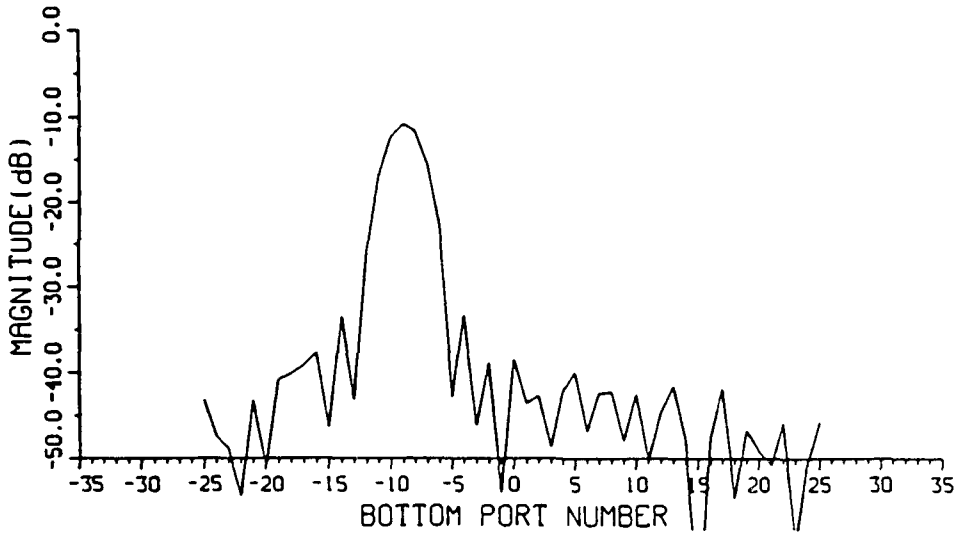

FREQ: 3.20000 GHz
PORT NUMBER
BOTTOM(1):791

BACK TO BACK(BOOTLACE LENS) TRANS. COEFF. MEASUREMENTS

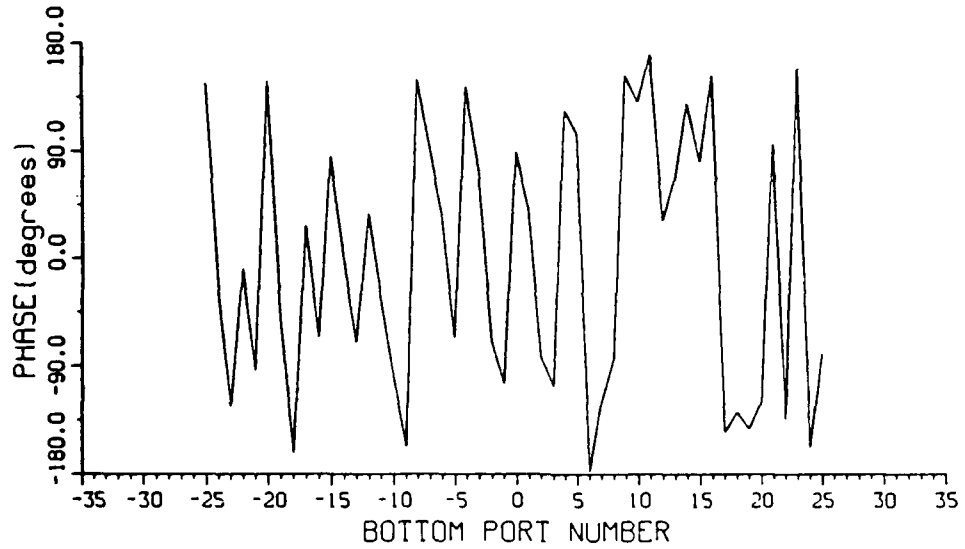

Figure V-35

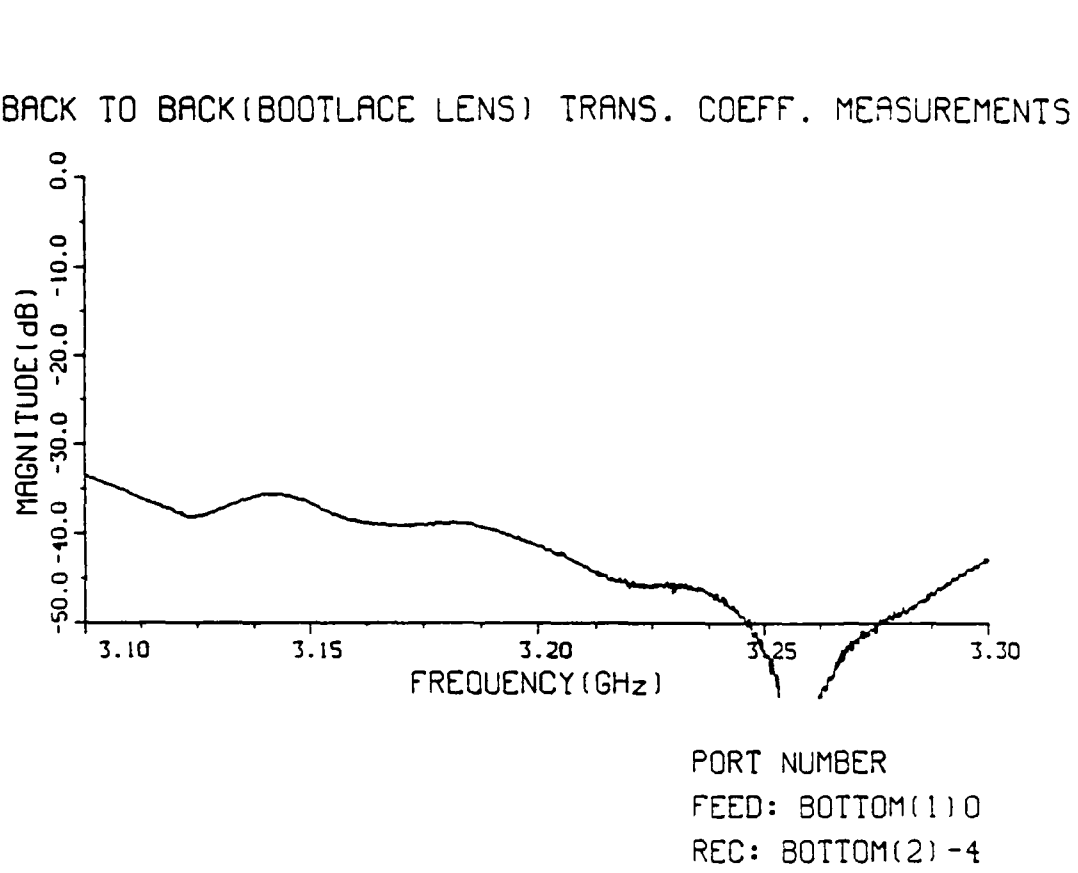
BACK TO BACK(BOOTLACE LENS) TRANS. COEFF. MEASUREMENTS
MAGNITUDE(dB)
0.0
-10.0
-20.0
-30.0
-40.0
-50.0
3.10
3.15
3.20
3.25
3.30
FREQUENCY(GHz)
PORT NUMBER
FEED: BOTTOM(1)0
REC: BOTTOM(2)-4

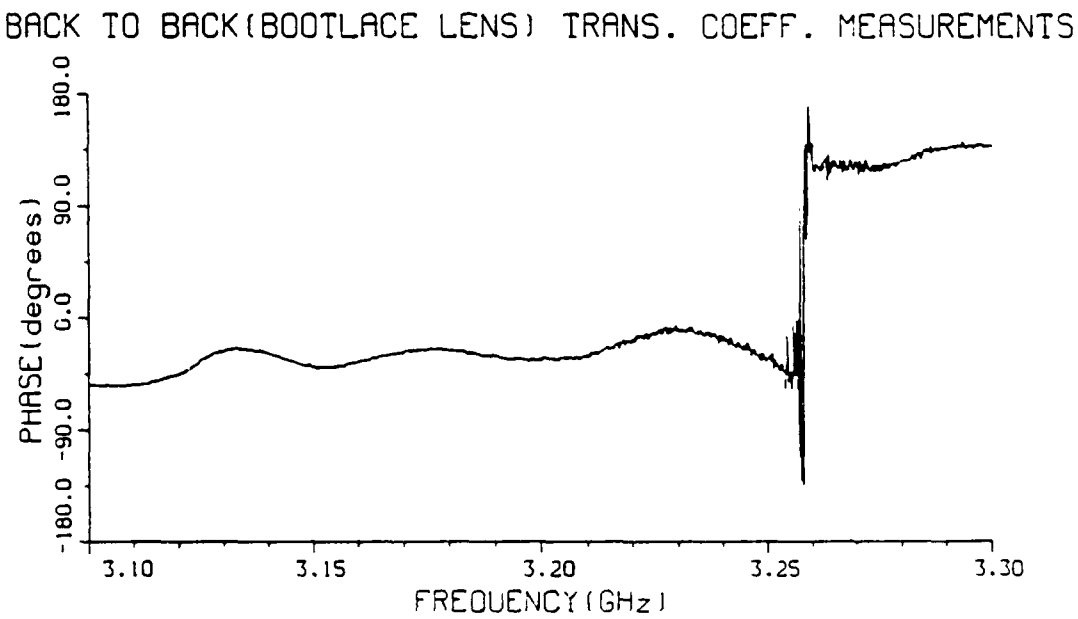
BACK TO BACK(BOOTLACE LENS) TRANS. COEFF. MEASUREMENTS
PHASE(degrees)
180.0
90.0
0.0
-90.0
-180.0
3.10
3.15
3.20
3.25
3.30
FREQUENCY(GHz)

Figure V-36

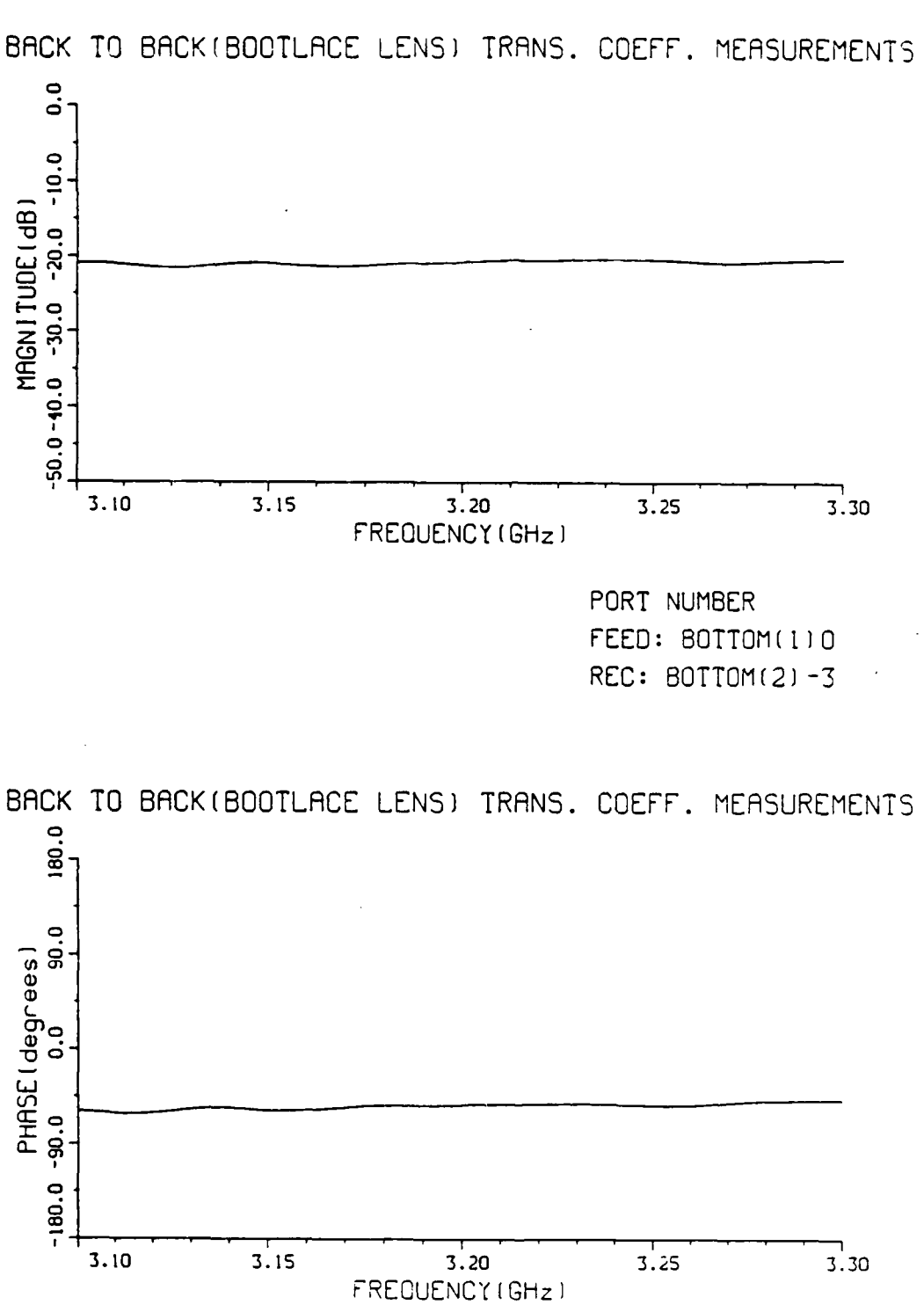
BACK TO BACK(BOOTLACE LENS) TRANS. COEFF. MEASUREMENTS
MAGNITUDE(dB)
0.0
-10.0
-20.0
-30.0
-40.0
-50.0
3.10
3.15
3.20
3.25
3.30
FREQUENCY(GHz)
PORT NUMBER
FEED: BOTTOM(1)0
REC: BOTTOM(2)-3
BACK TO BACK(BOOTLACE LENS) TRANS. COEFF. MEASUREMENTS
PHASE(degrees)
180.0
90.0
0.0
-90.0
-180.0
3.10
3.15
3.20
3.25
3.30
FREQUENCY(GHz)

Figure V-37

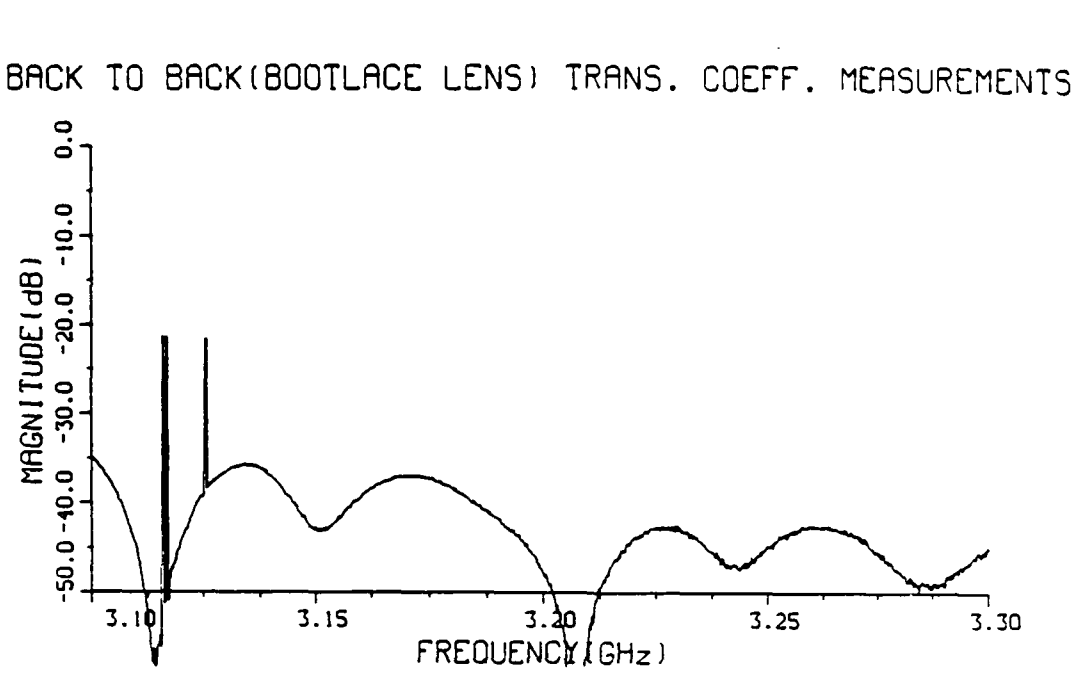
BACK TO BACK(BOOTLACE LENS) TRANS. COEFF. MEASUREMENTS
MAGNITUDE(dB)
0.0
-10.0
-20.0
-30.0
-40.0
-50.0
3.10
3.15
3.20
3.25
3.30
FREQUENCY(GHz)
PORT NUMBER
FEED: BOTTOM(1)0
REC: BOTTOM(2)-2

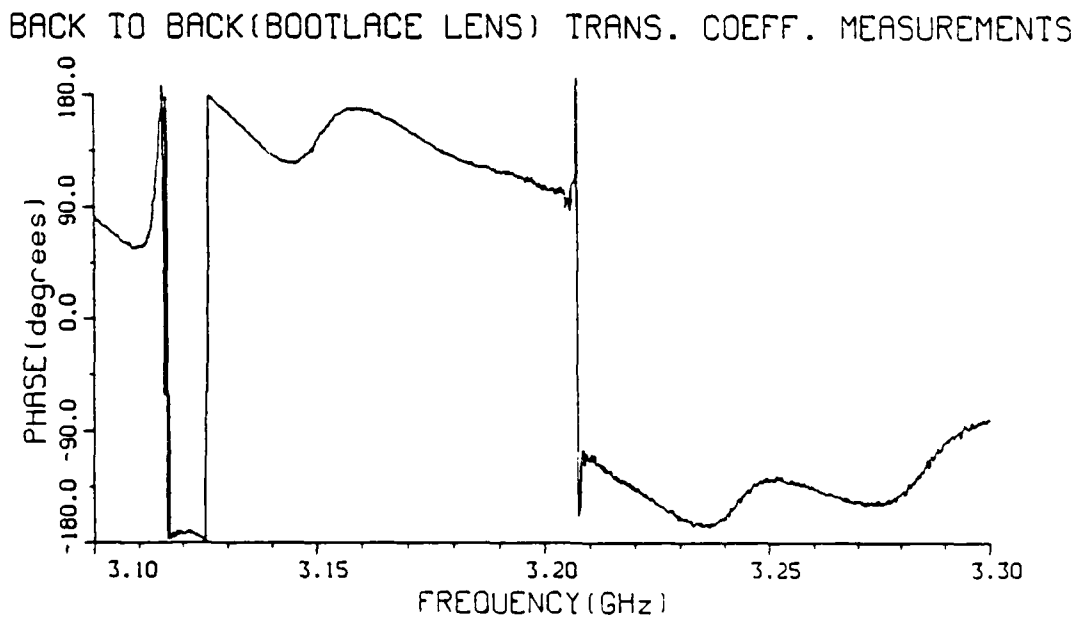
BACK TO BACK(BOOTLACE LENS) TRANS. COEFF. MEASUREMENTS
PHASE(degrees)
180.0
90.0
0.0
-90.0
-180.0
3.10
3.15
3.20
3.25
3.30
FREQUENCY(GHz)

Figure V-38

BACK TO BACK(BOOTLACE LENS) TRANS. COEFF. MEASUREMENTS

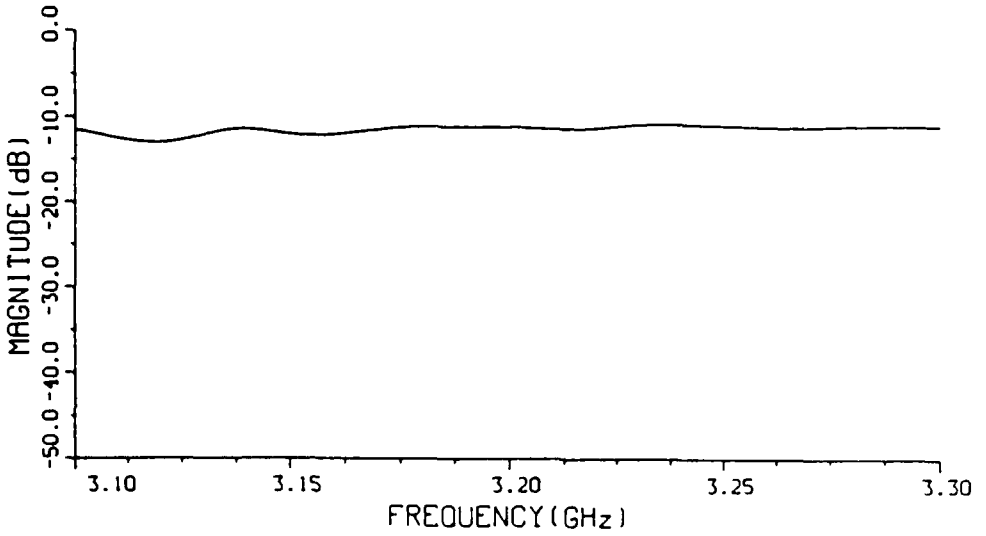

PORT NUMBER
FEED: BOTTOM(1)0
REC: BOTTOM(2)-1

BACK TO BACK(BOOTLACE LENS) TRANS. COEFF. MEASUREMENTS

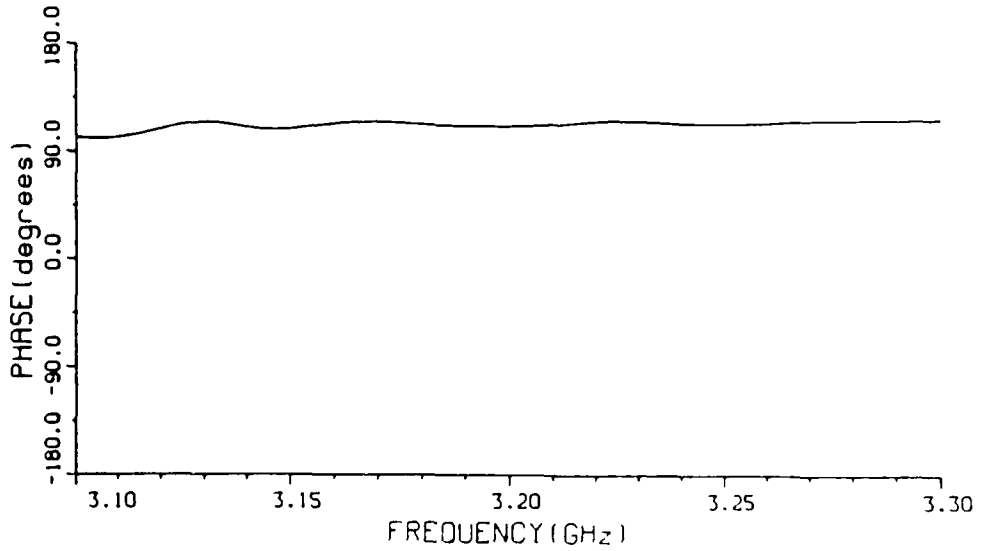

FigureV-39

BACK TO BACK(BOOTLACE LENS) TRANS. COEFF. MEASUREMENTS

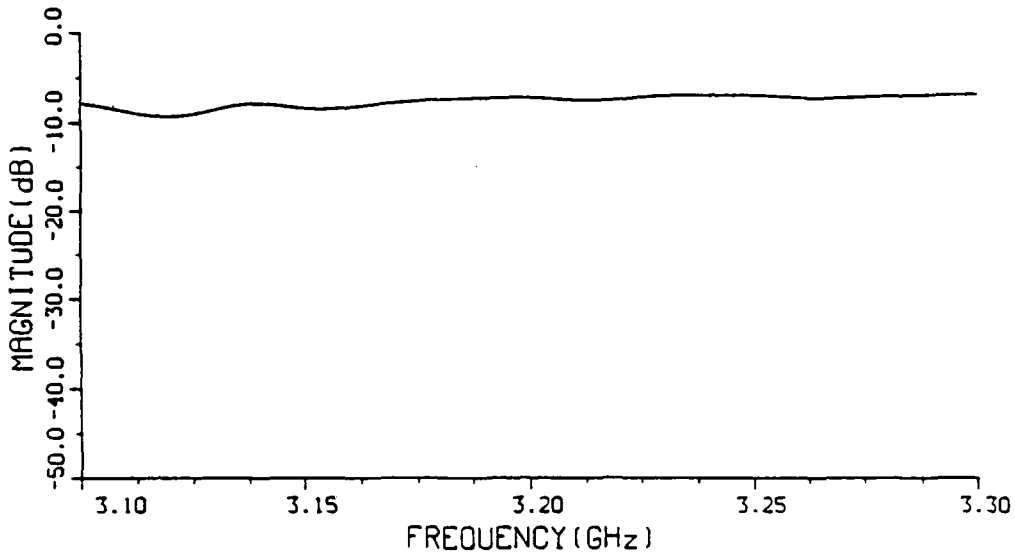

PORT NUMBER
FEED: BOTTOM(1)0
REC: BOTTOM(2)0

BACK TO BACK(BOOTLACE LENS) TRANS. COEFF. MEASUREMENTS

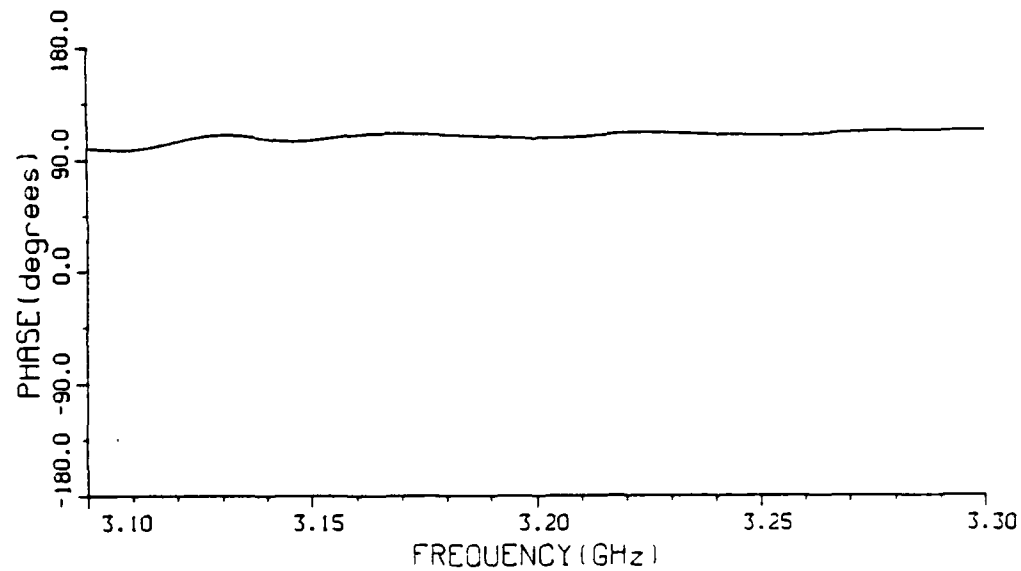

Figure V-40

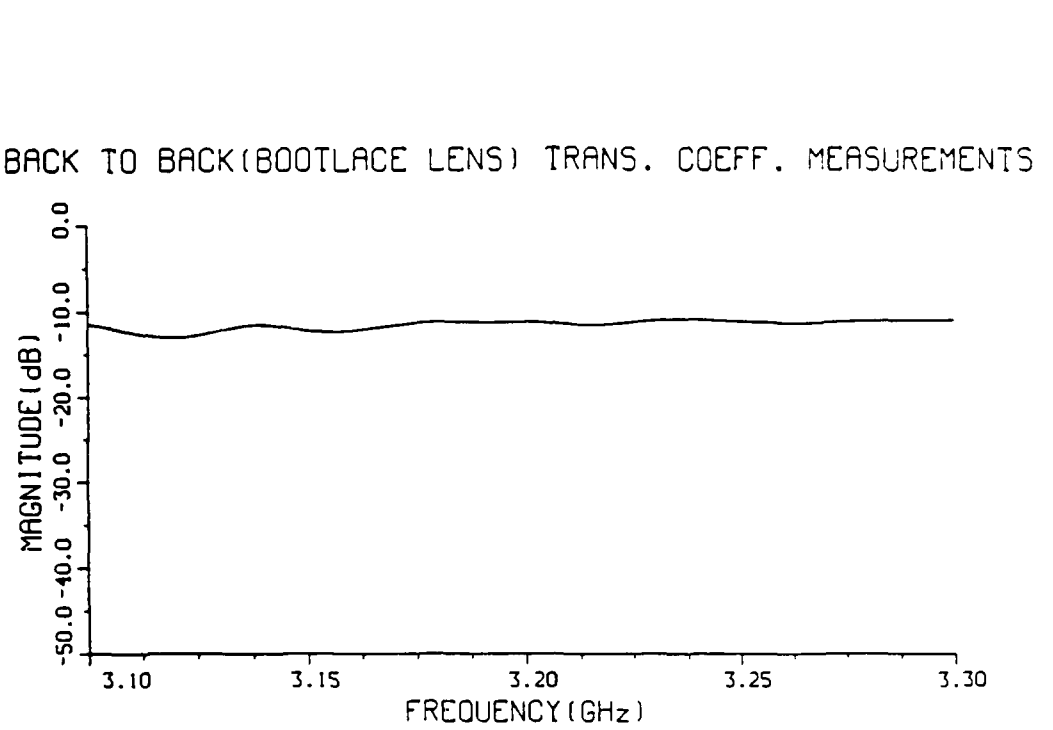
BACK TO BACK(BOOTLACE LENS) TRANS. COEFF. MEASUREMENTS
MAGNITUDE(dB)
0.0
-10.0
-20.0
-30.0
-40.0
-50.0
3.10
3.15
3.20
3.25
3.30
FREQUENCY(GHz)
PORT NUMBER
FEED: BOTTOM(1)0
REC: BOTTOM(2)1

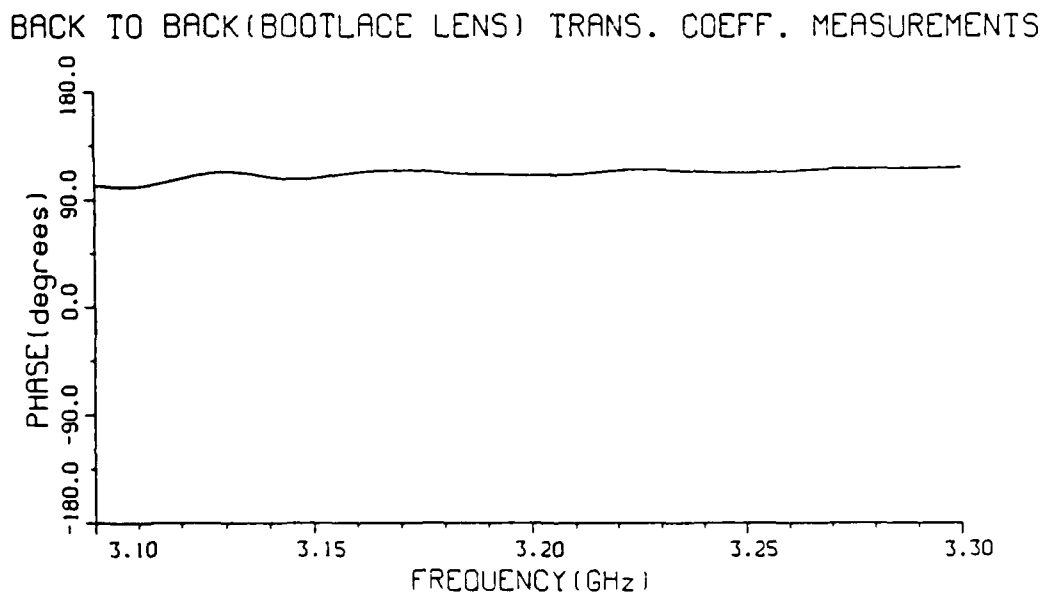
BACK TO BACK(BOOTLACE LENS) TRANS. COEFF. MEASUREMENTS
PHASE(degrees)
180.0
90.0
0.0
-90.0
-180.0
3.10
3.15
3.20
3.25
3.30
FREQUENCY(GHz)

Figure V-41

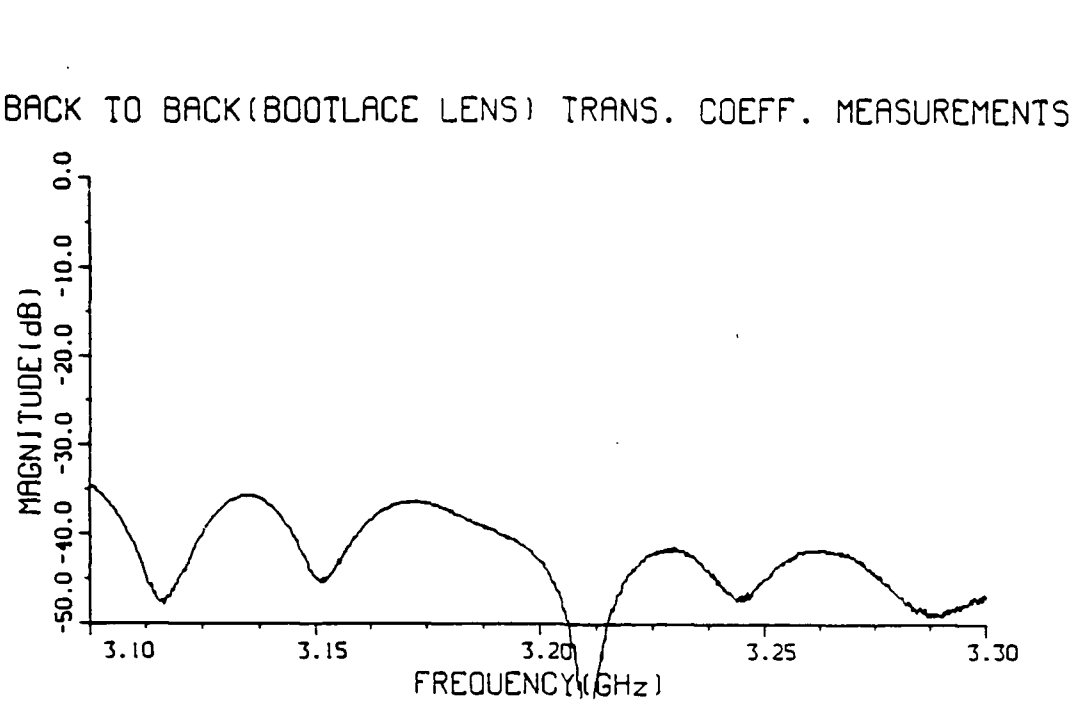
BACK TO BACK(BOOTLACE LENS) TRANS. COEFF. MEASUREMENTS
MAGNITUDE(dB)
0.0
-10.0
-20.0
-30.0
-40.0
-50.0
3.10
3.15
3.20
3.25
3.30
FREQUENCY(GHz)
PORT NUMBER
FEED: BOTTOM(1)0
REC: BOTTOM(2)2

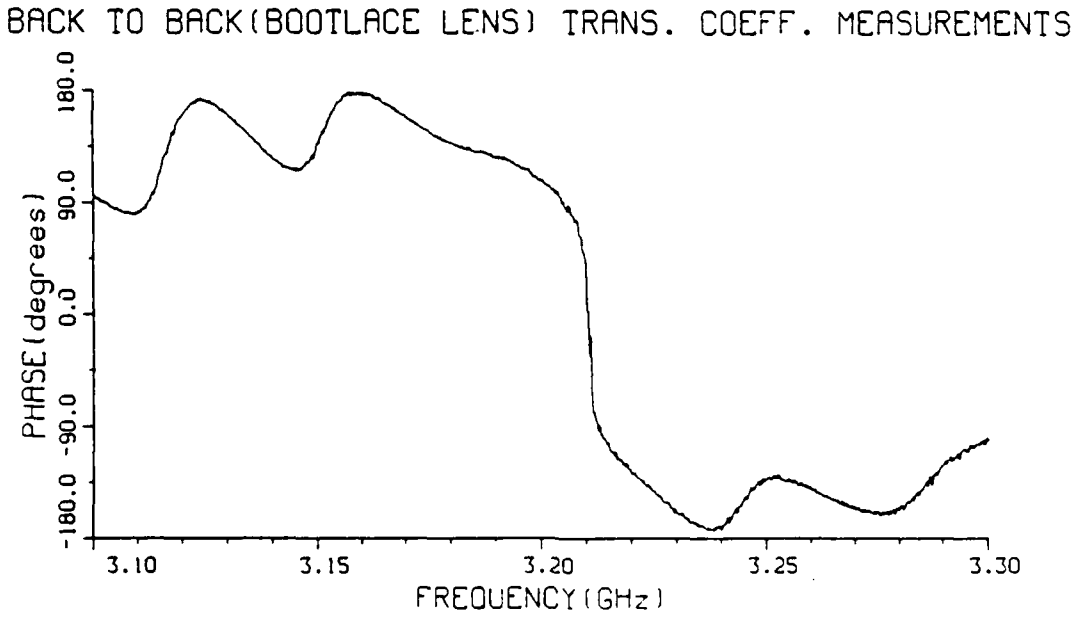
BACK TO BACK(BOOTLACE LENS) TRANS. COEFF. MEASUREMENTS
PHASE(degrees)
180.0
90.0
0.0
-90.0
-180.0
3.10
3.15
3.20
3.25
3.30
FREQUENCY(GHz)

Figure V-42

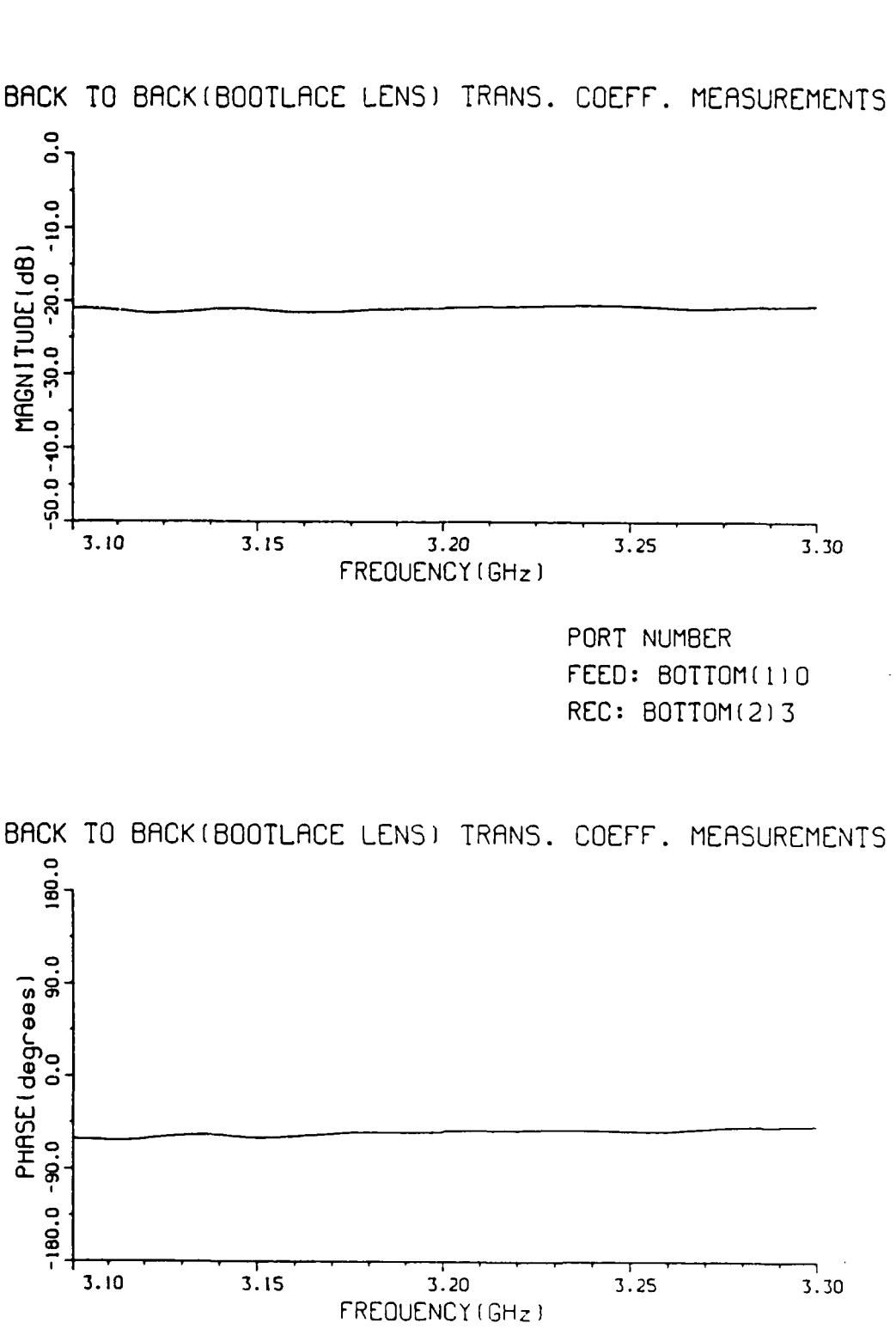
BACK TO BACK(BOOTLACE LENS) TRANS. COEFF. MEASUREMENTS
MAGNITUDE(dB)
0.0
-10.0
-20.0
-30.0
-40.0
-50.0
3.10
3.15
3.20
3.25
3.30
FREQUENCY(GHz)
PORT NUMBER
FEED: BOTTOM(1)0
REC: BOTTOM(2)3
BACK TO BACK(BOOTLACE LENS) TRANS. COEFF. MEASUREMENTS
PHASE(degrees)
180.0
90.0
0.0
-90.0
-180.0
3.10
3.15
3.20
3.25
3.30
FREQUENCY(GHz)

Figure V-43

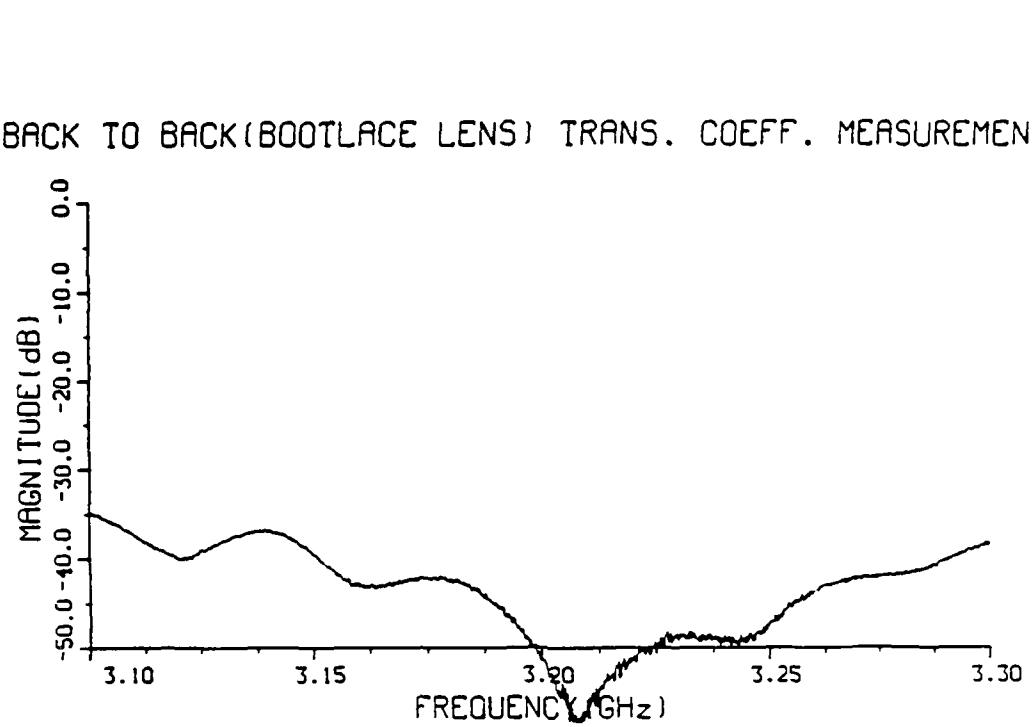
BACK TO BACK(BOOTLACE LENS) TRANS. COEFF. MEASUREMENTS
MAGNITUDE(dB)
0.0
-10.0
-20.0
-30.0
-40.0
-50.0
3.10
3.15
3.20
3.25
3.30
FREQUENCY(GHz)
PORT NUMBER
FEED: BOTTOM(1)0
REC: BOTTOM(2)4

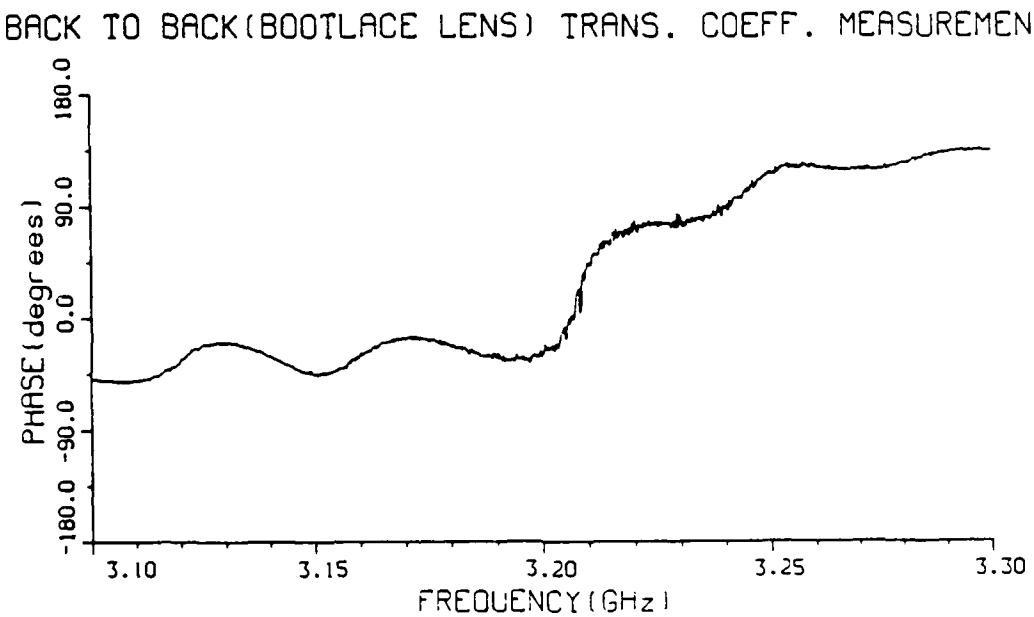
BACK TO BACK(BOOTLACE LENS) TRANS. COEFF. MEASUREMENTS
PHASE(degrees)
180.0
90.0
0.0
-90.0
-180.0
3.10
3.15
3.20
3.25
3.30
FREQUENCY(GHz)

Figure V-44

BACK TO BACK(BOOTLACE LENS) TRANS. COEFF. MEASUREMENTS

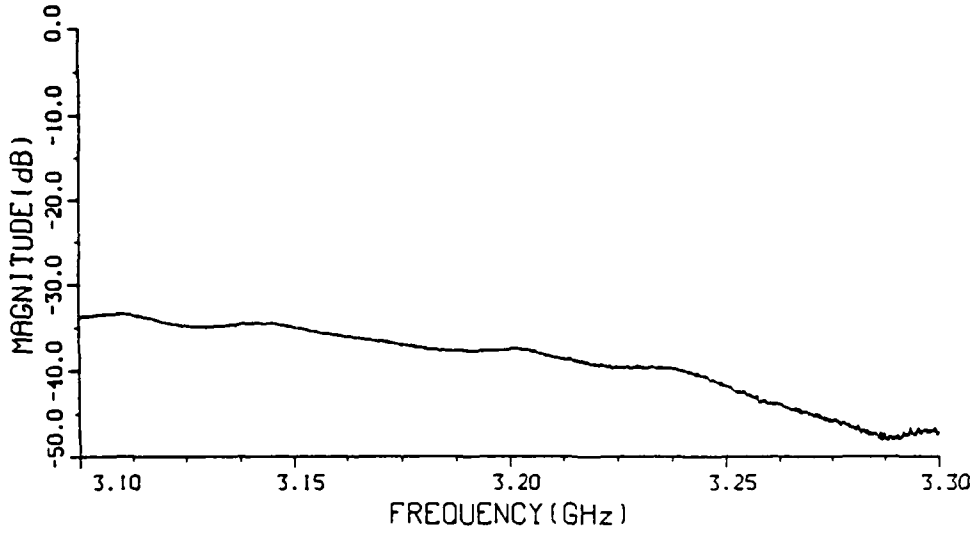

PORT NUMBER
FEED: BOTTOM(1)8
REC: BOTTOM(2)4

BACK TO BACK(BOOTLACE LENS) TRANS. COEFF. MEASUREMENTS

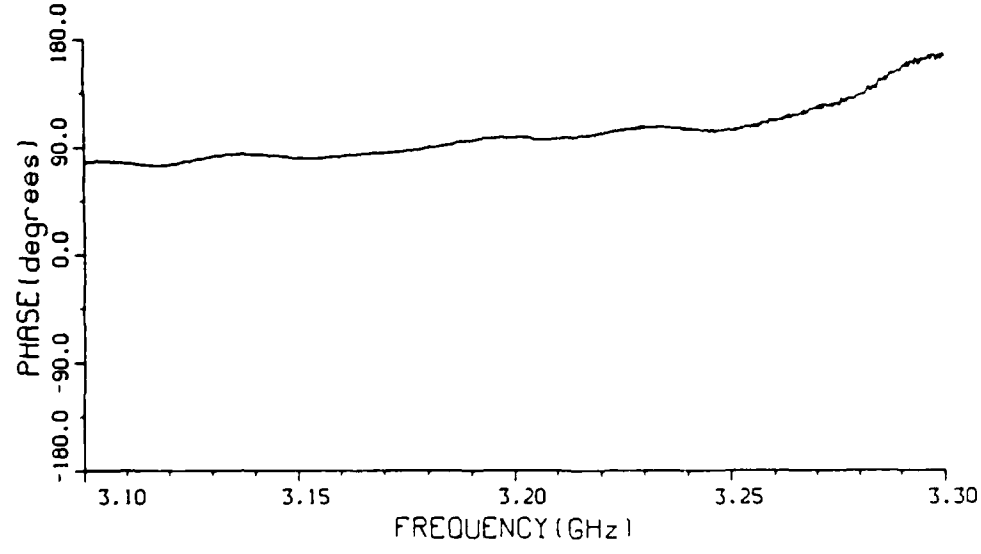

Figure V-45

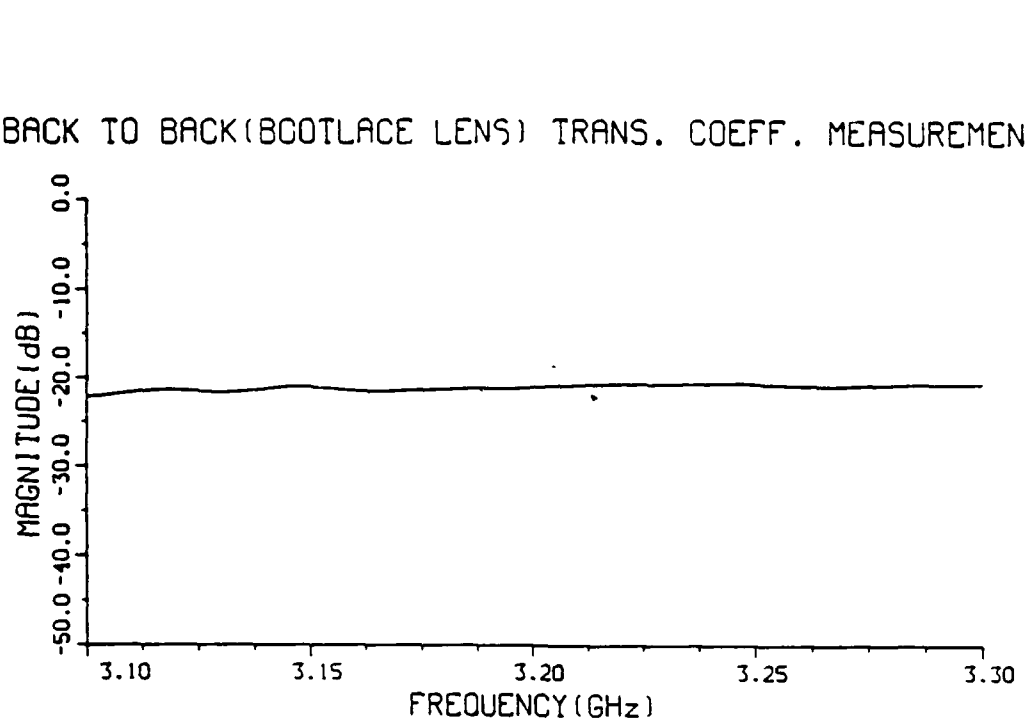
BACK TO BACK(BOOTLACE LENS) TRANS. COEFF. MEASUREMENTS
MAGNITUDE(dB)
0.0
-10.0
-20.0
-30.0
-40.0
-50.0
3.10
3.15
3.20
3.25
3.30
FREQUENCY(GHz)
PORT NUMBER
FEED: BOTTOM(1)8
REC: BOTTOM(2)5

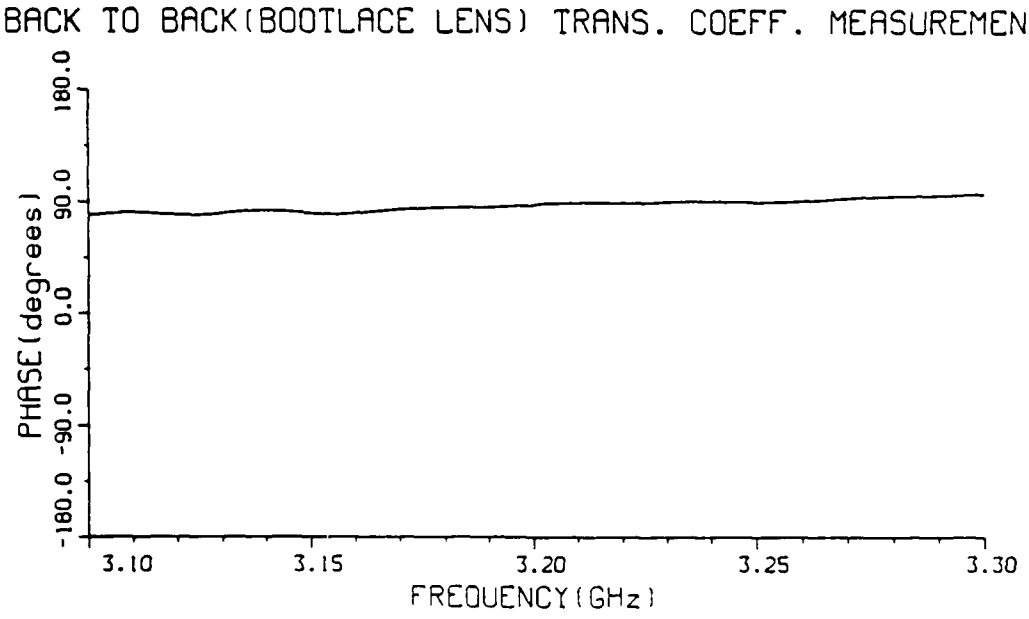
BACK TO BACK(BOOTLACE LENS) TRANS. COEFF. MEASUREMENTS
PHASE(degrees)
180.0
90.0
0.0
-90.0
-180.0
3.10
3.15
3.20
3.25
3.30
FREQUENCY(GHz)

Figure V-46

BACK TO BACK(BOOTLACE LENS) TRANS. COEFF. MEASUREMENTS

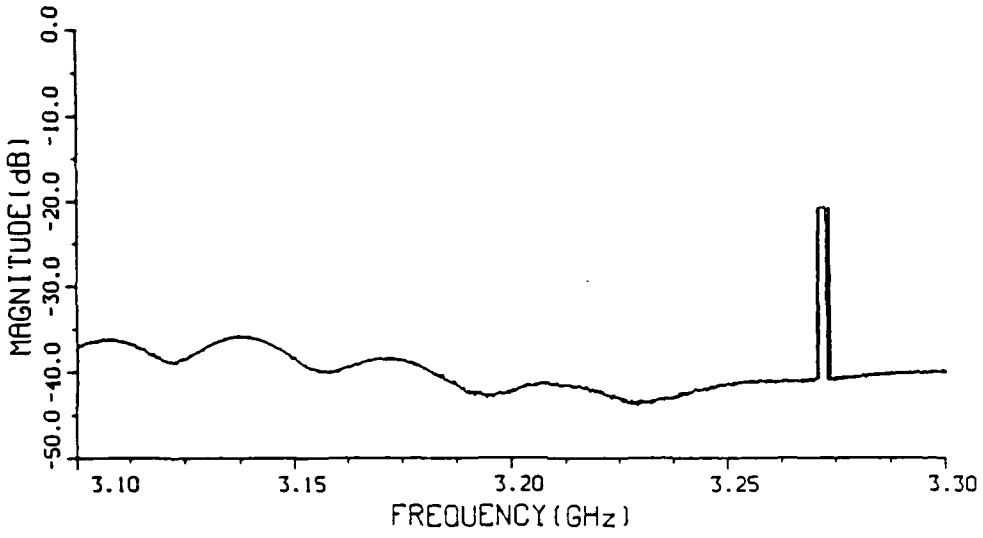

PORT NUMBER
FEED: BOTTOM(1)8
REC: BOTTOM(2)6

BACK TO BACK(BOOTLACE LENS) TRANS. COEFF. MEASUREMENTS

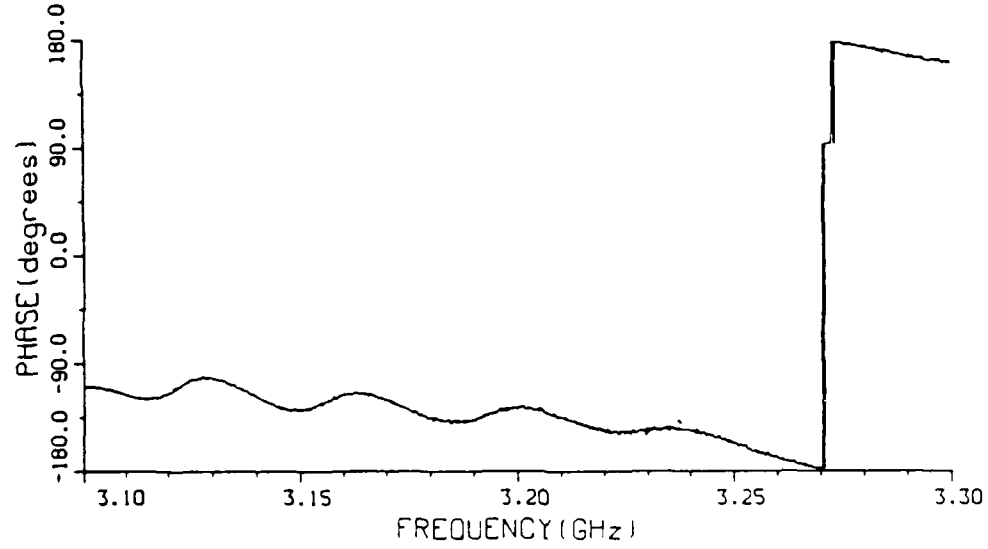

Figure V-47

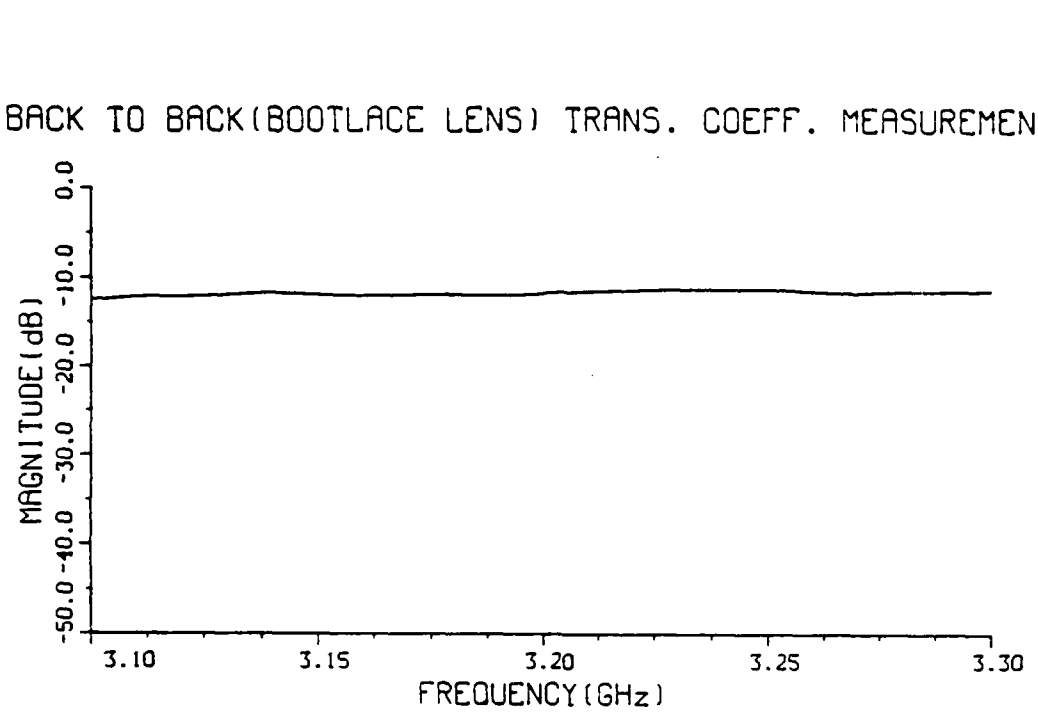
BACK TO BACK(BOOTLACE LENS) TRANS. COEFF. MEASUREMENTS
MAGNITUDE(dB)
0.0
-10.0
-20.0
-30.0
-40.0
-50.0
3.10
3.15
3.20
3.25
3.30
FREQUENCY(GHz)
PORT NUMBER
FEED: BOTTOM(1)8
REC: BOTTOM(2)7

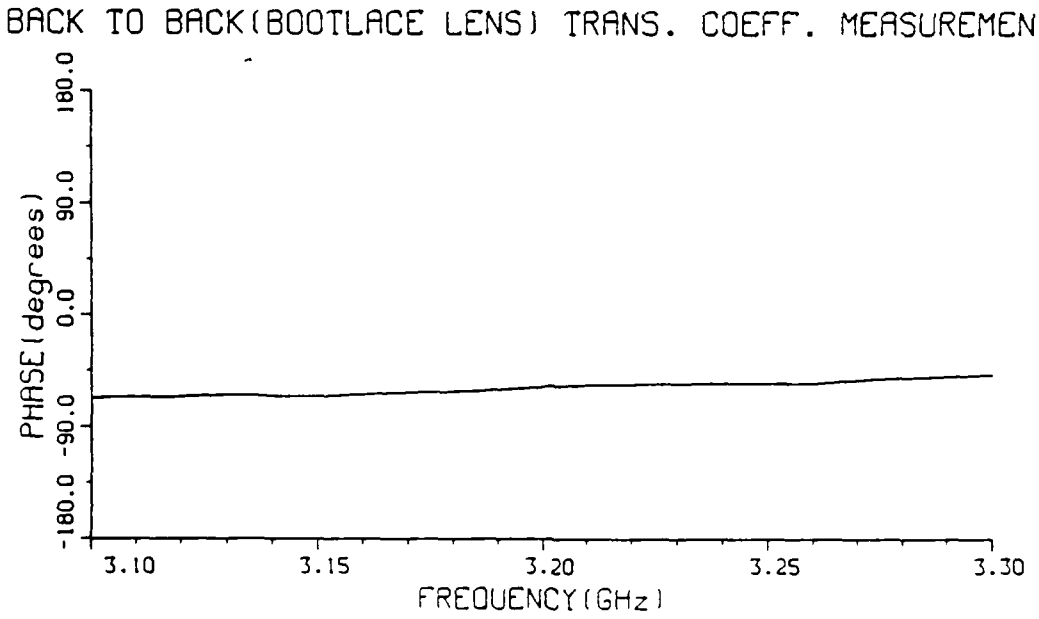
BACK TO BACK(BOOTLACE LENS) TRANS. COEFF. MEASUREMENTS
PHASE(degrees)
180.0
90.0
0.0
-90.0
-180.0
3.10
3.15
3.20
3.25
3.30
FREQUENCY(GHz)

Figure V-48

BACK TO BACK(BOOTLACE LENS) TRANS. COEFF. MEASUREMENTS

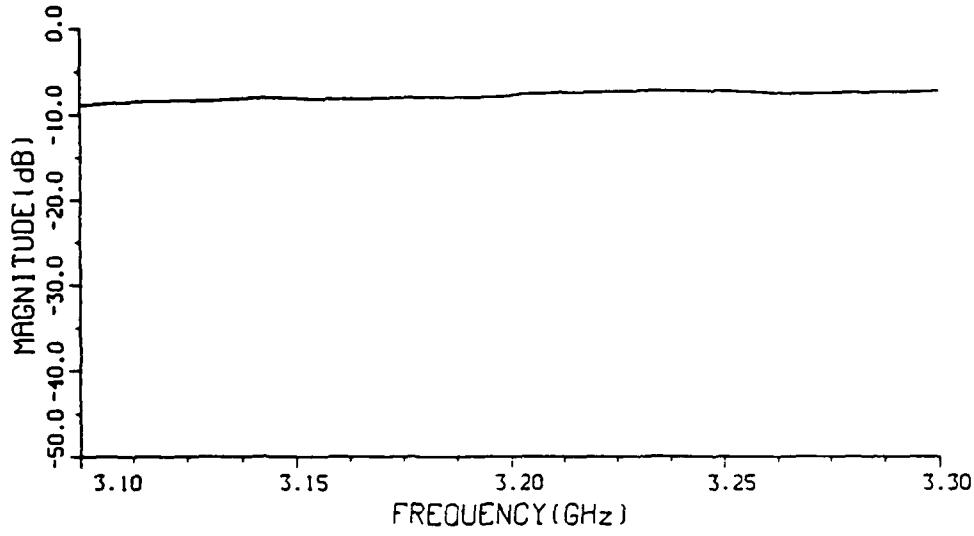

PORT NUMBER
FEED: BOTTOM(1)8
REC: BOTTOM(2)8

BACK TO BACK(BOOTLACE LENS) TRANS. COEFF. MEASUREMENTS

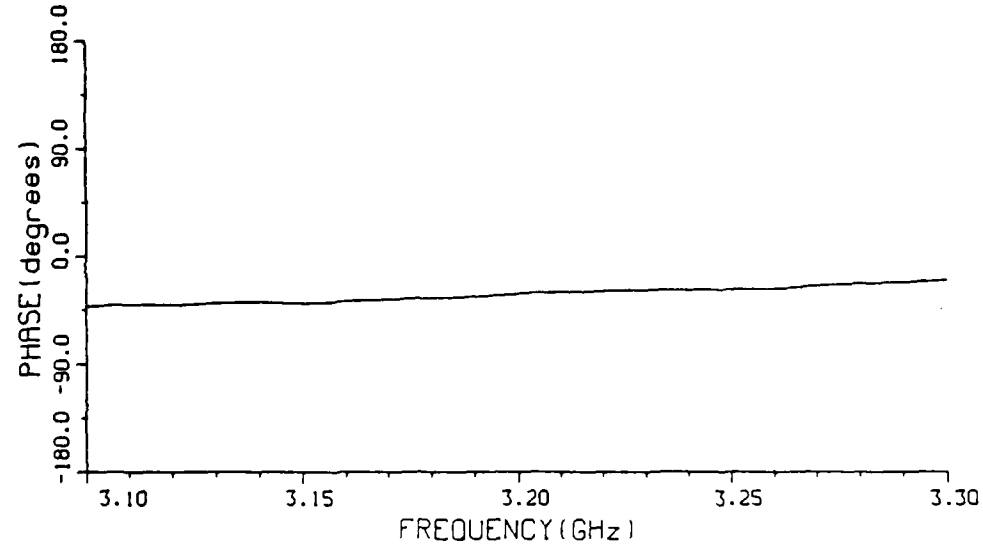

Figure V-49

BACK TO BACK(BOOTLACE LENS) TRANS. COEFF. MEASUREMENTS

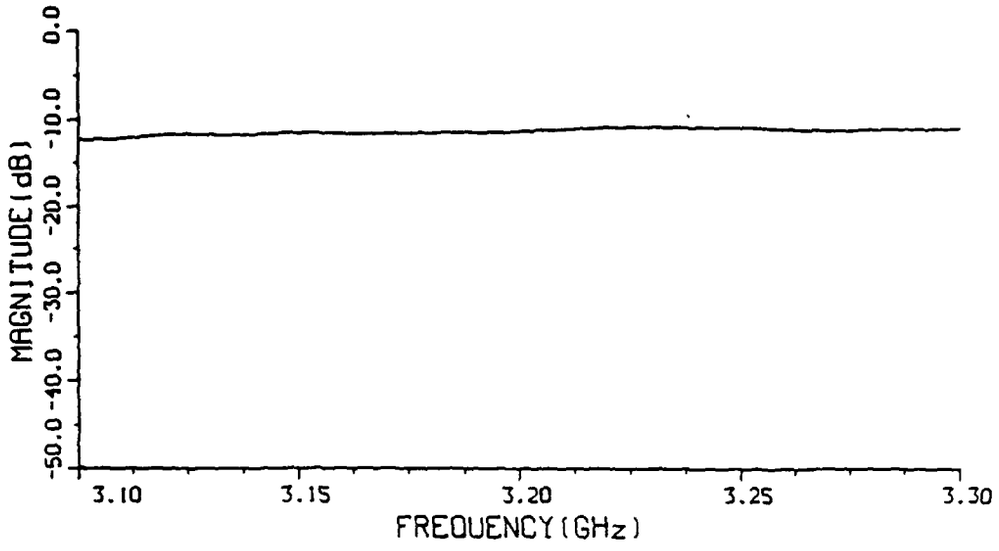

PORT NUMBER
FEED: BOTTOM(1)8
REC: BOTTOM(2)9

BACK TO BACK(BOOTLACE LENS) TRANS. COEFF. MEASUREMENTS

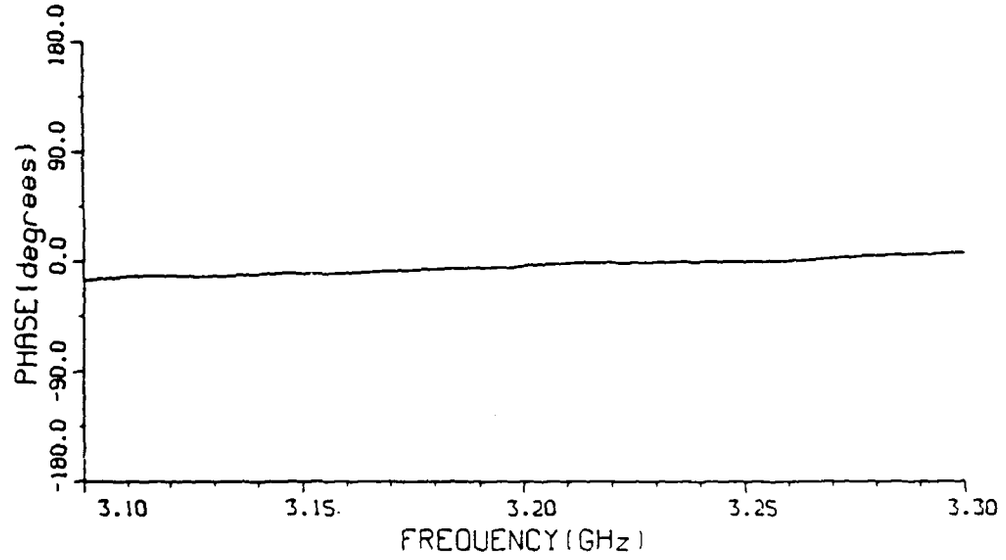

Figure V-50

BACK TO BACK(BOOTLACE LENS) TRANS. COEFF. MEASUREMENTS

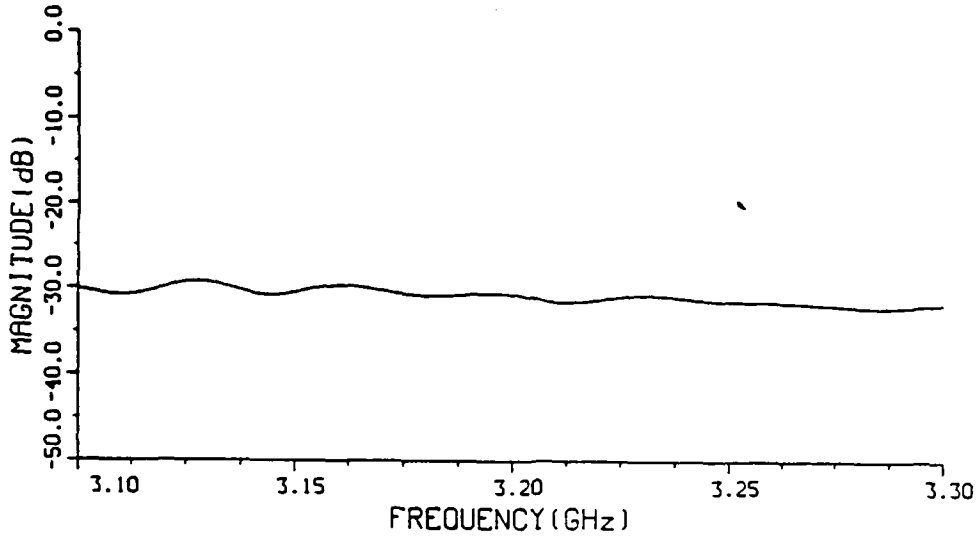

PORT NUMBER
FEED: BOTTOM(1)8
REC: BOTTOM(2)10

BACK TO BACK(BOOTLACE LENS) TRANS. COEFF. MEASUREMENTS

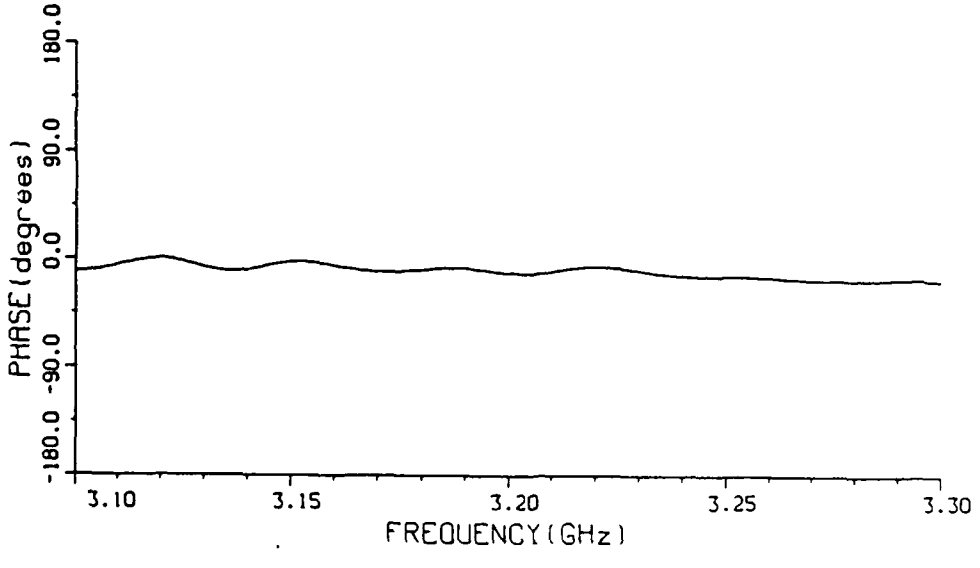

Figure V-51

BACK TO BACK(BOOTLACE LENS) TRANS. COEFF. MEASUREMENTS

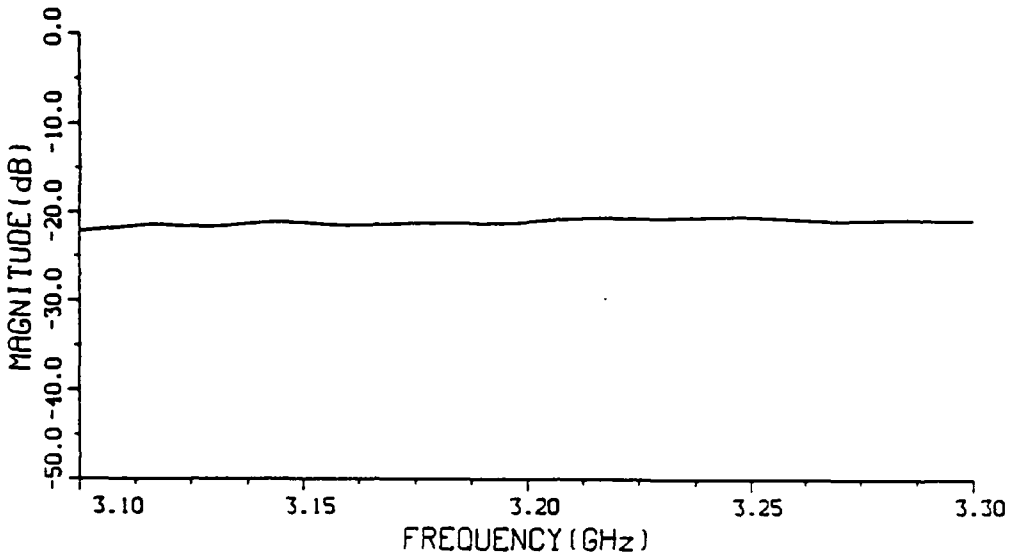

PORT NUMBER
FEED: BOTTOM(1)8
REC: BOTTOM(2)11

BACK TO BACK(BOOTLACE LENS) TRANS. COEFF. MEASUREMENTS

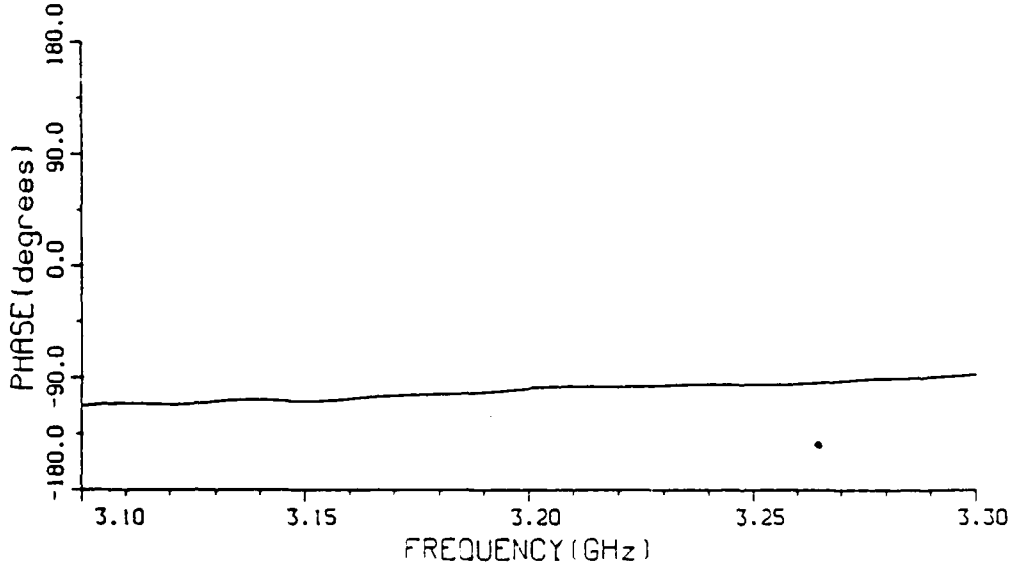

Figure V-52

BACK TO BACK(BOOTLACE LENS) TRANS. COEFF. MEASUREMENTS

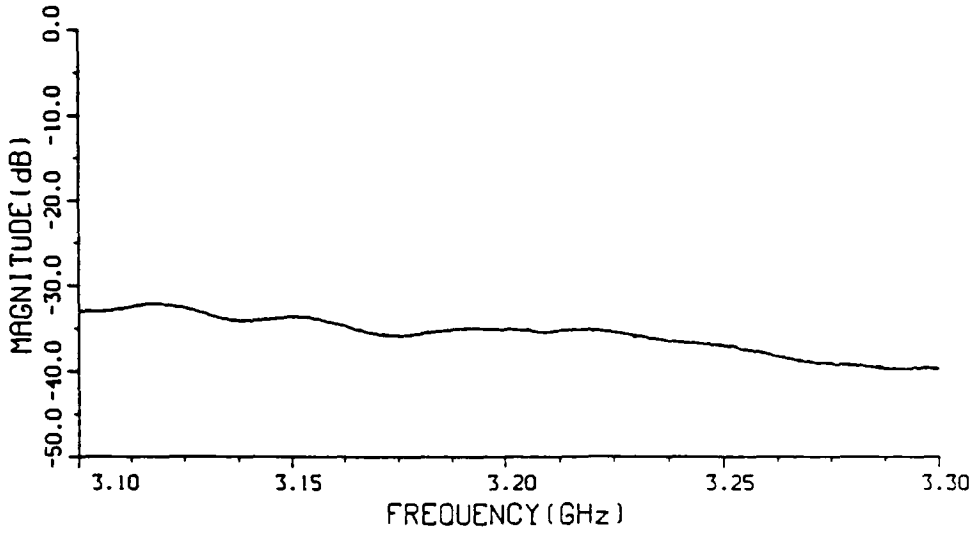

PORT NUMBER
FEED: BOTTOM(1)8
REC: BOTTOM(2)12

BACK TO BACK(BOOTLACE LENS) TRANS. COEFF. MEASUREMENTS

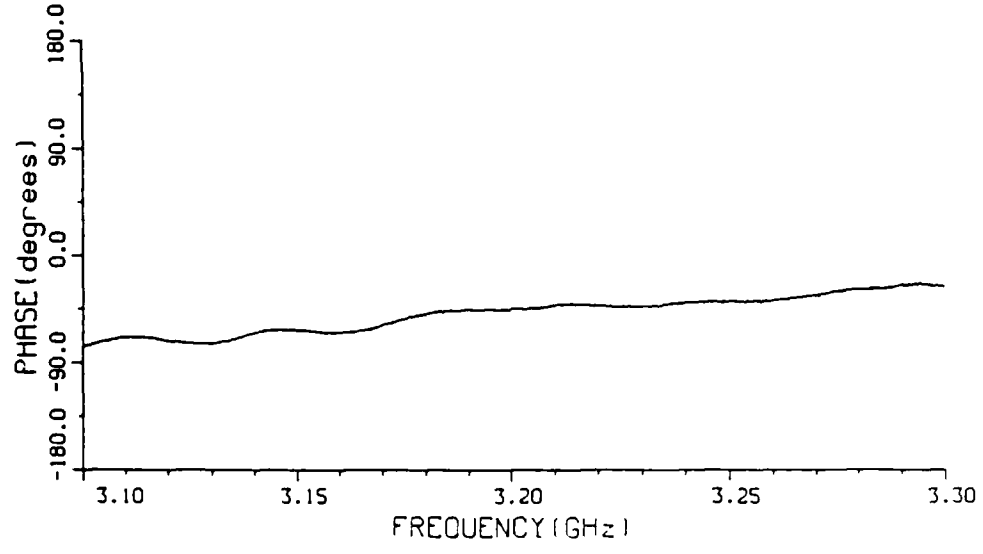

Figure V-53

END

DATE

FILMED

DTIC

9-88